MICROWAVE RADIOMETER DATA STUDY

Phase II Final Report

Report No. 1344R-2 June 1970

Contract No. NAS 9-9363

Prepared for

NATIONAL AERONAUTICS AND SPACE ADMINISTRATION
MANNED SPACECRAFT CENTER
Houston, Texas

Prepared by

AEROJET-GENERAL CORPORATION
MICROWAVE DIVISION
9200 East Flair Drive
El Monte, California

NASA CR 108561

MICROWAVE RADIOMETER DATA STUDY

Phase II Final Report

Prepared by

A. T. Edgerton

Report No. 1344R-2 - June 1970

Contract No. NAS 9-9363

Prepared for

NATIONAL AERONAUTICS AND SPACE ADMINISTRATION
MANNED SPACECRAFT
Houston, Texas

Prepared by

AEROJET-GENERAL CORPORATION
MICROWAVE DIVISION
9200 East Flair Drive
El Monte, California

FOREWORD

This document is the final technical report summarizing work performed by the Microwave Division of Aerojet-General Corporation, El Monte, California, during Phase II of the "Microwave Radiometer Data Study." Phase II of this study, sponsored by the NASA Manned Spacecraft Center, Houston, Texas, under Contract No. NAS 9-9363 is concerned with atmospheric and antenna pattern effects on measurements with the NASA P3A Multifrequency Microwave Radiometer System. This report summarizes equations and data flow developed to correct measurement data for these effects and includes results obtained from flight experiments designed to substantiate the equations. This work was performed between 7 October 1969 and 15 May 1970.

Personnel who have contributed to the data study and preparation of this report include A T Edgerton, A Stogryn, G Poe, S. Baker, G. T Chalfin, J. Kirwan, P. R Jordan and F Ruskey

ACKNOWLEDGEMENTS

The assistance of J. Carney and Nick Hatcher of NASA/MSC in planning and performing the verification tests is appreciated. In addition, the cooperation and help of the following MSC personnel is appreciated G. Flanagan, F Newman, W. Langenhenning, J. Williams, and R Mennella. Others, primarily flight crew personnel and operating technicians were also important contributors.

CONTENTS

ILLUSTRATIONS

ILLUSTRATIONS (Cont.)

Section 1

INTRODUCTION AND SUMMARY

This document is the final technical report summarizing work performed by Aerojet-General Corporation during Phase II of the Microwave Radiometer Data Study. Phase II of this study, sponsored by the NASA Manned Spacecraft Center under Contract No. NAS 9-9363, is concerned with the effects of atmospheric attenuation and emission, and the antenna patterns associated with the NASA P3A Multifrequency Microwave Radiometer System (MFMR). The object of this study is to develop equations and data flow for a computer program to correct measured radiometric data for these effects and to develop flight experiments and test procedures for verifying the equations. Data from this study were supplied to Manned Spacecraft Center's Computation and Analysis Division for computer programming.

This effort represents a portion of the over-all task of obtaining absolute brightness temperatures from raw MFMR data.

Absolute radiometric brightness temperatures can be derived from MFMR data by correcting raw data for effects of 1) instrumentation calibration (baseline drift, gain, radiometer system losses including waveguide and antenna insertion losses, etc.), 2) antenna patterns, 3) radome effects, and 4) atmospheric effects. The basic data reduction steps necessary for applying instrumentation and gross radome corrections to raw MFMR data have been developed by NASA/MSC and contractors The task of correcting measurement data for radome effects is the objective of a separate study.

This report deals with techniques for removing atmospheric and antenna pattern effects from MFMR data Section 2 contains a detailed description of equations, data flow, and experimental methods for removing atmospheric effects from measured data Section 3 contains equations, data flow, experimental and data reduction procedures for correcting MFMR data for antenna pattern effects Section 4 is a discussion of verification

tests designed to confirm the data reduction equations and rationale. Section 5 contains conclusions and recommendations based on the overall Phase II study.

In summary, Phase II of the Microwave Radiometer Data Study provides techniques for removing atmospheric contributions and antenna pattern effects from MFMR data The techniques are sufficiently general for use with other microwave radiometer systems, and computer programs are being developed by the Manned Spacecraft Center to apply these corrections to data acquired with the MFMR. Flight experiments were formulated and conducted to substantiate the data correction routines Data obtained during these experiments were inconsistent. Unrealistic brightness temperatures were obtained using antenna and radome loss values furnished for use in this study. Significant improvement was achieved by using an empirically determined loss factor However, quantitative results could not be obtained due to the sensitivity of measurement data to the empirically determined loss factor. After an adequate calibration of the MFMR is achieved, verification tests of the atmospheric and antenna pattern routines can be completed. The microwave radiometer data processing routines developed under Phase II of the data study will, for the first time, enable routine application of atmospheric and antenna pattern corrections. These refinements will facilitate use of MFMR data by the scientific community.

Section 2

ATMOSPHERIC ATTENUATION AND EMISSION STUDY

This section of the report documents equations and procedures developed to correct MFMR data for atmospheric attenuation and emission effects.

2.1 INTRODUCTORY COMMENTS

The brightness temperature of a surface observed by a radiometer at some height z above the surface is affected by the atmosphere in several ways. First, the radiation leaving the surface contains a component which consists of reflected incoming radiation emitted by the ionosphere above the surface (plus a component due to the cosmic background). Secondly, on leaving the surface, the radiation is attenuated by the atmosphere in propagating to the radiometer. Finally, the atmosphere between the radiometer and the surface itself emits radiation which contributes to the received signal. These contributions to microwave radiometric measurements can range from a negligible amount for a clear, dry day at frequencies below 15 GHz, to very substantial values for humid, cloudy and/or rainy conditions at frequencies above 20 GHz. Thus, the atmospheric contributions to airborne microwave radiometric data must generally be removed to obtain the true brightness temperature of the terrain surface The task is to devise a method for removing atmospheric contributions from radiometric measurements where the surface of interest and the intervening atmosphere are not necessarily uniform.

MFMR missions are flown for a variety of purposes and consequently, requirements for atmospheric corrections vary from mission to mission. Flights are conducted at various altitudes and under a wide range of climatic conditions. To accommodate the range of experimental conditions, a flexible atmospheric effects correction method must be devised. Moreover, planning of MFMR missions must include consideration of data requirements and mission constraints for performing an adequate atmospheric correction. Uniform atmospheric conditions are generally desirable.

Atmospheric contributions to MFMR measurements can be determined by (1) computation of atmospheric attenuation and emission using suitable mathematical expressions and known or estimated meteorological conditions, and/or (2) direct MFMR measurements of atmospheric radiation at selected heights above the terrain. Each approach possesses advantages and limitations. Both appear to be useful for MFMR data analysis. In the following discussion both approaches are considered.

To compute the effect of the atmosphere on measured brightness temperature, ideally one would like an air temperature and water vapor profile of the atmosphere together with a specification of the water droplet distribution within any clouds that may be present. Except for areas located near weather stations, such a detailed description of the atmosphere will not be available. Fortunately, the number of parameters that must be known to accurately predict atmospheric effects is small if the observations are made at sufficiently great height, (i e., above 20,000 feet). In fact, detailed numerical studies at a number of frequencies have shown that in the absence of rain, only the total water vapor content (the integral of the water vapor density, from sea level to the top of the atmosphere), the total cloud water droplet content, and the air temperature at cloud height will suffice to predict atmospheric effects to within 1 or $2^{o}K$. The P3A aircraft possesses sensors for determining height above terrain, barometric pressure, relative humidity and air temperature, so that many of the needed parameters can be obtained from on-board sensors. Section 2.2 contains a comprehensive discussion of numerical models for estimating atmospheric contributions to MFMR data.

The direct measurement approach requires more flight time than that needed for numerical approximations of atmospheric contributions. However, better accuracy can be realized with direct measurements when nonuniform weather, such as variable cloud conditions, is encountered. The number of MFMR sky measurements (flight altitudes) necessary to define atmospheric contributions to terrain observations is a function of prevailing weather conditions. Section 2.3 contains a comprehensive discussion of the direct measurement approach.

2.2 THEORY

The brightness temperature of a surface observed by a radiometer at some height z above the surface is affected by the atmosphere in several ways. First, the radiation leaving the surface contains a component which consists of reflected incoming radiation emitted by the atmosphere above the surface (plus a component due to the cosmic background). Secondly, on leaving the surface, the radiation is attenuated by the atmosphere in propagating to the radiometer Finally, the atmosphere between the radiometer and the surface itself emits radiation which contributes to the received signal The result of the last two effects on the brightness temperature of the radiation leaving the surface can be expressed in a simple way if scattering effects in the atmosphere are ignored while the mathematical expression of the first effect can involve rather complex equations if the surface is treated in a precise manner.*

Consider the situation illustrated in Figure 2-1 If the brightness temperature of the radiation with polarization p leaving the surface in the direction θ is $T_p(\theta, o)$, then the brightness temperature at the height z is

$$T_p(\theta, z) = L(\theta, z)\, T_p(\theta, o) + T_{atm}(\theta, z) \tag{2-1}$$

where the loss factor L is given by

$$L(\theta, z) = \exp\left[-\sec\theta \int_o^z \varkappa(u)du\right] \tag{2-2}$$

and the temperature of the radiation emitted by the atmosphere between the ground and the radiometer is

$$T_{atm}(\theta, z) = \sec\theta \int_o^z T_{air}(z')\,\varkappa(z')\exp\left[-\sec\theta \int_{z'}^z \varkappa(u)du\right] dz' \tag{2-3}$$

*For the frequencies of interest, scattering in the atmosphere can be ignored except for heavy rain storms

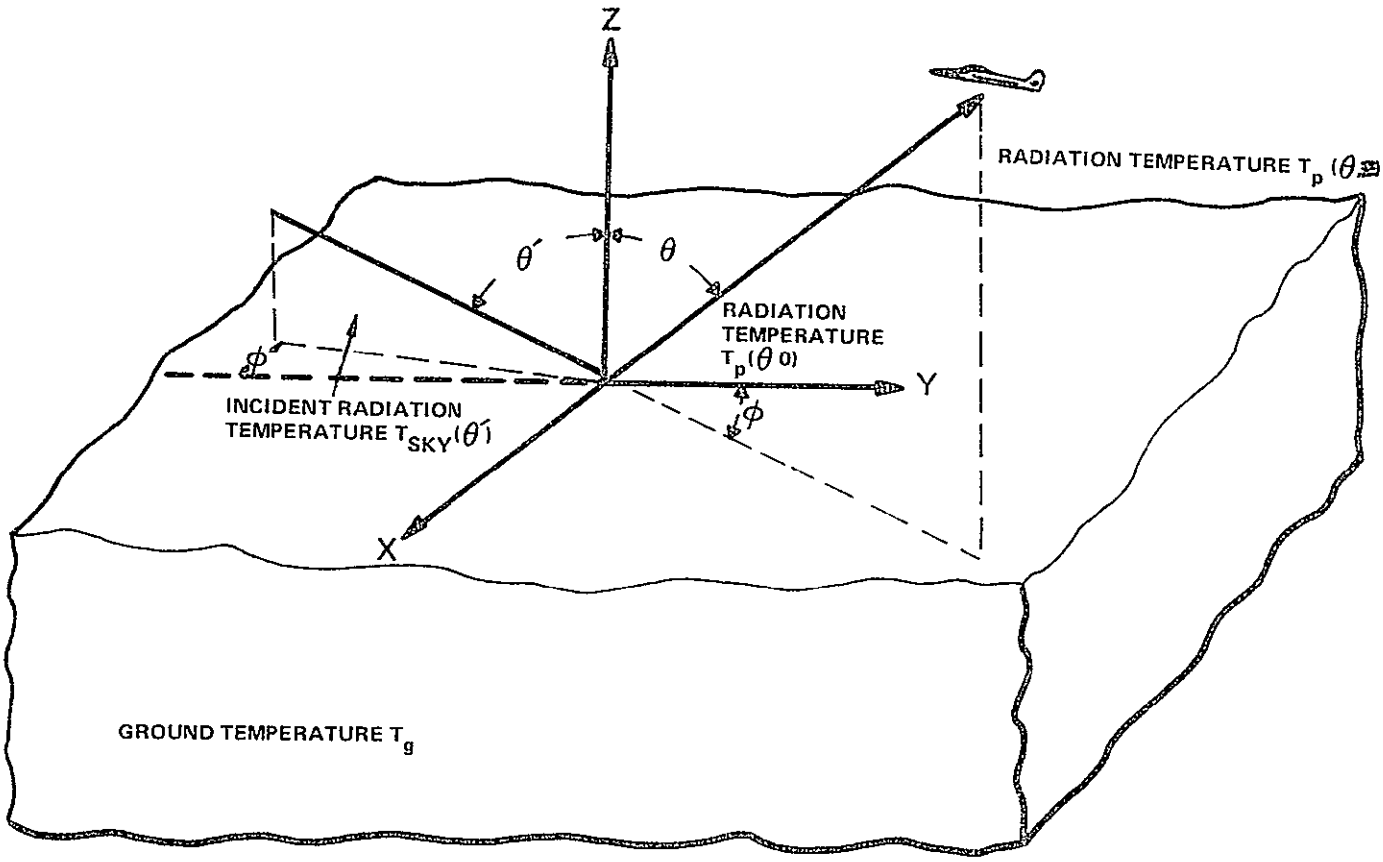

FIGURE 2-1 GEOMETRY FOR ATMOSPHERIC CORRECTIONS

In (2-2) and (2-3), $\varkappa(z)$ is the absorption coefficient per unit length in the atmosphere at the height z while $T_{air}(z)$ is the air temperature at the height z Note that $\varkappa$ is a function of the radiometric frequency although, in order to simplify the notation, the frequency dependence is not indicated in the equations

As mentioned above, the expression for $T_p(\theta, o)$ in terms of the properties of the surface and the atmosphere may be very complex Assuming that the incident sky radiation is unpolarized and that the ground temperature does not vary significantly over the depth from which most of the radiation is emitted,

$$T_p(\theta, o) = \epsilon_p(\theta) T_g + \frac{1}{4\pi} \int \left[\gamma_{ph} + \gamma_{pv}\right] T_{sky}(\theta') \, d\Omega' \qquad (2\text{-}4)$$

where $\epsilon_p(\theta)$ is the emissivity of the upper hemisphere ground in the direction θ, T_g the thermometric temperature of the ground and γ_{ph} and γ_{pv} are respectively coefficients for scattering with polarization p from the ground when the incident radiation has polarization h (horizontal) and v (vertical). Both γ_{ph} and γ_{pv} depend on the incidence angles θ', φ' and scattering direction θ, φ The quantity $T_{sky}(\theta')$ is the sky temperature which is given by

$$T_{sky}(\theta') = \sec\theta \int_o^\infty T_{air}(z') \varkappa(z') \exp\left[-\sec\theta' \int_o^z \varkappa(u) du\right] dz' + T_{CB} L(\theta' \infty) \qquad (2\text{-}5)$$

In (2-5), T_{air}, $\varkappa$, and L have the same meaning as above while $T_{CB}(=2\ 7^oK)$ is the temperature of the cosmic background radiation The convention that $z = \infty$ corresponds to the top of the atmosphere is used in (2-5) although in practice a finite number of the order of 20 km can be used to give adequate accuracy in numerical computations It is readily apparent, even apart from the problem of specifying the scattering

coefficients of the surface, that the use of (2-5) in (2-4) can lead to computations on a rather large scale. Therefore, the assumption is often made that the surface under investigation is perfectly flat and uniform (specular surface). In this case, the scattering coefficients contain delta functions of angle and (2-4) reduces to

$$T_p(\theta, o) = \epsilon_p(\theta) T_g + \left[1 - \epsilon_p(\theta) \right] T_{sky}(\theta) \tag{2-6}$$

For many applications, the set of equations (2-1), (2-2), (2-3), (2-5), and (2-6) provide a useful means of accounting for atmospheric effects even if the surface under observation is not strictly specular

2 2 1 Basic Integrals

The preceding discussion has indicated that atmospheric effects can be expressed in terms of the three basic quantities $L(\theta, z)$, $T_{atm}(\theta, z)$ and $T_{sky}(\theta)$ given by (2-2), (2-3) and (2-5). For realistic models of the atmosphere, it is clear that the integrals which occur in the definitions of these quantities cannot be evaluated analytically, and hence, a numerical quadrature must be performed. The most efficient quadrature scheme is obtained by noting that, except for the factor $T_{air}(z')$, the integrand in both (2-3) and (2-5) are exact differentials. Thus, if the integral over z' in these equations is written as a sum of integrals, each over a sufficiently small interval in which $T_{air}(z')$ may be considered a constant, the integral over z' may be performed analytically. For example, if z_{max} corresponds to the top of the atmosphere, and the interval (O, z_{max}) is subdivided by the points $O=z_1<z_2<z_3 \ldots <z_n = z_{max}$ in such a way that $T_{air}(z)$ is effectively a constant $\bar{T}_{air}(z_i)$ in the subinterval $z_i \le z \le z_{i+1}$, then

$$T_{sky}(\theta) = T_{CB} \exp\left[-\sec\theta \int_o^z \kappa(u)du\right] + \sum_{i=1}^{N-1} \bar{T}_{air}(z_i) \int_{z_i}^{z_{i+1}} \sec\theta\, \kappa(z') \exp\left[-\sec\theta \int_o^{z'} \kappa(u)du\right] dz'$$

$$= T_{CB} \exp\left[-\sec\theta \int_o^z \kappa(u)du\right] + \sum_{i=1}^{N-1} \bar{T}_{air}(z_i) \left\{ -\exp\left[-\sec\theta \int_o^{z'} \kappa(u)du\right] \right\}_{z'=z_i}^{z'=z_{i+1}}$$

$$= T_{CB} \exp\left[-\sec\theta \int_o^z \kappa(u)du\right] + \sum_{\imath=1}^{N-1} \bar{T}_{air}(z_\imath)\left\{\exp\left[-\sec\theta \int_o^{z_\imath} \kappa(u)du\right]\right.$$

$$\left. -\exp\left[-\sec\theta \int_o^{z_{\imath+1}} \kappa(u)du\right]\right\} \qquad (2\text{-}7)$$

If the height of the radiometer, z , is chosen to coincide with one of the above division points (say $z_{N'}$), then a similar calculation shows that

$$T_{atm}(\theta, z_{N'}) \approx \sum_{\imath=1}^{N'-1} \bar{T}_{air}(z_i)\left\{\exp\left[-\sec\theta \int_{z_{\imath+1}}^{z_{N'}} \kappa(u)du\right] - \exp\left[-\sec\theta \int_{z_\imath}^{z_{N'}} \kappa(u)du\right]\right\} \qquad (2\text{-}8)$$

Comparing (2-2), (2-7), and (2-8), it is seen that if the integral

$$f(z_i) = \int_o^{z_\imath} \kappa(u)du \qquad (2\text{-}9)$$

is calculated for $\imath = 1, 2, \ldots, N$, then the three basic quantities can be expressed as

$$L(\theta, z_{N'}) = \exp\left[-\sec\theta f(z_{N'})\right] \qquad (2\text{-}10)$$

$$T_{atm}(\theta, z_{N'}) = \sum_{\imath=1}^{N'-1} \bar{T}_{air}(z_i)\left\{\exp\left[-\sec\theta\left(f(z_{N'}) - f(z_{\imath+1})\right)\right] - \exp\left[-\sec\theta\left(f(z_{N'}) - f(z_i)\right)\right]\right\} \qquad (2\text{-}11)$$

$$T_{sky}(\theta) = T_{CB}\exp\left[-\sec\theta f(z_N)\right] + \sum_{i=1}^{N-1} \bar{T}_{air}(z_\imath)\left\{\exp\left[-\sec\theta f(z_\imath)\right]\right.$$

$$\left. - \exp\left[-\sec\theta f(z_{i+1})\right]\right\} \qquad (2\text{-}12)$$

To evaluate these expressions, all that remains is to specify the dependence of the absorption coefficient $\varkappa$ on atmospheric conditions and radiometric frequency.

2.2.2 The Absorption Coefficient

The absorption coefficient $\varkappa(z)$ may be written as a sum

$$\varkappa(z) = \varkappa_{O_2}(z) + \varkappa_{H_2O}(z) + \varkappa_{cloud}(z) + \varkappa_{rain}(z) \tag{2-13}$$

where $\varkappa_{O_2}$, $\varkappa_{H_2O}$, $\varkappa_{cloud}$, and $\varkappa_{rain}$ are respectively the absorption coefficients of oxygen, water vapor, condensed water droplets (liquid or ice) in clouds, and rain. The contribution of $\varkappa_{rain}$ to $\varkappa$ will not be considered further here because the occurrence of rain is somewhat less common than the occurrence of cloud cover and because $\varkappa_{rain}$ depends strongly on the rain drop size distribution function as well as rainfall rate, and hence, its computation depends on a detailed knowledge of the characteristics of a given rain storm The other three terms in (2-13) will be discussed below. The coefficients $\varkappa_{O_2}$ and $\varkappa_{H_2O}$ are usually expressed in terms of the attenuation γ in db/km The relation between γ and $\varkappa$ is

$$\varkappa = .2302581 \ \gamma \ km^{-1} \tag{2-14}$$

2.2.2.1 Oxygen Attenuation

The theory of absorption by oxygen was first given by Van Vleck [2-1]. Substituting numerical values for the coefficients and assuming an atmospheric content of 20.9% oxygen by volume, Van Vleck's formula for absorption by oxygen in air becomes

$$\gamma_{O_2} = 2\ 6742 \frac{P_{air}}{T_{air}^3} \nu^2 \sum_{\text{odd } K} \left[\frac{K(2K+3)}{K+1} S_{K_+} + \frac{(K+1)(2K-1)}{K} S_{K-} + \frac{2(K^2+K+1)(2K+1)}{K(K+1)} S_{K_o} \right] \exp\left[-2\ 06844K(K+1)/T_{air} \right] \text{ db/km} \tag{2-15}$$

where

P_{air} = air pressure in mm Hg

T_{air} = air temperature in ^{o}K

ν = radiometric frequency in GHz

$$S_{K\pm} = \frac{\Delta\nu}{(\nu-\nu_{K\pm})^2 + (\Delta\nu)^2} + \frac{\Delta\nu}{(\nu+\nu_{K\pm})^2 + (\Delta\nu)^2}$$

$$S_{Ko} = \frac{\Delta\nu}{\nu^2 + (\Delta\nu)^2}$$

$\Delta\nu$ = line width constant in GHz

$\nu_{K\pm}$ = resonant line frequencies in GHz

The first 46 resonant frequencies are listed in Table 2-1.

Experiments have shown that, for all lines except the 1- line, the line width constant is given by [2-2]

$$\Delta\nu = 1.9\times10^{-3} P_{air}\left(\frac{760}{760+P_{air}}\right)\left(\frac{290}{T_{air}}\right)^{.9} \text{ GHz} \qquad (2\text{-}16)$$

The 1- line width constant has been determined as 1.90 MHz/mm Hg at $300^{o}K$ [2-3] and is proportional to the air pressure. Assuming that the width varies as the reciprocal of the air temperature, this leads to

$$\Delta\nu_{1-} = 1.444 \left(\frac{P_{air}}{760}\right) \left(\frac{300}{T_{air}}\right) \text{ GHz} \qquad (2\text{-}17)$$

Table 2-1

MICROWAVE LINE FREQUENCIES (IN GHz) OF O_2

ν_{1+}	=	56 264752	ν_{1-}	=	118 7507
ν_{3+}	=	58.446577	ν_{3-}	=	62.486256
ν_{5+}	=	59.590979	ν_{5-}	=	60 306055
ν_{7+}	=	60.434779	ν_{7-}	=	59.164205
ν_{9+}	=	61.150567	ν_{9-}	=	58.323885
ν_{11+}	=	61.800163	ν_{11-}	=	57.612505
ν_{13+}	=	62.411224	ν_{13-}	=	56.968245
ν_{15+}	=	62 997980	ν_{15-}	=	56.363448
ν_{17+}	=	63 568535	ν_{17-}	=	55 783884
ν_{19+}	=	64 1276	ν_{19-}	=	55 221449
ν_{21+}	=	64.6782	ν_{21-}	=	54.6716
ν_{23+}	=	65 223961	ν_{23-}	=	54.1309
ν_{25+}	=	65.7626	ν_{25-}	=	53.595951
ν_{27+}	=	66.2978	ν_{27-}	=	53.0695
ν_{29+}	=	66.8313	ν_{29-}	=	52.5458
ν_{31+}	=	67.3627	ν_{31-}	=	52.0259
ν_{33+}	=	67.8923	ν_{33-}	=	51.5091
ν_{35+}	=	68.4205	ν_{35-}	=	50.9949
ν_{37+}	=	68 9478	ν_{37-}	=	50.4830
ν_{39+}	=	69.4741	ν_{39-}	=	49.9730
ν_{41+}	=	70.0000	ν_{41-}	=	49.4648
ν_{43+}	=	70.5249	ν_{43-}	=	48 9582
ν_{45+}	=	71.0497	ν_{45-}	=	48.4530

2 2.2.2 Water Vapor Attenuation

Water vapor has absorption lines located at 22 33, 183 6 and 324 GHz, as well as a great number of lines in the submillimeter range The attenuation due to water vapor can be written as

$$\gamma_{H_2O} = \gamma_{H_2O(22)} + \gamma_{H_2O(183)} + \gamma_{H_2O(324)} + \gamma_{H_2O(>324)} \qquad (2\text{-}18)$$

All numerical coefficients which are given below are based upon experimental measurements.

For the 22 GHz line [2-4]

$$\gamma_{H_2O(22)} = 4.23\times10^{2} \frac{\nu^2}{T_{air}^{5/2}} \rho_{H_2O}\left[\frac{\Delta\nu}{(\nu-22.33)^2+(\Delta\nu)^2} + \frac{\Delta\nu}{(\nu+22\ 33^2+(\Delta\nu)^2}\right] \text{db/km} \qquad (2\text{-}19)$$

where

$$\Delta\nu = 6\left(\frac{P_{air}}{760}\right)\cdot\left(\frac{293}{T_{air}}\right) \qquad (2\text{-}20)$$

Here and in the following

ρ_{H_2O} = water vapor density in gm/m^3

T_{air} = air temperature in ^{o}K

P_{air} = air pressure in mm Hg

ν = radiometric frequency in GHz

For the 183 GHz line [2-5]

$$\gamma_{H_2O(183)} = 1.361\times10^{3} \frac{\nu^2}{T_{air}^{5/2}} \rho_{H_2O}\left[\frac{\nu^2}{(\nu-183.6)^2+(\Delta\nu)^2} + \frac{\Delta\nu}{(\nu+183.6)^2+(\Delta\nu)^2}\right] \text{db/km} \qquad (2\text{-}21)$$

where

$$\Delta\nu = 5.4\left(\frac{P_{air}}{760}\right)\left(\frac{293}{T_{air}}\right) \qquad (2\text{-}22)$$

There is less reliable information on the 324 GHz line. We will write

$$\gamma_{H_2O(324)} = 4\ 22\times10^{2}\ \frac{\nu^2}{T_{air}^{5/2}}\ \rho_{H_2O}\left[\frac{\Delta\nu}{(\nu-324)^2+(\Delta\nu)^2}+\frac{\Delta\nu}{(\nu+324)^2+(\Delta\nu)^2}\right] \text{db/km} \qquad (2\text{-}23)$$

and assume that

$$\Delta\nu = 6\left(\frac{P_{air}}{760}\right)\left(\frac{293}{T_{air}}\right) \qquad (2\text{-}24)$$

Finally, for frequencies below 300 GHz, the effect of all higher frequency lines can be combined and written as

$$\gamma_{H_2O}\,(>324) = 1\ 510\ \frac{\nu^2\ P_{air}}{T_{air}^{7/2}}\ \rho_{H_2O}\ \text{db/km} \qquad (2\text{-}25)$$

2.2.2.3 Absorption by Condensed Water

Clouds consist of minute droplets of water or ice If these droplets are assumed to be spherically shaped, the Mie theory of scattering is applicable. Since the particle sizes are so small compared to the wavelengths under consideration, the limiting form of the theory may be used In the limit of small particle sizes, it can be shown that, after averaging over-particle sizes, the absorption depends only on the mass of the water or ice. The result is [2-6]

$$\varkappa_{cloud} = \frac{6\pi\times10^{9}\ \nu}{c}\ \frac{M}{\rho}\ \mathrm{Im}\left[\frac{K-1}{K+2}\right] \qquad (2\text{-}26)$$

where

M = mass of droplets per unit volume
ρ = density of water (or ice)
K = dielectric constant of water (or ice)
c = speed of light (= 2.997925×10^{8} m/sec)
ν = radiometric frequency in GHz

and Im means "imaginary part" of the bracketed quantity.

Since the imaginary part of the dielectric constant of ice is small, it is found that ice particles contribute very little to the absorption coefficient unless they are near a melting condition in which case their surfaces may be wet. Consequently, attention will be confined to water droplets. Inserting numerical values for the constants, (2-26) becomes

$$\kappa_{cloud} = 6.2875342 \times 10^{-2} M\nu \, \mathrm{Im}\left[\frac{K-1}{K+2}\right] \tag{2-27}$$

where M is the density of the condensed water in gm/m^3 and ν the frequency in GHz.

The dielectric constant of water, which appears in (2-27), may be expressed by a formula of the Debye type·

$$K = \frac{\epsilon_o - \epsilon_\infty}{1 - i\frac{\nu\Delta\lambda}{c}} + \epsilon_\infty \tag{2-28}$$

where ϵ_o , ϵ_∞ , and the relaxation wavelength $\Delta\lambda$ are functions of the temperature. A number of investigations of these parameters have been made. Hasted [2-7] gives

$$\epsilon_o = 87.44 - .4008\,(T_w-273) + 9.398 \times 10^{-4}\,(T_w-273)^2 + 1\ 41 \times 10^{-6}(T_w-273)^3 \tag{2-29}$$

where T_w is the water temperature in ^oK. This may be assumed equal to the air temperature T_{air} at the height of the cloud There is less information about the temperature dependence of ϵ_∞ . The current evidence suggests that it is independent of temperature. We will take $\epsilon_\infty = 5.5$ When ν is expressed in GHz, $\frac{\Delta\lambda}{c}$ is given by

$$\frac{\Delta\lambda}{c} = \frac{10^{-4}}{3}\Big[-.555(T_w-263)(T_w-253)(T_w-243) + 1.19\,(T_w-273)\,(T_w-253)\,(T_w-243)$$

$$-.87\,(T_w-273)\,(T_w-263)\,(T_w-243) + .227\,(T_w-273)\,(T_w-263)\,(T_w-253)\Big] \tag{2-30}$$

2.3 DETERMINATION OF ATMOSPHERIC CORRECTIONS

The factors determining the atmospheric contribution to the total brightness temperature of a target have been discussed in the previous section In determining the correction to be applied in a given situation, there are essentially two methods of approach. The first consists in assuming that atmospheric conditions are sufficiently well known (e.g., from data supplied by a nearby Weather Bureau station or by direct meteorological measurements from the aircraft) that an a priori calculation of the atmospheric effects can be made. This will be called Option A. The second approach (Option B) assumes that the necessary parameters for an a priori calculation are not known (or known only partially) and thus requires that some measurements be performed before atmospheric corrections can be made. Option B, of course, is a more general procedure than Option A, but has the concomittant disadvantage of requiring some flight time to be set aside specifically for atmospheric measurements. In addition, precise calibration of the radiometers is mandatory if the direct measurement method is to succeed.

These two approaches are discussed in more detail below

2.3.1 COMPUTATION OF ATMOSPHERIC ATTENUATION AND EMISSION - OPTION A

If the air temperature, air pressure, atmospheric water vapor profile, and condensed water distribution in the atmosphere are known, the calculation of the three basic quantities $L(\theta, z)$, $T_{atm}(\theta, z)$, and T_{sky}, which were discussed in the theory, proceeds in a straightforward manner. The computer program or subroutine will require the following input data

A. Radiometric frequency or frequencies ν (in GHz).
B. Radiometer look angle (or angles) θ.
C. Aircraft altitude z_N (in kilometers). z_N should coincide with one of the z_i mentioned in D.
D. A description of atmospheric conditions in the form of a table This should consist of a sequence of altitudes z_i (in kilometers) $i = 1, \ldots, N$ at which the air temperature (^oK), air pressure (mm Hg), water vapor density (gm/m^3), and cloud water droplet content (gm/m^3) are specified.

The calculation proceeds in the following manner:

A At each z_i, and frequency ν of interest calculate γ_{O_2} according to equations (2-15) - (2-17) Change γ to κ_{O_2} according to (2-14).

B At each z_i, and frequency ν of interest calculate γ_{H_2O} according to equations (2-18) - (2-25). Change γ to κ_{H_2O} according to (2-14)

C At each z_i and frequency of interest calculate κ_{cloud} according to (2-27) - (2-30).

D. Calculate κ according to (2-13).

E. Evaluate the sequence of integrals (at each frequency ν).

$$f(z_i) = \int_0^{z_i} \kappa \, du \qquad i=1,\ldots N$$

by any standard numerical integration rule. The trapezoidal rule will yield adequate accuracy and provide an easy implemental scheme if $z_{i+1} - z_i \lesssim 1/3$ km.

F. For each angle θ and frequency ν calculate L, T_{atm}, and T_{sky} according to (2-10) - (2-12). If the trapezoidal rule is used in E above, $\bar{T}_{air}(z_i)$ may be taken simply as $\frac{1}{2}\left[T_{air}(z_{i+1}) + T_{air}(z_i)\right]$.

2.3.2 DIRECT MEASUREMENT OF ATMOSPHERIC EFFECTS OPTION B

If sufficient a priori information concerning atmospheric conditions is not available, then specific measurements for this purpose must be made. The basic set of quantities that need to be estimated for atmospheric corrections is $L(\theta, z)$, $T_{atm}(\theta, z)$ and T_{sky} as in Option A. It will be assumed that the angle θ is fixed in the following discussion (recall, also, that these quantities are frequency dependent, although the frequency dependence has been suppressed in the notation).

The required measurements consist of the following. Starting at a very low altitude (i.e., sufficiently low so that the atmosphere between the aircraft and ground does not contribute significantly to L, T_{atm}, or T_{sky} - typically this may be about 300 to 500 feet) and with

the radiometers pointed skyward, a measurement of the brightness temperature is made at each of the frequencies of interest. A measurement of the air temperature is also necessary. The aircraft then increases its altitude by an increment Δz and the measurements are repeated. This process is continued until the aircraft has reached an altitude at which the measured brightness temperature does not differ significantly from the cosmic background temperature or, if this is not feasible, to an altitude above which little water exists in the air (the contribution of the atmosphere above this altitude to the three basic quantities may be approximated with sufficient accuracy by the use of an a priori model).

The data which is so obtained may be analyzed in the following manner. At the lowest altitude, z_1, the brightness temperature is approximately the quantity T_{sky}. The loss factor $L(\theta, z_1)$ is approximately equal to 1 and $T_{atm}(\theta, z_1)$ is approximately equal to zero (see equations (2-2) and (2-3) in Section 2.2). These estimates may be used to determine $L(\theta, z)$ and $T_{atm}(\theta, z)$ inductively. Thus, suppose that at some altitude z_1, $L(\theta, z_1)$ and $T_{atm}(\theta, z_1)$ are known To determine $L(\theta, z_1+\Delta z)$ and $T_{atm}(\theta, z_1+\Delta z)$ we may write equation (2-2) as

$$T_{atm}(\theta, z_1+\Delta z) = \sec\theta \int_0^{z_1+\Delta z} T_{air}(z')\, K(z') \exp\left[-\sec\theta \int_{z'}^{z_1+\Delta z} K(u)du\right] dz'$$

$$= \sec\theta \left[\int_0^{z_1} + \int_{z_1}^{z_1+\Delta z}\right] \tag{2-31}$$

$$= e^{-\sec\theta \int_{z_1}^{z_1+\Delta z} K(u)du}\, T_{atm}(\theta, z_1)$$

$$+ \sec\theta \int_{z_1}^{z_1+\Delta z} T_{air}(z')\, K(z') \exp\left[-\sec\theta \int_{z}^{z_1+\Delta z} K du\right] dz' .$$

But, if the altitude increment Δz is not too large, then $T_{air}(z')$ may, under most circumstances, be well approximated by $\bar{T}_{air}(z_1) = \frac{1}{2}\left[T_{air}(z_1) + T_{air}(z_1 + \Delta z)\right]$ which will be a known quantity. Hence, we see that

$$T_{atm}(\theta, z_1 + \Delta z) = \frac{L(\theta, z_1 + \Delta z)}{L(\theta, z_1)} T_{atm}(\theta, z_1) + \bar{T}_{air}(z_1) \left[1 - \frac{L(\theta, z_1 + \Delta z)}{L(\theta, z_1)}\right]. \qquad (2\text{-}32)$$

At the same time, the difference in the measured brightness temperatures at altitudes z_1 and $z_1 + \Delta z$ is given by

$$T_b(\theta, z_1) - T_b(\theta, z_1 + \Delta z) = \sec\theta \int_{z_1}^{\infty} T_{air}(z') K(z') \exp -\left[\sec\theta \int_{z_1}^{z'} K du\right] dz'$$

$$+ \frac{L(\theta,\infty)}{L(\theta, z_1)} T_{CB} - T_b(\theta, z_1 + \Delta z)$$

$$= \sec\theta \left[\int_{z_1}^{z_1 + \Delta z} + \int_{z_1 + \Delta z}^{\infty}\right] + \frac{L(\theta,\infty)}{L(z_1)} T_{CB} - T_b(\theta, z_1 + \Delta z).$$

But

$$\sec\theta \int_{z_1}^{z_1 + \Delta z} T_{air} K \exp\left[-\sec\theta \int_{z_1}^{z'} K du\right] dz' \approx T_{air}(z_1) \left[1 - \frac{L(\theta, z_1 + \Delta z)}{L(\theta, z_1)}\right]$$

and

$$\sec\theta \int_{z_1 + \Delta z}^{\infty} T_{air} K \exp\left[-\sec\theta \int_{z_1}^{z'} K du\right] dz'$$

$$= e^{-\sec\theta \int_{z_1}^{z_1 + \Delta z} K du} \sec\theta \int_{z_1 + \Delta z}^{\infty} T_{air} K \exp\left[-\sec\theta \int_{z_1 + \Delta z}^{z'} K du\right] dz'$$

$$= \frac{L(\theta, z_1 + \Delta z)}{L(\theta, z_1)} \left[T_b(\theta, z_1 + \Delta z) - \frac{L(\theta,\infty)}{L(\theta, z_1 + \Delta z)} T_{CB}\right]$$

Therefore,

$$T_b(\theta, z_1) - T_b(\theta, z_1+\Delta z) = T_{air}(z_1) - T_b(\theta, z_1+\Delta z)\left[1 - \frac{L(\theta, z_1+\Delta z)}{L(\theta, z_1)}\right]$$

or

$$\frac{L(\theta, z_1+\Delta z)}{L(\theta, z_1)} = 1 - \frac{T_b(\theta, z_1) - T_b(\theta, z_1+\Delta z)}{T_{air}(z_1) - T_b(\theta, z_1+\Delta z)} \qquad (2\text{-}33)$$

Hence, (2-32) and (2-33) form a pair of equations which may be used recursively to determine $T_{atm}(\theta, z_1+\Delta z)$ and $L(\theta, z_1+\Delta z)$ from the measurements when use is made of the known values of these quantities at the altitude z_1

For this procedure to be useful, an accurate calibration of the radiometers is required since (2-32) and (2-33) contain references to measured brightness temperatures which can be expected to be small under most circumstances.

A second, more approximate, method of determining atmospheric corrections may be useful when it is known that the atmospheric conditions of radiometric frequencies are such that the attenuation coefficient K is so small that $\sec\theta \int_o^\infty K dz \ll 1$. In this case, $L(\theta, z) \approx 1$ and

$$\begin{aligned} T_{sky} &\approx \sec\theta \int_o^\infty K\, T_{air}\, dz + T_{CB} \\ T_{atm}(\theta, z) &\approx \sec\theta \int_o^z K\, T_{air}\, dz \qquad (2\text{-}34) \\ &= \sec\theta \left[\int_o^\infty - \int_o^\infty\right] \\ &= T_{sky} - T_{CB} - T_b(\theta, z) \end{aligned}$$

This approximation can be used with data obtained in clear, low humidity weather

Thus, only two measurements are required. The first, a measurement of T_{sky} near ground level, is analogous to the more precise method discussed above. However, the measurements of the air temperature and brightness temperatures at a number of intermediate altitudes are eliminated and replaced by a single upward looking measurement of the brightness temperature, $T_b(\theta, z)$ at the experiment altitude. As in the case of the more detailed procedure, the calibration of the radiometers must be sufficiently good so that a measurement of the brightness temperatures with the radiometers pointed skyward may be made more accurately than can be achieved with an a priori model.

REFERENCES

2-1 Van Vleck, J , "The Absorption of Microwaves by Oxygen," Phys Rev. 71, 413(1947)

2-2 Tolbert, C and Straiton, A., "Synopsis of Attenuation and Emission Investigations of 58 to 62 KMC Frequencies in the Earth's Atmosphere," Proc. IEEE 51, 1754 (1963)

2-3. Tolbert, C., Krause, L., and Straiton, A., "Attenuation of the Earth's Atmosphere Between the Frequencies of 100 and 140 Gigacycles per Second," J. Geophys Rec 69, 1349 (1964)

2-4. Tolbert, C., Straiton, A., and Britt, C., "Propagation Studies Between 18.0 and 25 5 KMC," EERL Report No. 110, Univ. of Texas (1959)

2-5. Coats, G., Bond, R., and Tolbert, C., "Propagation Measurements in the Vicinity of the 183 GC/S Water Vapor Line," EERL Report No. 7-20, Univ. of Texas (1962)

2-6. Gunn, K. and East, T., "The Microwave Properties of Precipitation Particles," Quart. J. Roy. Meteorol Soc., London, XXX, 522 (1954)

2-7 Hasted, J., "The Dielectric Properties of Water" Progress in Dielectrics, vol 3 J. Birks and J. Hart, Eds., New York, Wiley (1961)

Section 3

ANTENNA PATTERN STUDY

This section of the report documents equations and procedures developed to correct MFMR data for antenna pattern effects.

3.1 GENERAL CONSIDERATIONS

An antenna detects energy propagating not only along its boresight axis but also from other directions in space. The energy which is detected or, equivalently, the antenna temperature T_A may be expressed as

$$T_A(\theta_o, \varphi_o) = \int G(\theta_o, \varphi_o, \theta, \varphi) T_r(\theta, \varphi) d\Omega \qquad (3\text{-}1)$$

where the angles (θ_o, φ_o) specify the direction of the antenna boresight axis with respect to some reference coordinate system, $T_r(\theta, \varphi)$ is the temperature of the radiation propagating along the ray specified by the angles (θ, φ), $d\Omega$ is a differential solid angle about (θ, φ), and G is the antenna gain function. The gain function, which essentially describes the effectiveness of the antenna in detecting radiation propagating in directions other than the boresight direction, may be normalized by requiring that

$$\int G(\theta_o, \varphi_o; \theta, \varphi) d\Omega = 1 \qquad (3\text{-}2)$$

Since the cone of angles which contribute significantly to the antenna temperature will, in general, intersect the ground in an area which contains several different terrestrial features, it is clear that the antenna temperature will be a weighted average of many distinct ray temperatures. However, in the quantitative interpretation of

radiometric signals in terms of their relation to geophysical phenomena, it is the ray temperatures belonging to the distinct features which are desired instead of a weighted average. Thus, the problem of solving the integral equation (3-1) for the ray temperatures when the antenna temperature is known arises.

There are some practical difficulties which severely limit any program designed to solve (3-1). First, there is the problem of measuring the antenna temperature at a sufficient number of points. Temperatures over a two-dimensional set are required (i.e., both along the aircraft flight path and perpendicular to the flight path). Since the antennas on the P3V are not scanned perpendicular to the flight path, the information which will be obtained will be confined to a narrow strip, which is essentially one dimensional. This is not adequate to solve (3-1) on the basis of microwave data alone. The situation can be improved somewhat by making several passes over the target area with the flight path displaced slightly on each pass. Another procedure for circumventing the lack of two-dimensional information is to make an a priori estimate of the temperature connected with features outside of the strip over which data is gathered. This may be done, for example, by an interpreter using optical data.

A second problem that arises in connection with solving (3-1) and which is, perhaps, even more fundamental than the first is that of numerical instability. This problem will occur even if antenna temperatures are specified over a two-dimensional surface and will limit the degree to which the antenna beam may be "split" in any analytical scheme. The situation is as follows. In solving (3-1) numerically, the integral will be approximated by a finite sum of terms (obtained by the application of some numerical quadrature scheme) and the resultant system of linear equations with specified lefthand sides will be solved It will be found that if an attempt is made to resolve too many features by approximating the integral by a sum consisting of a large number of terms that a small change in the input data (i.e., antenna temperature) will produce a large change in the computed ray temperatures. Thus, the extraction of meaningful ray temperatures becomes impossible.

The reasons for such behavior are common for all Fredholm integral equations of the first kind, of which (3-1) is an example in two dimensions. For simplicity in exposition, however, the problem will be discussed in one dimension in the following. Thus, we consider an equation of the form

$$T(x) = \int_a^b G(x, y)\ T_r(y)dy \tag{3-3}$$

The limits of integration, a and b, are fixed. Suppose that the result $T(x)$ is obtained with a given $T_r(y)$. Now, let us examine the effect of modifying $T_r(y)$ by the addition of a term of the form A sin ny where A is a constant and n is a parameter. Then $T(x)$ is changed by a term of the form

$$A\int_a^b G(x, y)\ \sin ny\ dy \tag{3-4}$$

However, in the limit where $n \to \infty$, the integral in (3-4) approaches zero. This result follows rigorously from the Riemann Lebesgue lemma with certain mild restrictions on the class of functions from which G is taken (this class certainly includes functions which represent real antenna gain functions). Intuitively, the result is expected because the rapid oscillation of the term sin ny in the integrand will lead to cancellation between nearly equal positive and negative parts of the integral Thus, we see that even if A is a large constant (i.e , there is a large change in $T_r(y)$ that the function $T(x)$ is essentially unchanged when n is large. Conversely, we see that a small change in $T(x)$ (say, due to errors in measurement of the antenna temperature) may be ascribed to large changes in the ray temperature.

The argument presented above is not quite as artificial as it may seem at first sight in connection with ray temperature variations that will actually occur. It is only necessary to realize that the true temperature variation can be Fourier analyzed. Thus, we see that in the presence of small errors in measurement no information can be obtained about the high spatial frequency components of the ray

temperature. In fact, a numerical analysis using measured data can be expected to yield spurious, large high frequency components which will completely obscure the true nature of T_r. Numerical experiments have indeed demonstrated that this phenomenon occurs and, unfortunately, is a serious problem even when only a small amount of "beam splitting" is attempted. Naturally, the problem manifests itself more severely as the error in the measured data is increased.

In view of the above remarks, it is clear that stringent measures must be taken if meaningful antenna pattern corrections are to be made. This may be done by imposing certain smoothness requirements on the computed ray temperatures. Such a procedure can be used quite successfully if sufficient a priori information concerning the target characteristics is available. Unfortunately, this type of information cannot be expected to be available in general. Thus, another approach must be taken. Probably the simplest technique which can be used is to write (3-1) as

$$T_A(\theta_o, \varphi_o) = \int_M GT_r \, d\Omega + \int_S GT_r \, d\Omega \tag{3-5}$$

where M is the main lobe of the antenna and S includes all of the sidelobes. A detailed description of the ray temperatures is not attempted. Instead, we attempt simply to obtain the average ray temperature in the main lobe. The contributions of the sidelobes to the antenna temperature may be estimated by a procedure which is discussed in the next section.

3.2 DESCRIPTION OF CORRECTION TECHNIQUE

The basic idea behind any sidelobe correction scheme is to determine the value of the first integral in the expression

$$T_A = \int_M T(\theta, \phi)G(\theta, \phi)d\Omega + \int_S T(\theta, \phi)G(\theta, \phi)d\Omega \tag{3-6}$$

where T_A is the observed antenna temperature, M represents the solid angle subtended by the main lobe, S represents the solid angle subtended by the sidelobes, $T(\theta, \phi)$ is the brightness temperature at the surface in the direction (θ, ϕ) and $G(\theta, \phi)$ is the gain of the antenna in the direction (θ, ϕ).

To solve the equation we must know $G(\theta, \phi)$ for each point in S and also $T(\theta, \phi)$ for each point in S where $G(\theta, \phi)$ is significant. In other words, we need to know the intensity of all significant sidelobes, and what these sidelobes were looking at

The values of $G(\theta, \phi)$ for the MFMR antennas were determined by comparison with a gain standard

Determination of $T(\theta, \phi)$ for (θ, ϕ) in S can be rather difficult, because the ground is scanned along a single line. Thus, on the basis of radiometric data, some correction may be made for the sidelobes observing the region immediately ahead and behind the main lobe. However, it is unlikely that merely having data on what the sidelobes were seeing fore and aft of the main beam will be sufficient to provide an acceptable correction. For most types of terrain, information will be needed on the terrain on all sides of the main lobe It is expected that temperature values accurate enough for this purpose can be estimated using the optical photography obtained at the same time as the microwave measurements.

Using the uncorrected microwave data and the photography, one would estimate the temperatures seen by the sidelobes within a specified angle of the ground track of the main lobe. This would be done for whatever portion of the ground track that sidelobe-corrected data was required The estimates would then be entered onto punch cards or other computer-input media, and would be read into the computer along with the uncorrected microwave data.

The computer would then calculate the integral

$$\int_S T(\theta, \phi) G(\theta, \phi) d\Omega \tag{3-7}$$

for each point on the ground track, and subtract this value from the observed antenna temperature. The result would be the true main lobe temperature

$$\int_M T(\theta, \phi) G(\theta, \phi) d\Omega \ . \tag{3-8}$$

If these values differed excessively from the estimates used initially for a given type of terrain, a better set of estimates could be formulated and the procedure repeated. It is expected that after sufficient experience in preparing such estimates, the second iteration would not be required.

3.3 CORRECTION PROGRAMMING PROCEDURE

The available information on the MFMR antennas indicates a main beam efficiency of around 95% for the L-band (1.420 GHz) antenna, and around 90% for the higher frequency antennas. Either of these values is sufficiently below 100% to require a sidelobe correction procedure if the desired $1^{o}K$ to $2^{o}K$ absolute accuracy is to be achieved.

It should be noted that all of the efficiency measurements were made by antenna range techniques, i.e., by using a distant transmitter and receiving through the antenna under test. When this is done, the receiver is normally adjusted so as not to saturate on the peak main lobe signal. This means that sidelobe responses below about -40 dB will not be detected, and so will not contribute to the sidelobe portion of the main lobe efficiency calculation. This would result in the main lobe efficiency being measured higher than it actually is This effect would be significant only if a substantial part of the far-out sidelobe pattern were above -30 dB. This is unlikely, but all flight data should be examined for any suggestion of such effects.

The available patterns seem to be adequate for determining the total power in the sidelobes. This is the case for the TRG antennas, because beam efficiency measurements made by TRG by use of ordinary measured patterns and symmetry assumptions agree fairly well with Aerojet measurements which were made by integrating the entire solid pattern with a pattern integrator. The 1 GHz antenna efficiency was determined by the pattern integrator method.

3.3.1 COMPUTER PROGRAM OUTLINE

a. The computer must be programmed to accept an approximation of the microwave temperature of a strip of terrain centered on the ground track of the antenna beams and having a width equal to several times the aircraft altitude. Presumably, the ground track will either be straight or will curve sufficiently slow so that all points in the area of interest can be specified by a Cartesian coordinate system with, for example, x representing distance perpendicular to the ground track and y representing distance along the ground track measured from an arbitrary reference - say, the beginning of the run Expressions for relating antenna beam position with ground position are derived in Section 3 4.

b. The microwave temperature values for each point (x, y) would come from estimates prepared by someone familiar with the radiometers (and preferably familiar with the terrain) and having access to the uncorrected microwave data, as well as photographs, maps, etc.

c. Since the antenna beams will, by definition, be tracking down the center of the specified terrain swath, the incidence angle will vary only with x, and then in a known manner. Therefore, the effects of varying incidence angle can be accounted for by specifying appropriately lower temperatures at larger values of x.

d. Significant portions of the sidelobe pattern will often point off the specified terrain region or even into the sky. For this reason it is necessary to specify "default options" giving an approximation to the terrain temperature at shallow incidence angles in various directions from the aircraft. The required number of different temperature versus incidence angle "curves" will depend on how variable the terrain is, but will probably not exceed 4 or 5 for any given run. Also, the sky temperature will have to be specified as a function of incidence angle, and as a function of direction from the aircraft, when the sky conditions vary considerably with azimuth. The distance-terrain curves and the sky curves will vary from flight to flight, but can be selected (by the user) from a "catalog" of curves stored in the computer.

e. In addition to specifying the radiometric nature of the terrain and sky it is also necessary to specify the time at which the antenna beams encounter a prescribed point on the Y-axis. This is done by specifying the time of encountering a small number of the points, and specifying the average ground speed between each pair of points. Also, the sidelobe pattern of each of the antennas must be specified and the incidence angle of the antenna beams fed into the computer.

f. It will be most convenient to specify the sidelobe pattern in polar coordinates, centered on the main beam. Then the θ coordinate will be "degrees off boresight" and the ϕ coordinate will be degrees circumferentially from some reference. When the antenna assembly is rotated to change polarization it is then only necessary to add 90° to each ϕ coordinate. The existing antenna patterns indicate that the cross-polarized response of all the antennas is negligible in the main lobe, and the aggregate response in the sidelobes can probably be accounted for with acceptable accuracy as a "bias" in the conventional (i.e., non-cross-polarized) sidelobe pattern.

g. The parameter that would be used in specifying the sidelobe pattern is the fractional contribution to the total power received due to the given (θ, ϕ) "bin." This depends on both the gain

at (θ, ϕ) and the values of θ and ϕ. The latter is necessary because the bin size, in steradians, varies with θ and ϕ while the gain is usually specified per steradian. However, it is only necessary to read in the usual gain pattern. The computer should be programmed to account for the size of each (θ, ϕ) bin. Also, since it is necessary to read the antenna pattern into the computer only once for each antenna, it is reasonable to use punch cards or something similar as the input medium for this purpose Once the computer has the terrain information, the timing information, the incidence angle, the antenna pattern, and the microwave data available, the correction proceeds automatically as outlined in steps h through k and in the flow diagram, Figures 3-1 to 3-5. The flow diagram steps may be followed exactly to generate the antenna pattern effects program.

h. The computer considers each point in the antenna pattern, for example, starting with θ_{min} (just outside the main lobe) and incrementing ϕ through 360^{o}, then going to the next θ "ring" and again incrementing ϕ through 360^{o}, and so on until θ_{max} is reached.

i. For each (θ, ϕ) point where the gain is significant (say above -50 dB) the program determines where within the (x, y) terrain grid the (θ, ϕ) direction intercepts the ground, or else which one of the default-option terrain or sky temperature curves should be used. The program then could either use the temperature at that point (or nearest to that point) or, to obtain greater accuracy, the computer could determine the average temperature within the region of the ground intercepted by the boundary of the (θ, ϕ) bin In either case, the temperature, multiplied by the fractional contribution of the given (θ, ϕ) bin, yields the contribution to the observed temperature due to that bin. The computer adds the contributions from all the bins where the gain is significant, thus obtaining the total sidelobe contribution

j. This total sidelobe contribution is then subtracted from the observed microwave temperature, and the result multiplied by the reciprocal of the fractional contribution of the main lobe to the total received power. The result is then the temperature seen by the main

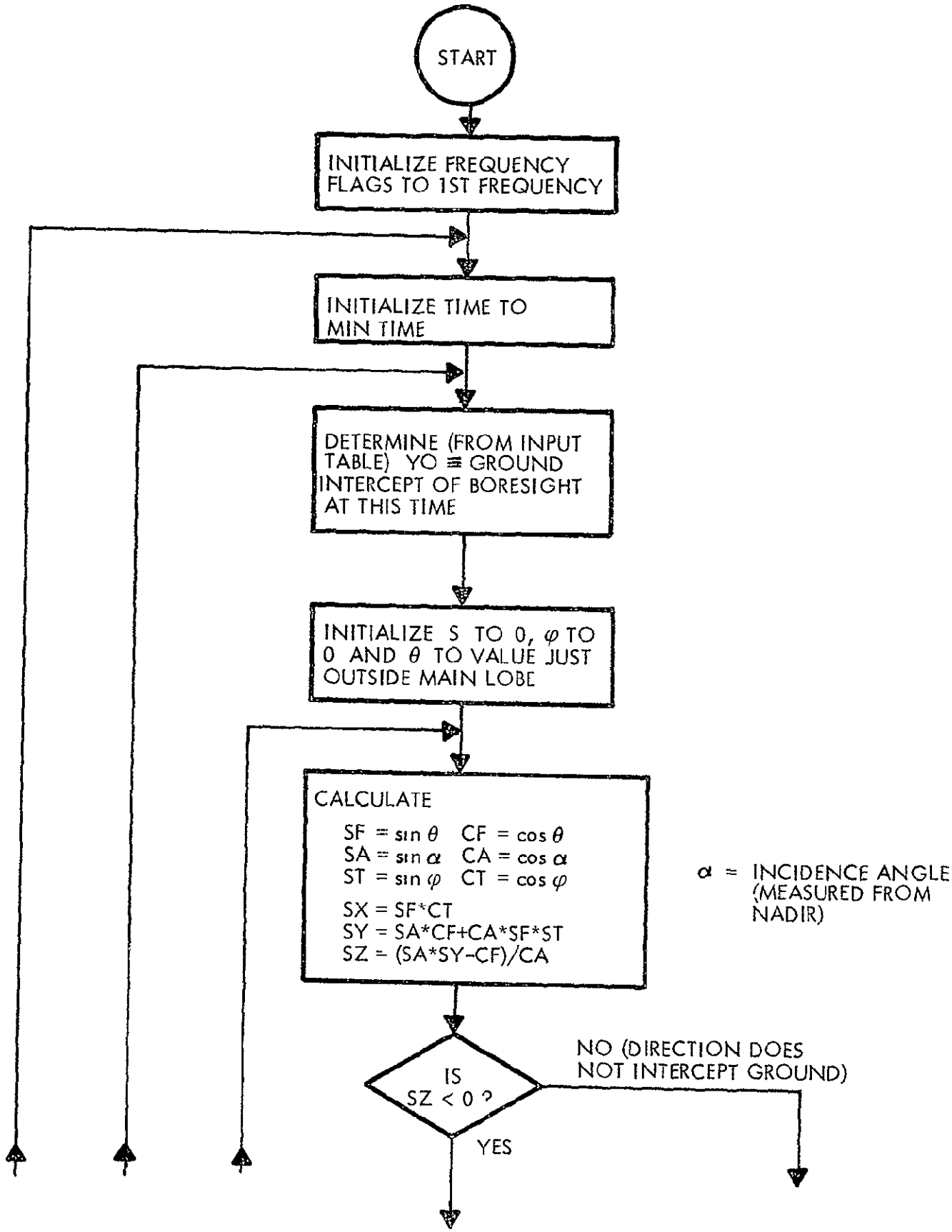

FIGURE 3-1 ANTENNA PATTERN CORRECTION FLOW DIAGRAM

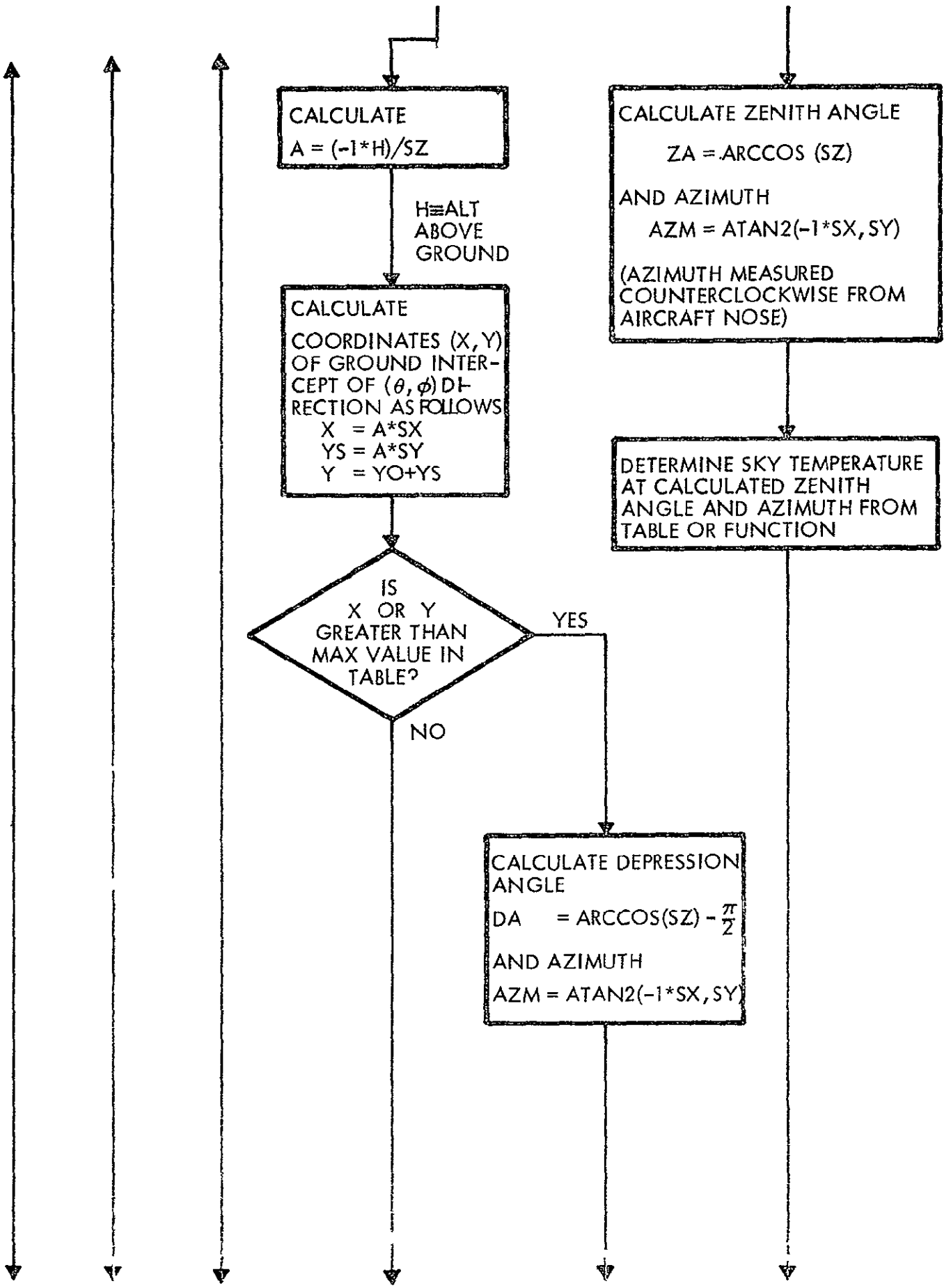

FIGURE 3-2 ANTENNA PATTERN CORRECTION FLOW DIAGRAM

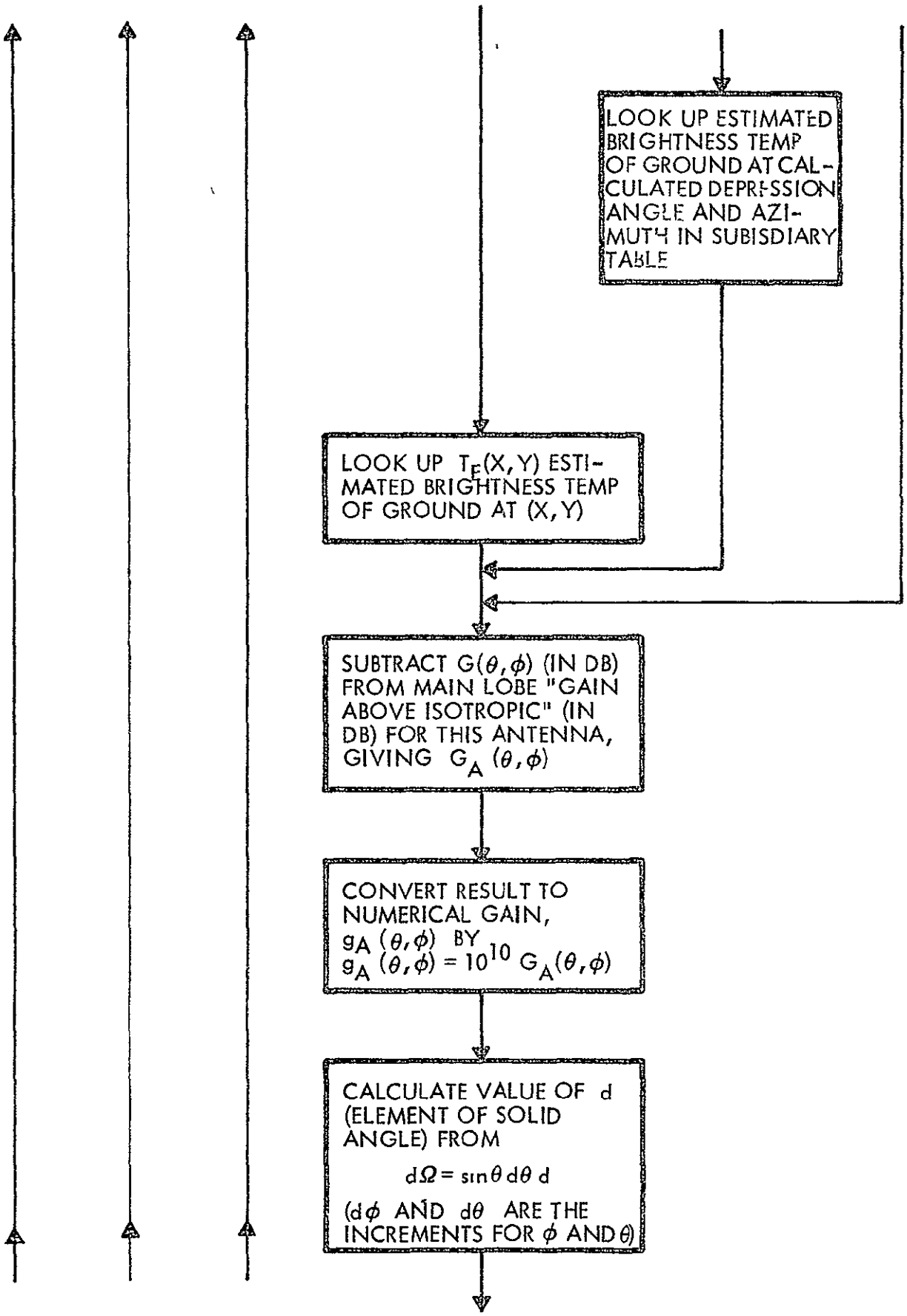

FIGURE 3-3 ANTENNA PATTERN CORRECTION FLOW DIAGRAM

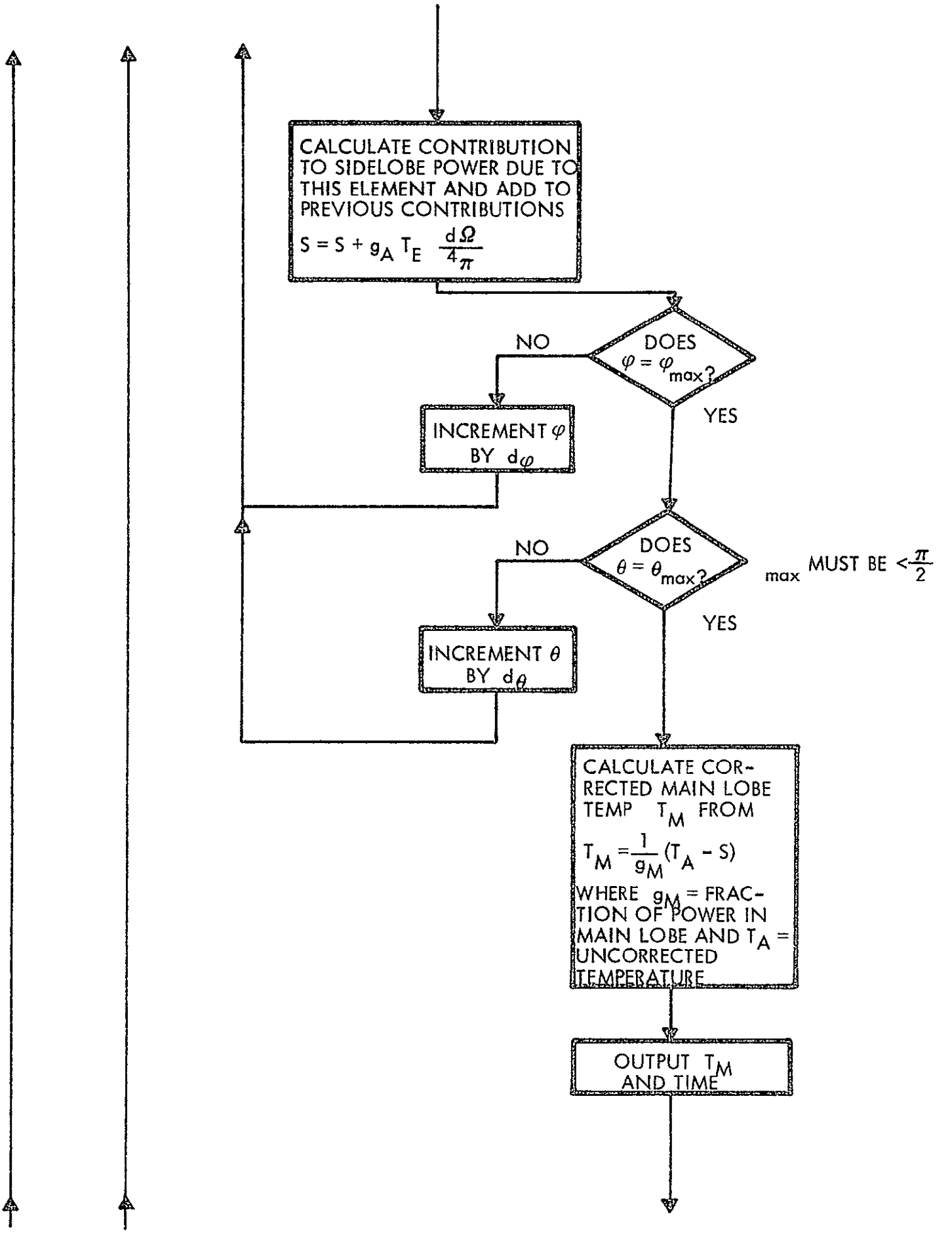

FIGURE 3-4. ANTENNA PATTERN CORRECTION FLOW DIAGRAM

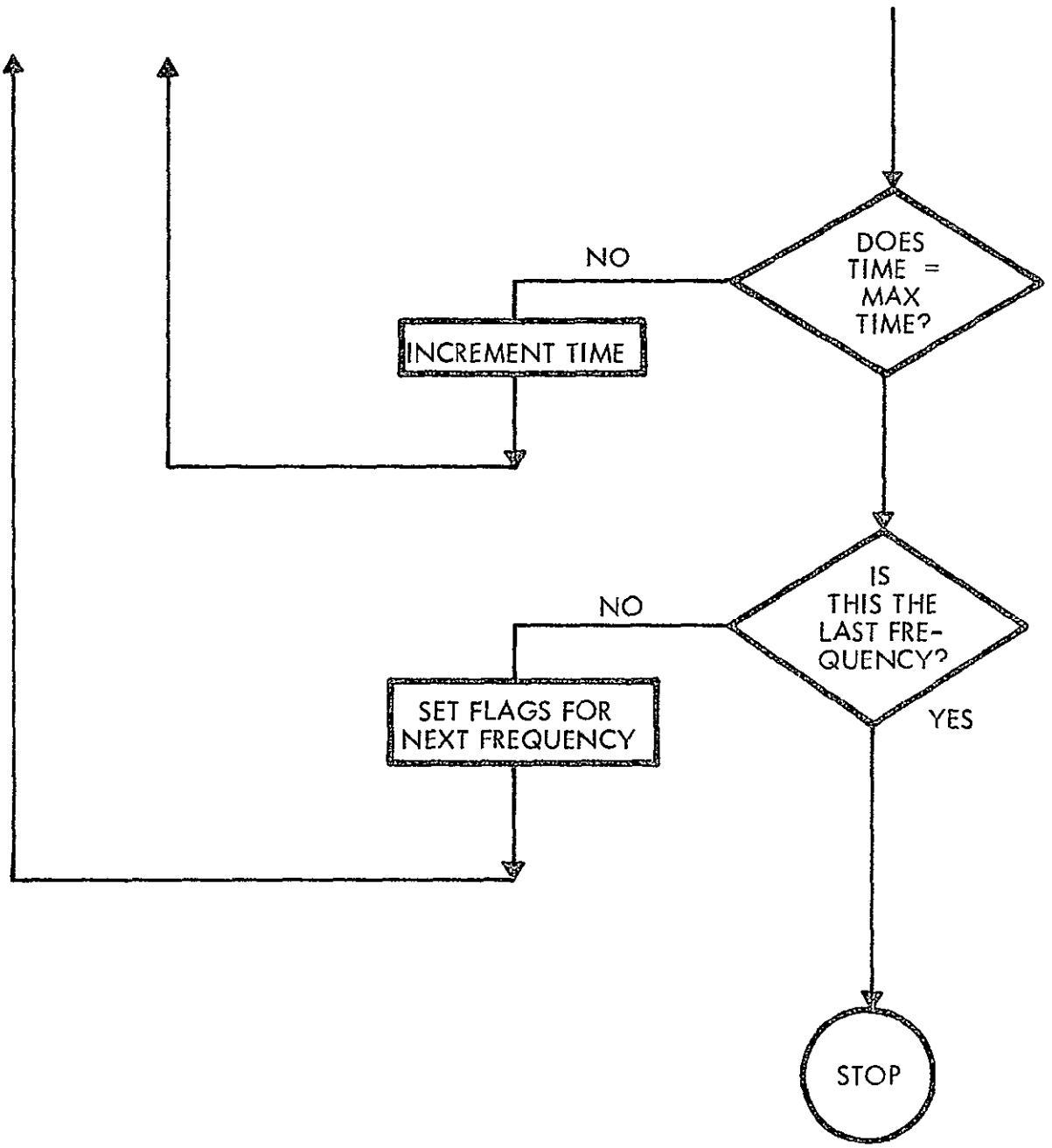

FIGURE 3-5. ANTENNA PATTERN CORRECTION FLOW DIAGRAM

lobe alone.

k. This can be expressed mathematically as follows. The temperature T_A observed at the antenna port is given by

$$T_A = T_M G_M + T_1 G_1 + T_2 G_2 + \ldots \tag{3-9}$$

Where T_M is the temperature seen by the main lobe, T_1 is the temperature seen by bin 1 of the sidelobe pattern, T_2 is the temperature seen by bin 2, and so on. G_M is the fractional contribution to the total received power provided by the main lobe, G_1 is the fractional contribution provided by bin 1, G_2 is the fractional contribution provided by bin 2, and so on. Solving for T_M we get

$$T_M = \frac{1}{G_M} T_A - (T_1 G_1 + T_2 G_2 + \ldots) \tag{3-10}$$

The above procedure solves this equation exactly and will thus give the correct value of T_M, provided the specified terrain and sky temperatures are correct. If, after running the program, it is found that the corrected main lobe temperatures for various terrain types fail to match the estimates used in the sidelobe correction procedure, then the newly-obtained information can be used to re-specify the terrain temperature and the program can be re-run. This procedure can be repeated as many times as necessary until the values converge. Presumably, after some familiarization with the radiometers and the terrain, only one or two runs will be required.

3.4 DERIVATION OF ANTENNA BEAM POSITION EXPRESSIONS

The problem is to find the coordinates (x, y) on the ground representing the intercept of the direction (θ, ϕ), where the (θ, ϕ) coordinate system has its origin at $(0, y_o, h)$ and its polar axis coincident with the boresight axis (i.e., in the YZ plane and elevated by an angle α from nadir toward the +Y direction).

Let $\vec{u}_x$, $\vec{u}_y$, and $\vec{u}_z$ be unit vectors directed along the positive X, Y and Z axes, respectively. See Figure 3-6

Let $\vec{s}_o$ be a unit vector directed away from the aircraft along the boresight axis.

Then

$$\vec{s}_o = \sin \alpha \vec{u}_y - \cos \alpha \vec{u}_z \tag{3-11}$$

Let $\vec{s}$ be a unit vector pointing from the aircraft toward the point (x, y, o) on the ground.

Let $\vec{s} = s_x \vec{u}_x + s_y \vec{u}_y + s_z \vec{u}_z$

(Note $s_x^2 + s_y^2 + s_z^2 = 1$)

Then, from the definition of dot products

$$\vec{s} \cdot \vec{s}_o = \cos \theta = \sin \alpha s_y - \cos \alpha s_z \tag{3-12}$$

Now, from the definition of cross products, the vector $\vec{s} \times \vec{s}_o$ is perpendicular to the plane defined by $\vec{s}$ and $\vec{s}_o$. Also, $\vec{s}_o \times (\vec{s} \times \vec{s}_o)$ is perpendicular to both $\vec{s}_o$ and $\vec{s} \times \vec{s}_o$. Therefore, $\vec{s}_o \times (\vec{s} \times \vec{s}_o)$ is in the plane defined by $\vec{s}$ and $\vec{s}_o$, and is also perpendicular to the boresight axis.

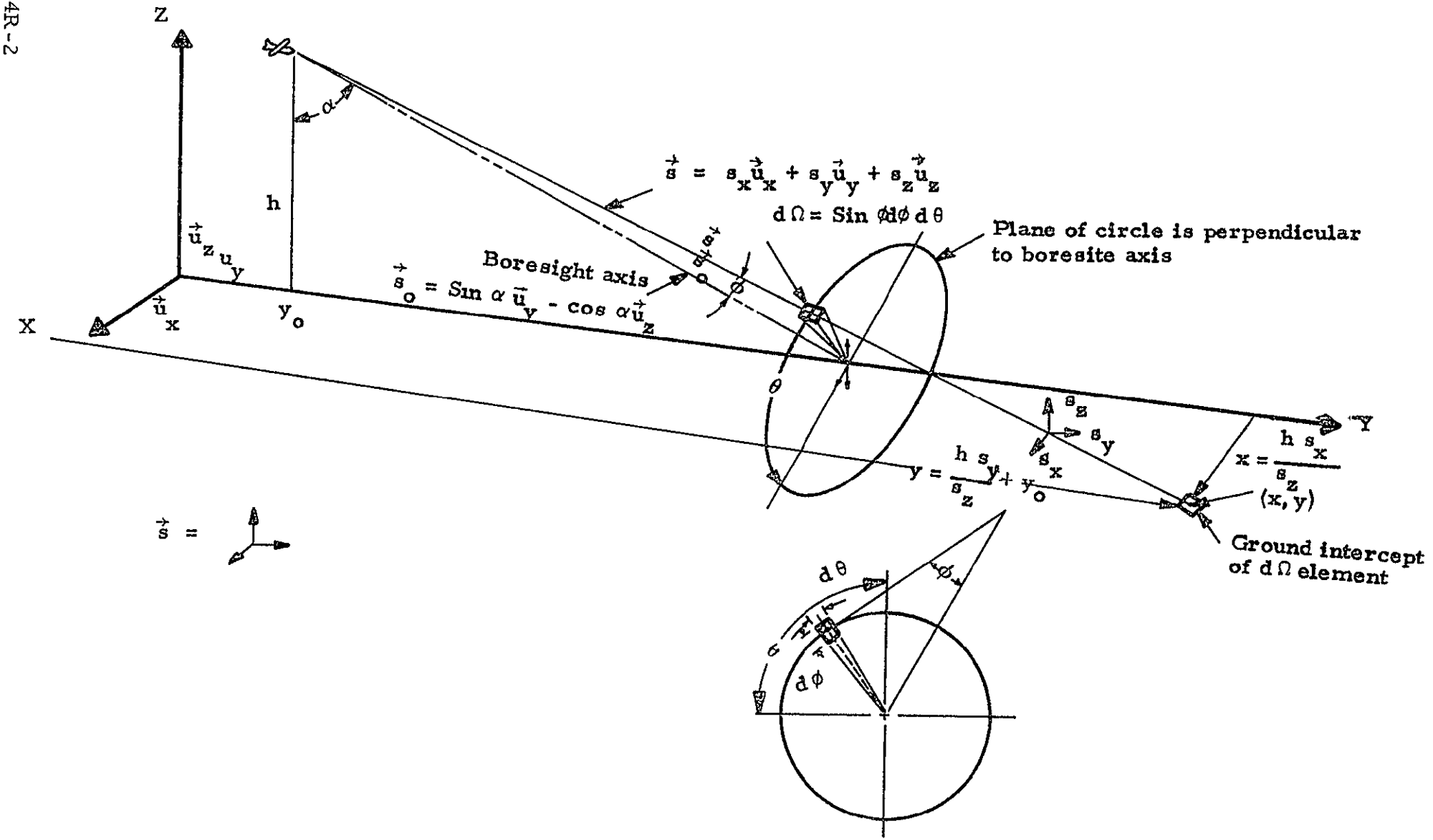

FIGURE 3-6. ANTENNA BEAM POSITION GEOMETRY

From vector theorems·

$$\vec{s}_o x(\vec{s} x \vec{s}_o) = (\vec{s}_o \cdot \vec{s}_o)\vec{s} - (\vec{s} \cdot \vec{s}_o)\vec{s}_o = \vec{s} - \cos\theta \vec{s}_o \tag{3-13}$$

Therefore, the unit vector in the $\vec{s}_o \times (\vec{s} \times \vec{s}_o)$ direction is·

$$\frac{\vec{s} - \cos\theta \vec{s}_o}{\left|\vec{s} - \cos\theta \vec{s}_o\right|}$$

Now,

$$\vec{s} - \cos\theta \vec{s}_o = \sqrt{(\vec{s} - \cos\theta \vec{s}_o)\cdot(\vec{s} - \cos\theta \vec{s}_o)} \tag{3-14}$$

$$= \sqrt{\vec{s}\cdot\vec{s} - 2\cos\theta \vec{s}\cdot\vec{s}_o + \cos^2\theta \vec{s}_o \cdot \vec{s}_o}$$

$$= \sqrt{1 - \cos^2\theta}$$

$$= \sin\theta$$

Also,

$$\cos\phi = \vec{u}_x \cdot \frac{\vec{s} - \cos\theta \vec{s}_o}{\left|\vec{s} - \cos\theta \vec{s}_o\right|} \tag{3-15}$$

$$= \frac{\vec{u}_x \cdot \vec{s}}{\sin\theta}$$

$$= \frac{s_x}{\sin\theta}$$

Thus

$$s_x = \sin\theta \cos\phi \tag{3-16}$$

Now applying the fact that $s_x^2 + s_y^2 + s_z^2 = 1$ to equation (3-11) we get:

$$\cos\theta = \sin\alpha\, s_y - \cos\alpha \sqrt{1 - s_x^2 - s_y^2} \tag{3-17}$$

From which·

$$\cos\theta - \sin\alpha\, s_y = -\cos\alpha \sqrt{1 - s_x^2 - s_y^2}$$

Squaring both sides

$$\cos^2\theta - 2\sin\alpha\cos\theta\, s_y + \sin^2\alpha\, s_y^2 = \cos^2\alpha - \cos^2\alpha\, s_x^2 - \cos^2\alpha\, s_y^2$$

$$\cos^2\theta + s_y^2(\sin^2\alpha + \cos^2\alpha) - 2\sin\alpha\cos\theta\, s_y - \cos^2\alpha(1-s_x^2) = 0.$$

But

$$\sin^2\alpha + \cos^2\alpha = 1.$$

Thus,

$$s_y^2 - 2\sin\alpha\cos\theta\, s_y + \cos^2\theta - \cos^2\alpha\,(1-s_x^2) = 0. \tag{3-18}$$

Solving the quadratic in s_y^2.

$$s_y = \frac{1}{2}\left[2\sin\alpha\cos\theta \pm 2\sqrt{\sin^2\alpha\cos^2\theta + \cos^2\alpha(1-s_x^2) - \cos^2\theta}\right]$$

Now by trigonometric identies

$$\sin^2 \alpha \cos^2 \theta - \cos^2 \theta = (1-\cos^2 \alpha)\cos^2 \theta - \cos^2 \theta$$

$$= -\cos^2 \alpha \cos^2 \phi$$

Therefore

$$s_y = \sin \alpha \cos \theta \pm \sqrt{-\cos^2 \alpha \cos^2 \theta + \cos^2 \alpha(1-s_x^2)}$$

Taking $\cos^2 \alpha$ outside the radical and using the $s_x^2 = \sin^2 \theta \cos^2 \phi$ we get

$$s_y = \sin \alpha \cos \theta \pm \cos \alpha \sqrt{-\cos^2 \theta + 1 - \sin^2 \theta \cos^2 \phi}$$

$$= \sin \alpha \cos \theta \pm \cos \alpha \sin \theta \sin \phi$$

By continuity and by considering the situation near $\phi = \pi/2$, we see that the + sign should be used. (This assumes that ϕ runs from 0 to 2π). Thus:

$$s_y = \sin \alpha \cos \theta + \cos \alpha \sin \theta \sin \phi \qquad (3\text{-}19)$$

and solving equation (3-11) for s_z we get

$$s_z = \frac{\sin \alpha \, s_y - \cos \theta}{\cos \alpha} \qquad (3\text{-}20)$$

The vector $\vec{s}$ is now completely determined in terms of θ, ϕ, and α.

Now consider the line through the aircraft and the point (x, y, o), i.e., the point where the (θ, ϕ) direction intercepts the ground. This line is defined by the locus of points given by the vector $y_o\vec{u}_y + h\vec{u}_z + \lambda\vec{s}$ where λ is a parameter. Now the point on this line corresponding to (x, y, o) is the point for which the vector has zero z-component, i.e., when $\lambda = -(h/s_z)$.

Now, the x and y components of $y_o\vec{u}_y + h\vec{u}_z + \lambda\vec{s}$ are simply λs_x and λs_y, respectively. Therefore, substituting $-(h/s_z)$ for λ we get the x and y coordinates of the desired point (x, y, o), namely

$$x = \frac{hs_x}{s_z} \tag{3-21}$$

$$y = \frac{hs_y}{s_z} + y_o \tag{3-22}$$

The criterion for the (θ, ϕ) direction intercepting the ground is obviously $s_z < 0$. If this is not met, or if the x or y coordinates are beyond the area for which temperatures have been predicted, then we can use either zenith angle and aximuth to find the sky temperature in the (θ, ϕ) direction or depression angle and azimuth as a guide to finding the brightness temperature of the ground

The zenith angle is simply the angle between $\vec{s}$ and the + z-axis, which is $\cos^{-1} s_z$. The depression angle is $\pi/2$ less than the zenith angle, namely, $(\cos^{-1} s_z) - \pi/2$ and the azimuth is $\tan^{-1}(-s_y/s_x)$ measured counterclockwise from the Y-axis, (i.e., counterclockwise from the direction of the nose of the aircraft).

It should be noted that the FORTRAN function ATAN2 (or equivalent) should be used to calculate $\tan^{-1}(-s_y/s_x)$ to insure that the angle is in the correct quadrant.

EXPERIMENTAL VERIFICATION OF CORRECTION ROUTINES

4.1 GENERAL

This section documents experimental tests developed to verify the adequacy of atmospheric and antenna pattern correction routines outlined in Sections 2 and 3 of this report. These experiments included bench and in-flight calibration of the MFMR system, along with airborne measurements to evaluate the correction equations.

MFMR missions were flown on 13 and 16 February 1970 in an attempt to verify the correction routines. These flights were over the Gulf of Mexico and the Houston area Cold and hot load calibration data acquired during late January 1970 and late February 1970 were utilized in conjunction with mission data. Experimental data taken to substantiate the atmospheric correction routines show that gross inconsistencies exist in the MFMR data. Unrealistic brightness temperature values were obtained using the antenna and radome loss values furnished for this study Significant improvement was achieved by using an empirically determined loss factor. However, quantitative results could not be obtained due to the sensitivity of measurement data to the empirically determined loss factor This uncertainty, discussed in detail in Section 4.2, must be resolved before the reported atmospheric and antenna pattern routines can be substantiated.

4.2 EXPERIMENTAL VERIFICATION OF ATMOSPHERIC CORRECTION ROUTINE

4.2.1 MISSION PLAN

An experimental mission was configured to test the validity of atmospheric correction routines developed in Section 2 The mission was approved by cognizant NASA/MSC personnel and is outlined below.

ATMOSPHERIC MISSION PLAN

A. Flight Conditions

1) Flight should be over ocean, prefereably having constant sea state characteristics. A cloudless day with calm seas is preferred.

2) Flights should be level and repeated passes made over the same flight line, in the same direction for stated angle scans.

3) Flight line one (1) consists of repeated passes as shown on Table 1. Total passes = 40.

4) Radiometers pointing downward (0^{o}) except for part of low level run and part of high level run. See Table 4-1.

5) Record vertical polarization only.

6) Record output during 500 ft elevation and ~ 20,000 ft elevation pass when swinging from vertically downward (0^{o}) to ~ vertically upward (150^{o}) in 10^{o} steps. Record for 30 seconds at each 10^{o} increment.

7) Record baseline and cal "1" before and after each flight run. (10 secs each.) Note The cal "after" a given run becomes the cal "before" the next run, etc.

8) Boresight camera imagery is required during each data run.

9) Repeat all steps in a descending flight

10) Estimated total flight time, both ascending and descending - 80 to 100 minutes.

11) Low level pass, 500 ft, high level pass, 20,000 ft; steps (ascending), approximately 1100 ft, steps (descending), approximately 3,000 ft.

12) Elevation control should be by radar and not barometric pressure.

13) Integration times should be 1.0 sec for 10.625 GHz radiometer (X-Band) and 0.1 sec for the other radiometers.

Table 4-1

ATMOSPHERIC MISSION PLAN (FLIGHT LINE 1)

Table 4-1

ATMOSPHERIC MISSION PLAN (Flight Line 1)

Run No	Flight Line Pass	Absolute Flight Altitude***	Record Time	Sensors*	Laser Profilometer	Meteorological Data	Polarization	View Angle
1	1- 1	500	30 secs	Yes	Yes	Yes	Vert	0° **
2		500	10 mins					0° to 150 in 10° Steps
3		500	30 secs					150°
4	1- 2	1,600						0°
5	1- 3	2,700				?		
6	1- 4	3 800				?		
7	1- 5	4,900				?		
8	1- 6	6,000						
9	1- 7	7 100						
10	1- 8	8,200						
11	1- 9	9,300						
12	1-10	10 400						
13	1-11	11 500						
14	1-12	12,600						
15	1-13	13 700						
16	1-14	14 800						
17	1-15	15,900						
18	1-16	1 700						
19	1-17	18,100						
20	1-18	19,200						
21	1-19	20,300	30 secs			?		0°
22		20 300	10 mins			?		0° to 150° in 10° steps
23		20,300	30 secs			?		150°
24	1-20	19,200						0°
25	1-21	18,100						
26	1-22	17 000						
27	1-23	15 900						
28	1-24	14,800						
29	1-25	13,700						
30	1-26	12 600						
31	1-27	11,500	30 secs	Yes		? Yes	Vert	0°
32	1-28	10 400						
33	1-29	9 300						
34	1-30	8 200						
35	1-31	7 100						
36	1-32	6,000						
37	1-33	4 900						
38	1-34	3,800						
39	1-35	2 700						
40	1-36	1,600						
41	1-37	500	30 secs					0°
42		500	10 mins					0° to 150° in 10° steps
43		500	30 secs	yes	yes	yes	vert	150°

Note * Sensors include multifrequency radiometers boresight camera, analog recorder

** 0° view angle is vertically downward, 150° view angle is towards sky

*** Altitudes may approximate ±200 of given altitudes however exact altitude of pass must be recorded

B. Recorded Flight Data

1) Radiometer outputs and radiometer calibration data on PCM system and on 5-pen analog recorder (use 1.0 sec integrators) (record 4 frequencies, plus time).

2) Radiometer Frequencies

L-Band	1.42	GHz
X-Band	10.625	GHz
K-Band	22.2	GHz
K_a-Band	31.4	GHz

3) Complete ADAS

4) Boresight camera imagery during all recording periods. (Must be time or frame correlated with radiometer data.)

5) Air temperature at each elevation

6) Air pressure at each elevation

7) Humidity at each elevation

8) Occurrence of water droplets (if any) at each elevation. Quantitative cloud cover. Note height of cloud base and cloud tops in flight line (if any).

9) Record laser altimeter data at applicable lower elevations.

C. Ground Truth Data

1) Nominal wind speed (steady or gusting)

2) Nominal wind direction

3) Nominal wave height

4) Nominal water temperature

5) Description of weather in general area. (Meteorological maps) Presence of fronts, cloud cover descriptions, ceiling (if any).

6) Cold load and hot load calibrations should be run within a day or two "before" and "after" the flight.

4.2 2 FLIGHT TEST RESULTS

A mission was flown on February 13, 1970 in an attempt to verify the atmospheric correction equations described in Section 2.2 1. Data were gathered over the Gulf of Mexico with the radiometers pointing both toward the sea and skyward. Of particular interest from the point of view of testing the basic equations without the extraneous influence of emissions from other sources is the case where the radiometers were pointing skyward. These data also provide a good test of the radiometer calibration (including radome effects) since low temperature targets generally provide sensitive indications of possible calibration errors. The following discussion will be restricted to a consideration of only this portion of the flight test data since the gross inconsistencies which were encountered seem to preclude a precision estimate of temperatures from other targets until corrective steps are taken.

The sky temperature measurements can be conveniently divided into two groups for the purpose of discussion. The first part of the data was gathered as the aircraft climbed from an altitude of 550 to 21,000 feet, while the second part of the data was obtained during a descent from an altitude of 19,900 to 485 feet. In the following, these portions of the flight will be referred to simply as the ascent and descent. In both cases the air temperature and dew point (from which the absolute humidity can be determined) were recorded at a number of altitudes. No clouds were present.

The measured air temperatures for the ascent and descent are shown in Figure 4-1. Since the calculation of sky brightness temperatures requires atmospheric data at altitudes higher than were attained by the aircraft, an extrapolation is required. A glance at Figure 4-1 shows that the measured air temperatures below 6 km do not differ greatly from the ARDC model tropical atmosphere. Hence, in the calculation of sky brightness temperatures, measured air temperatures were used from sea level to the peak flight altitude (slightly greater than 6 km), between the peak flight altitude and 8 km, a smooth transition into a tropical air temperature profile was introduced, above 8 km, the model tropical atmosphere was used.

FIGURE 4-1 AIR TEMPERATURE PROFILE - ATMOSPHERIC EFFECTS TEST FLIGHT - 2/13/70

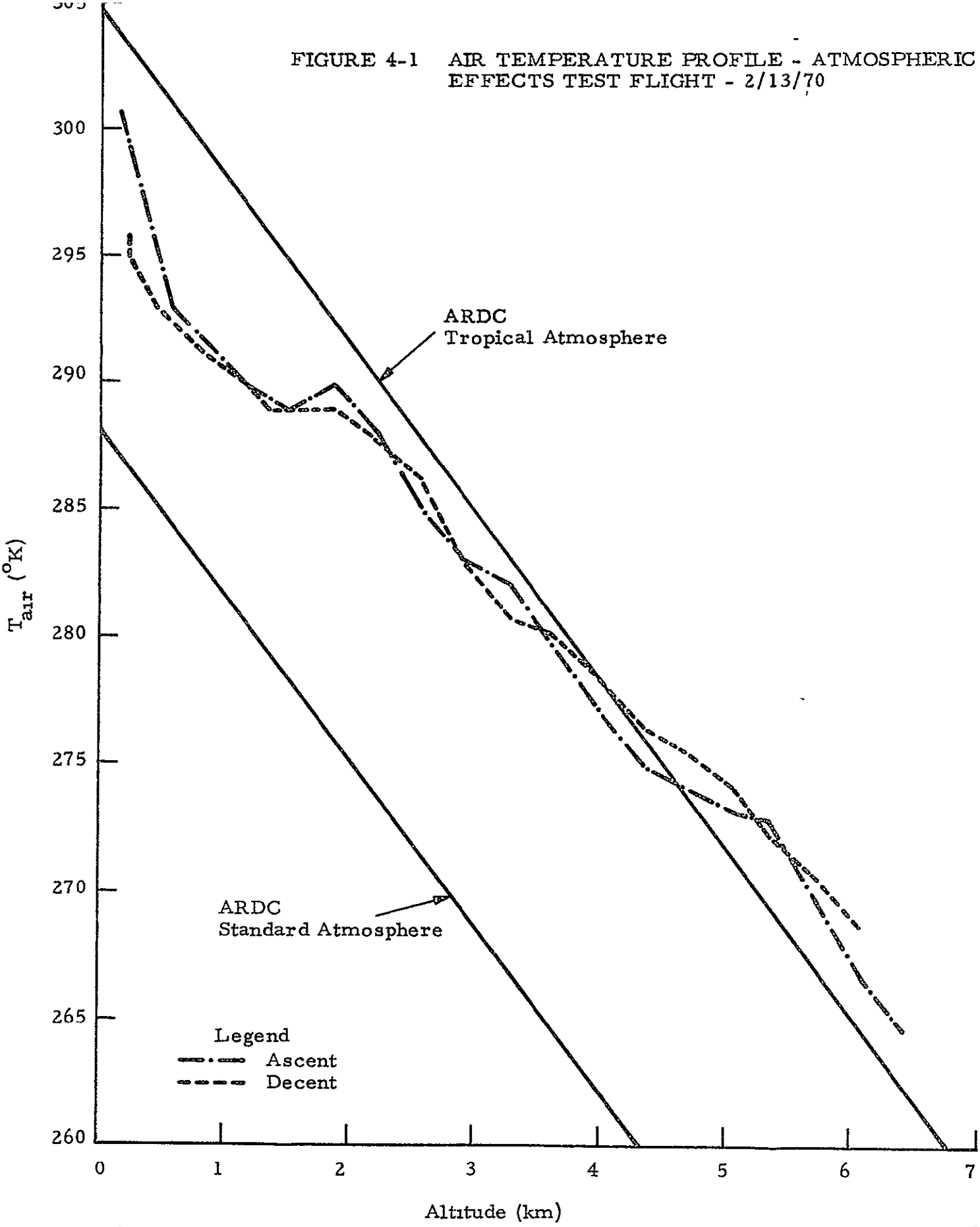

The absolute humidity, $\rho_{H_2O}(z)$, during the ascent and descent is shown in Figure 4-2. A few of the measured dew points lead to relative humidities which are greater than 100 percent (assuming that the recorded air temperature is correct). There is clearly some error here and the points which are plotted (indicated by question marks in the figure) are the absolute humidities assuming 100 percent relative humidity. Both the ascent and descent measurements indicate that the water vapor density decreases approximately in an exponential manner with altitude. Thus, since information at altitudes higher than were achieved in the flight is needed for a theoretical calculation, the assumption was made that the water vapor profile is adequately described by

$$\rho_{H_2O}(z) = \rho_{H_2O}(0)\, e^{-\lambda z} \quad .$$

For both the ascent and descent, $\rho_{H_2O}(0)$ was chosen to be 22.0 gm/m^3 while a reasonable fit to the data is given by $\lambda = 0.523\ km^{-1}$ for the ascent and $\lambda = 0.618\ km^{-1}$ for the descent portion of the flight.

On the basis of the model discussed above, sky brightness temperatures were calculated for frequencies of 1.42, 10.625, 22.235, and 31.4 GHz at a number of viewing angles and aircraft altitudes. The results are shown in Figures 4-3 to 4-12. The uncertainty in the calculated values due to the required extrapolation of air temperature profile is small. There is more uncertainty due to the approximate water vapor density profile which was used. The uncertainty is greatest at 22.235 GHz (near the peak water vapor absorption) and negligible at 1.42 GHz Except near grazing (i.e., angles less than 110°), the uncertainty at 22.235 GHz should be less than $10^{\circ}K$ near sea level and less than $2^{\circ}K$ near 20,000 feet.

These results may be compared with measured brightness temperatures. Comparisons, using several different procedures in processing the data, are shown in Figures 4-13 to 4-15 for frequencies of 1.42, 22.235, and 31.4 GHz.

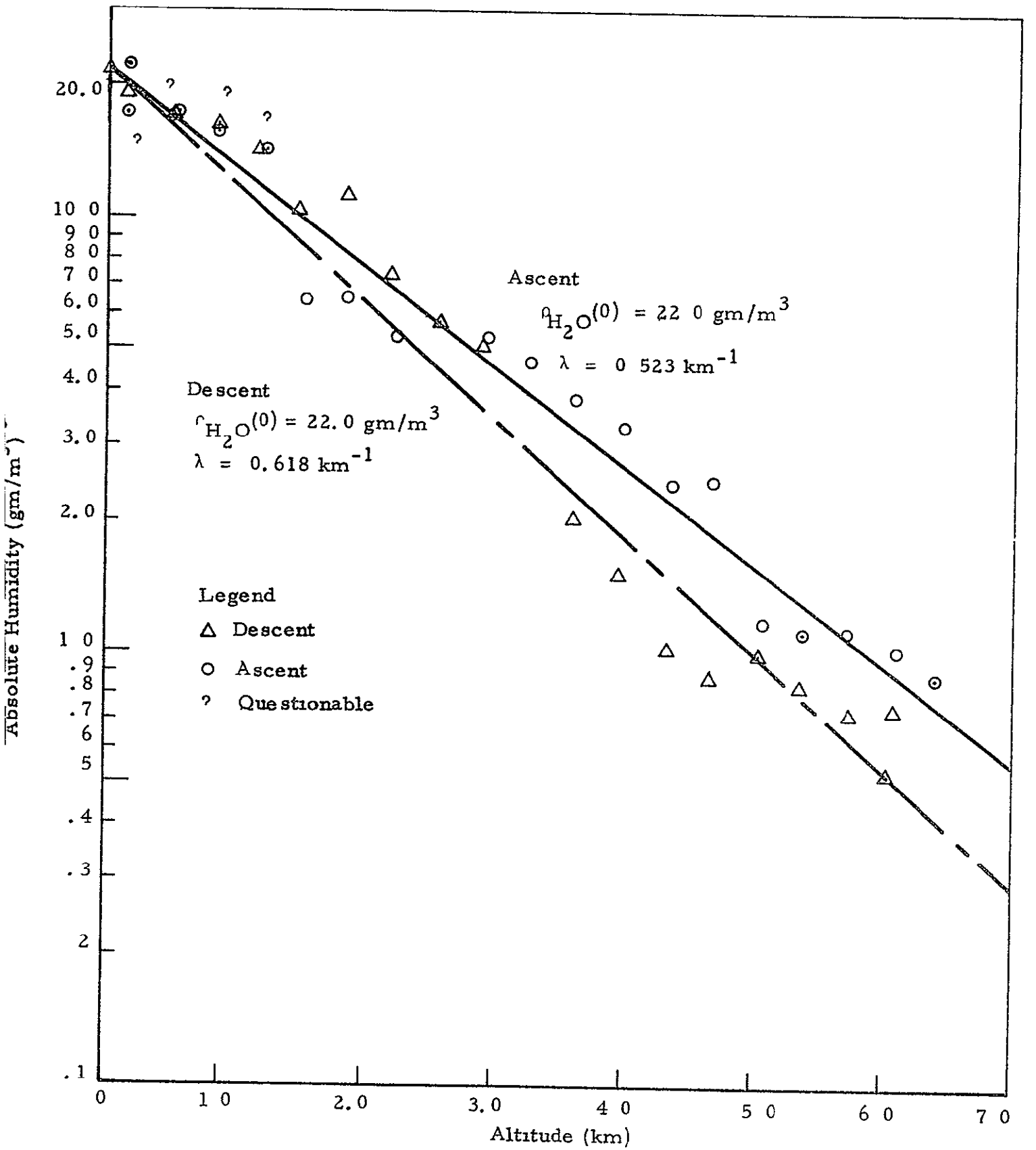

FIGURE 4-2 WATER VAPOR DENSITY PROFILE - ATMOSPHERIC EFFECTS TEST FLIGHT, 2/13/70

FIGURE 4-3 T_b VS VIEW ANGLE AND ELEVATION

1.42 GHz

ρ_{H_2O} Ascent

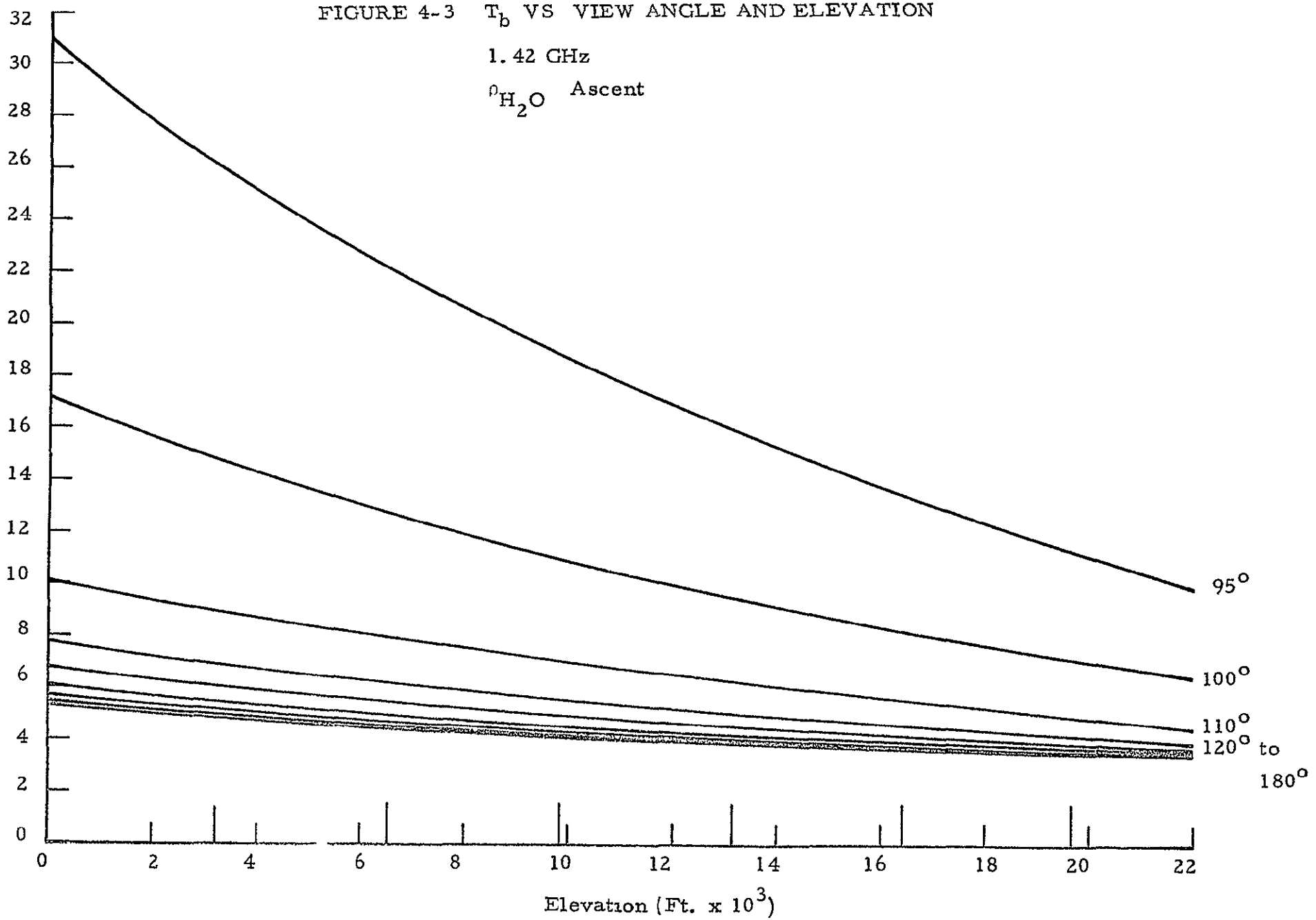

FIGURE 4-4 T_b VS. VIEW ANGLE AND ELEVATION

1.42 GHz

$^{\rho}H_2O$ Descent

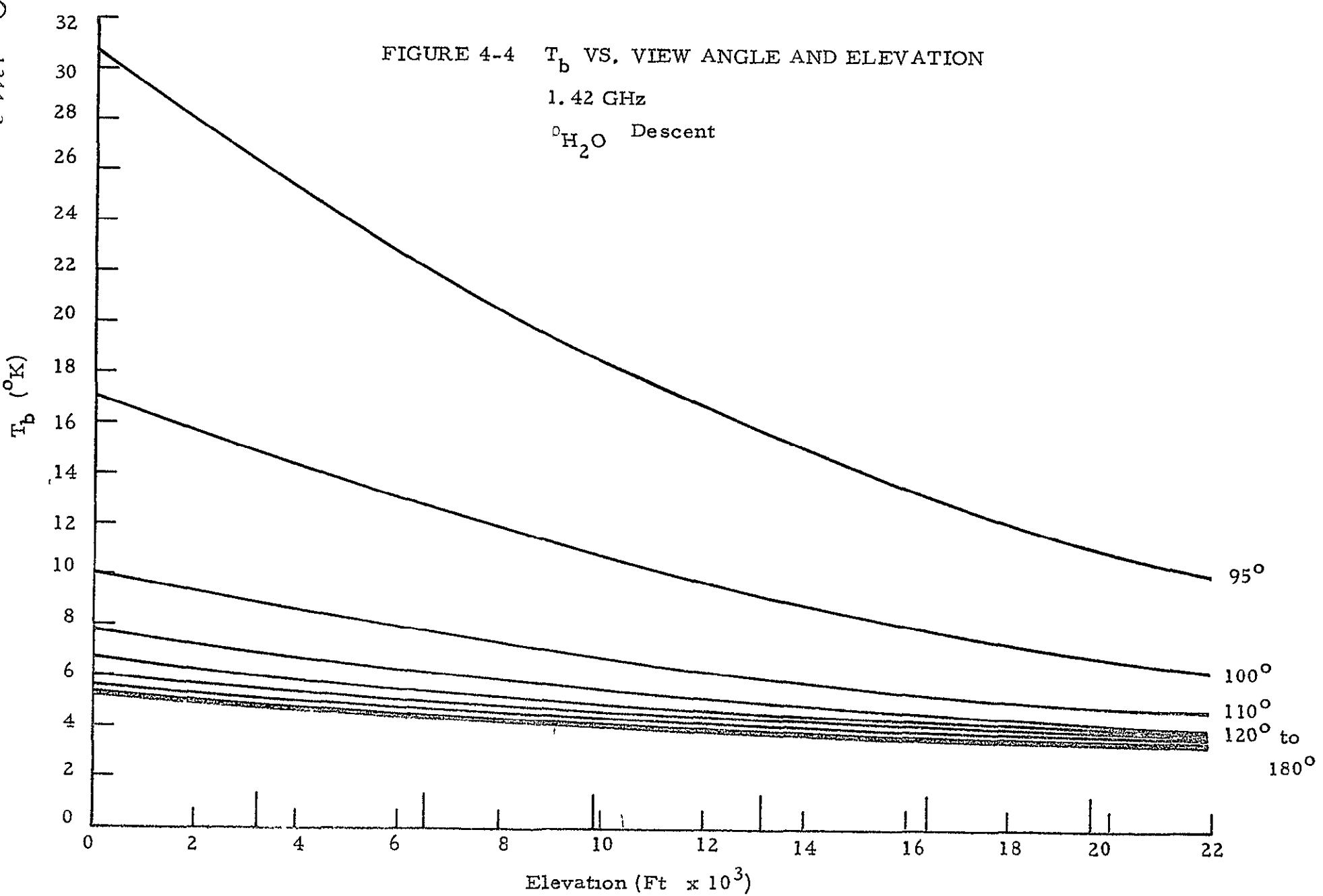

FIGURE 4-5. T_b VS VIEW ANGLE AND ELEVATION

10.625 GHz

ρ_{H_2O} Ascent

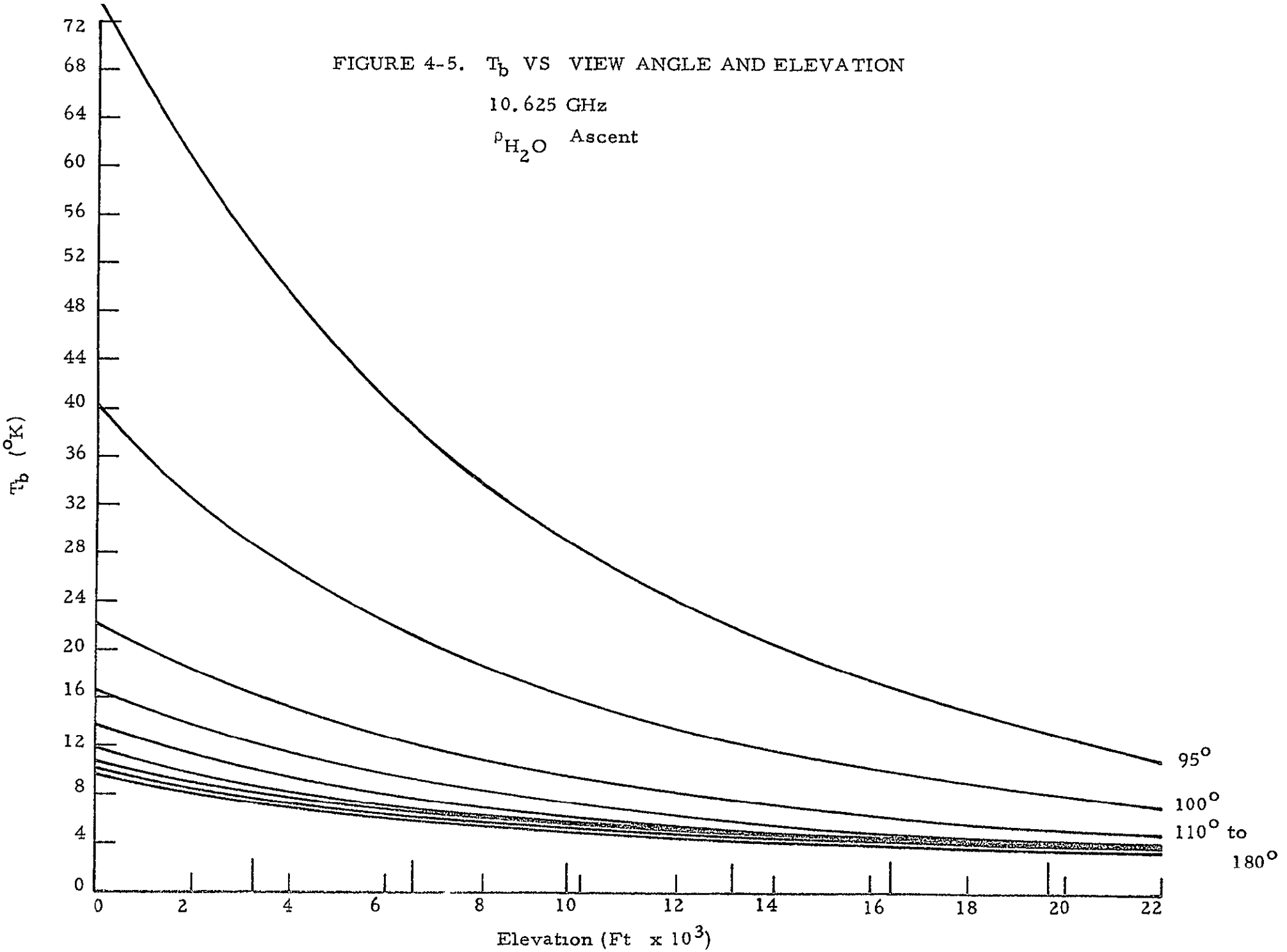

FIGURE 4-6 T_b VS VIEW ANGLE AND ELEVATION

10 625 GHz

ρ_{H_2O} Descent

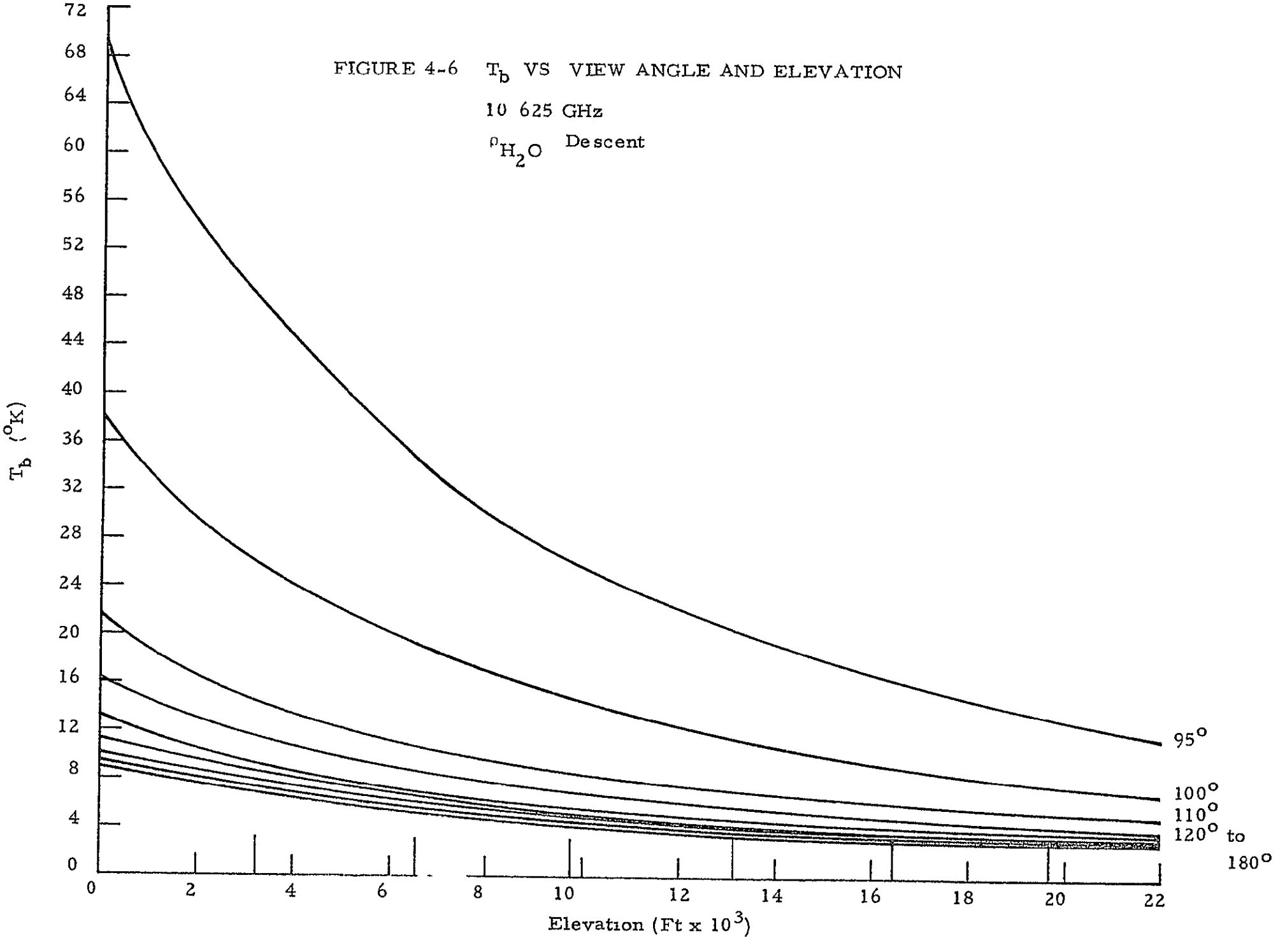

FIGURE 4-7 T_b VS VIEW ANGLE AND ELEVATION

22 235 GHz

ρ_{H_2O} Ascent

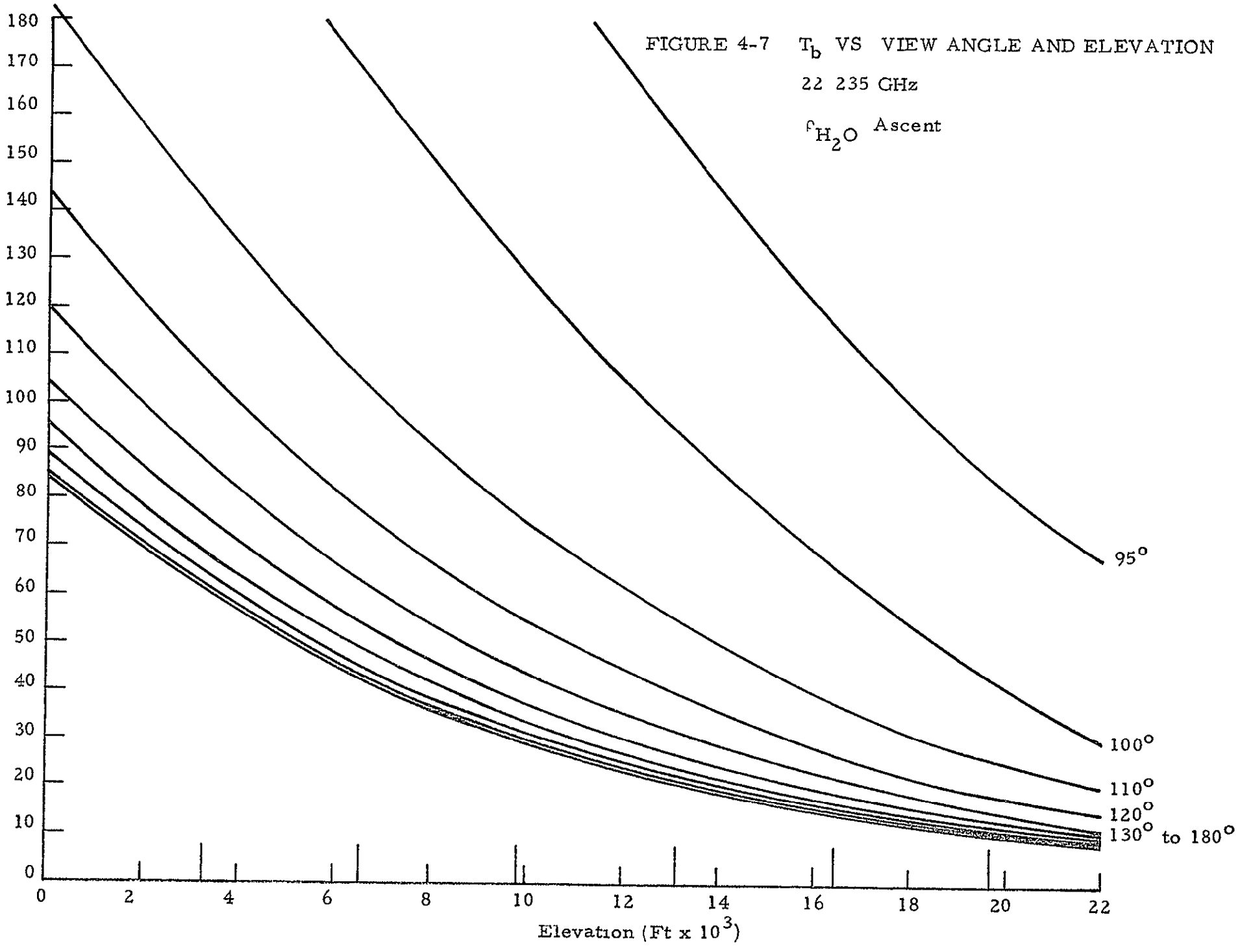

FIGURE 4-8 T_b VS VIEW ANGLE AND ELEVATION

22 235 GHz

ρ_{H_2O} Descent

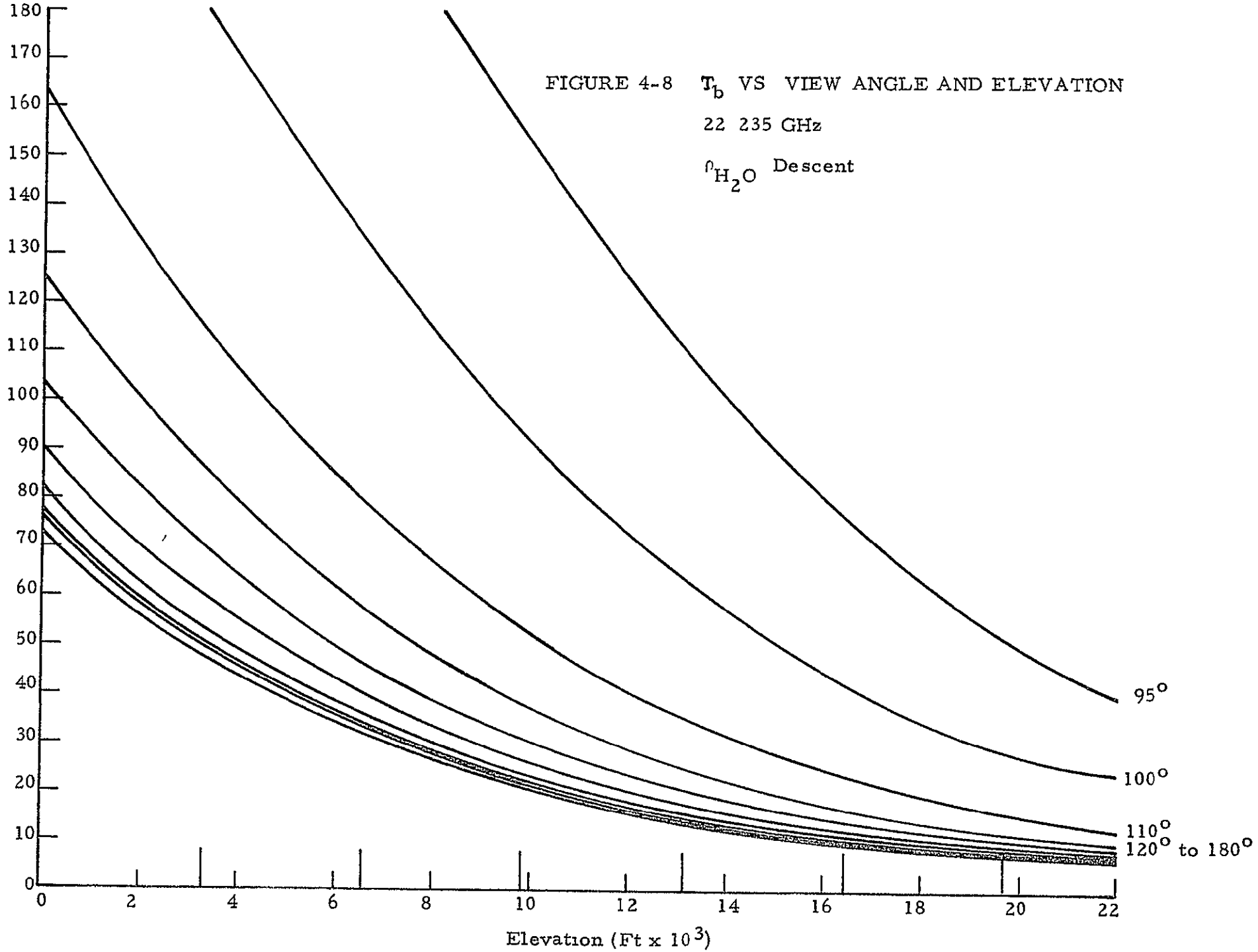

FIGURE 4-9 T_b VS VIEW ANGLE AND ELEVATION

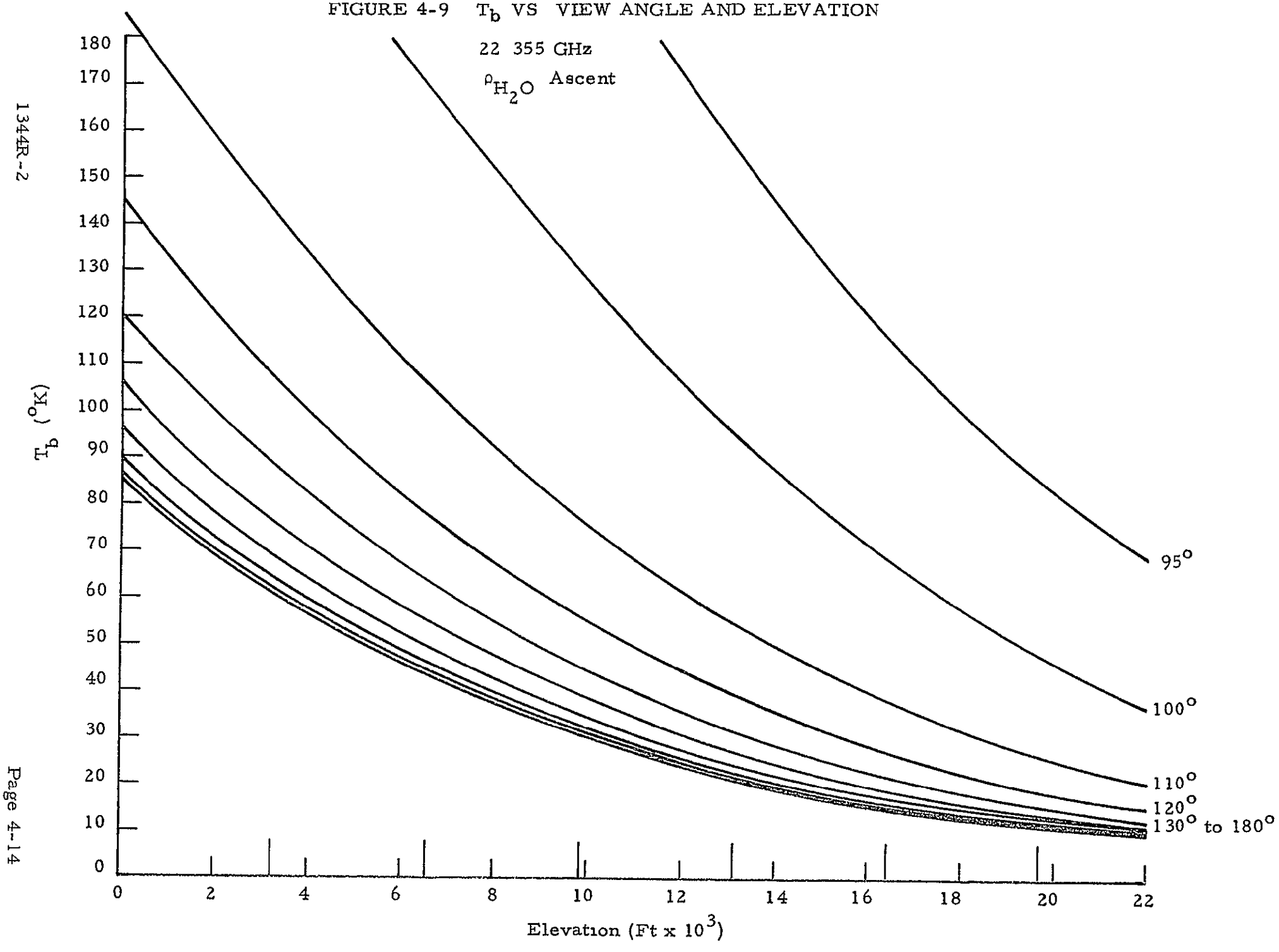

FIGURE 4-10 T_b vs VIEW ANGLE AND ELEVATION
22 355 GHz
ρ_{H_2O} Descent

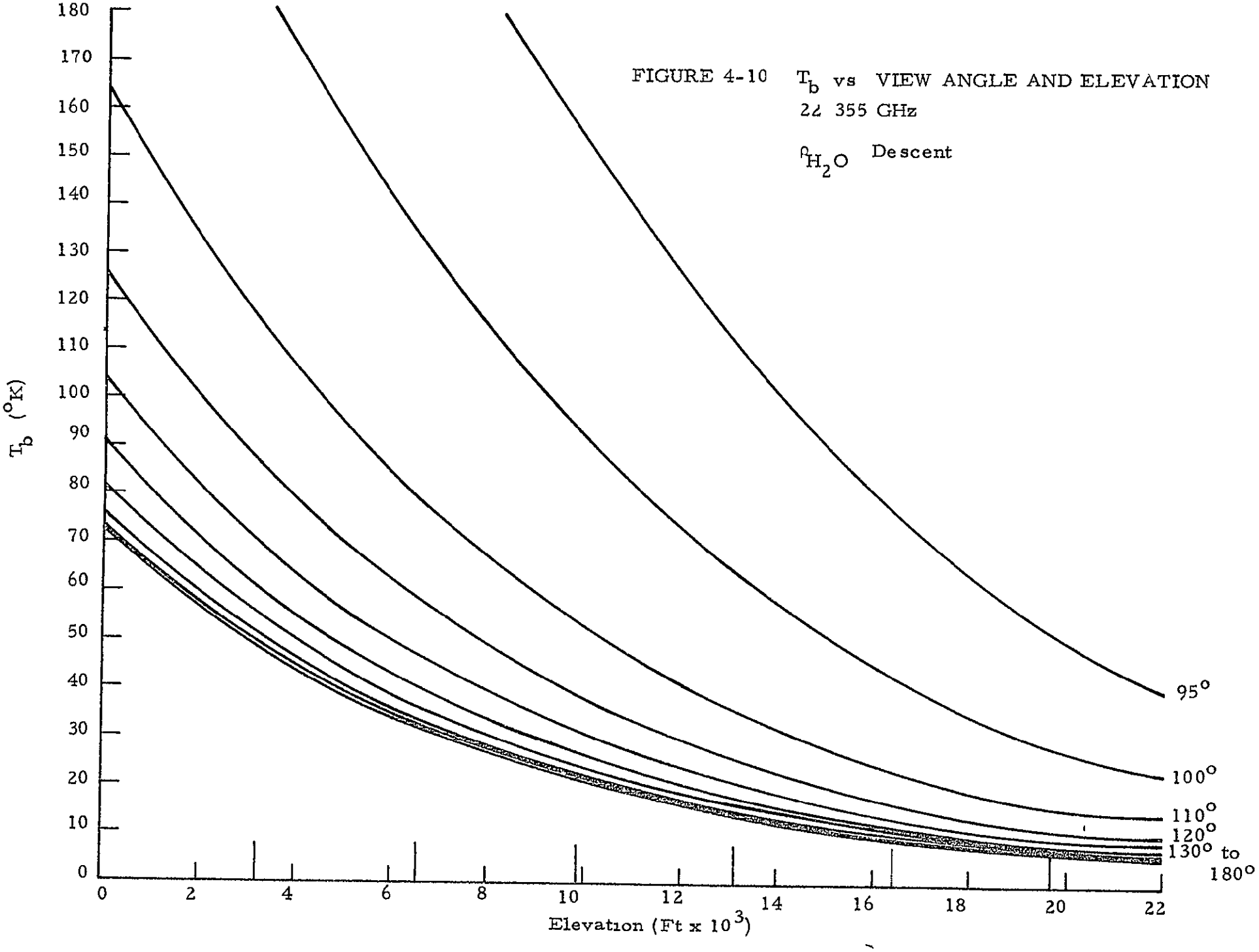

FIGURE 4-11 T_b vs VIEW ANGLE AND ELEVATION
31.4 GHz

ρ_{H_2O} Ascent

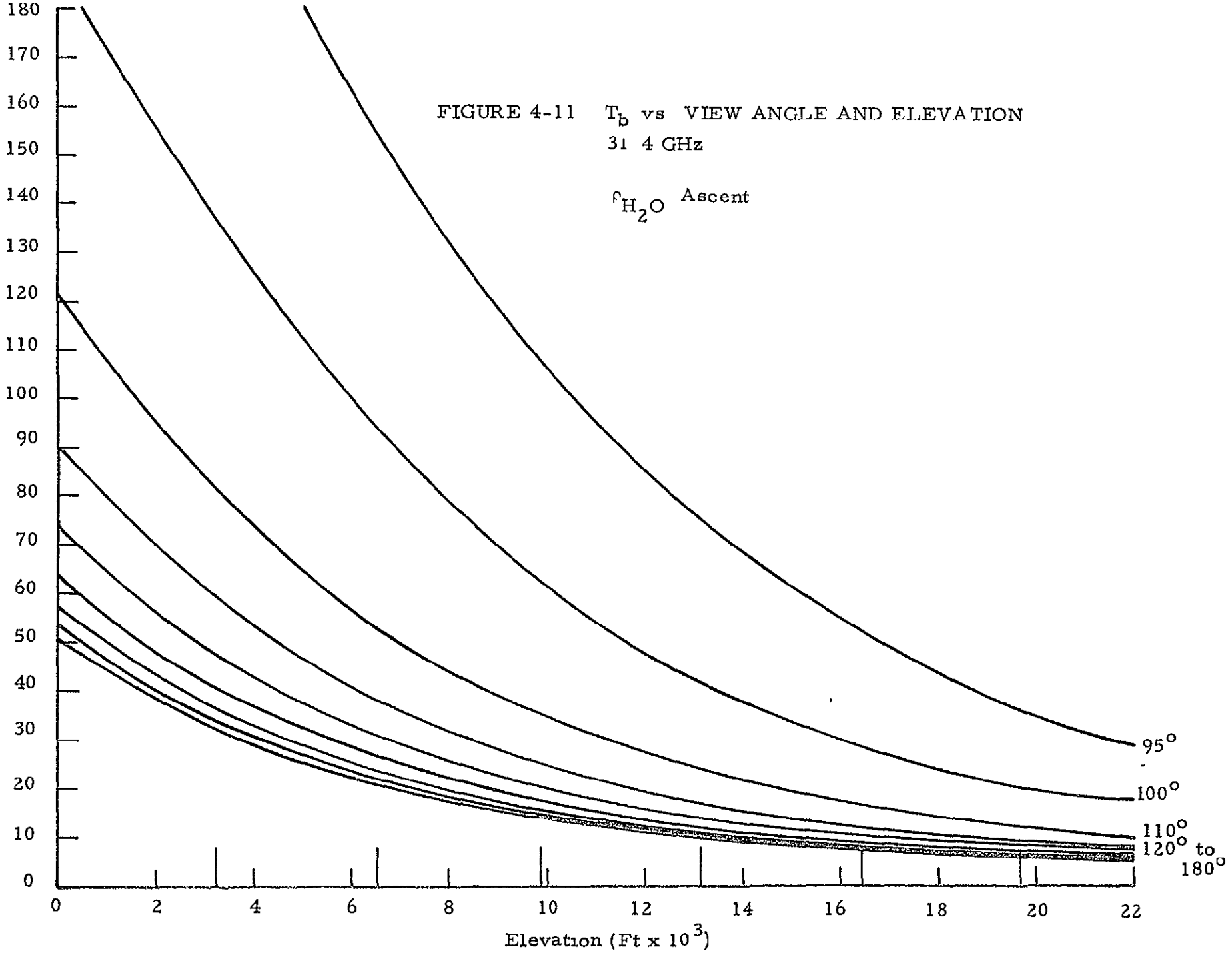

FIGURE 4-12 T_b vs VIEW ANGLE and ELEVATION

31 4 GHz

ρ_{H_2O} Descent

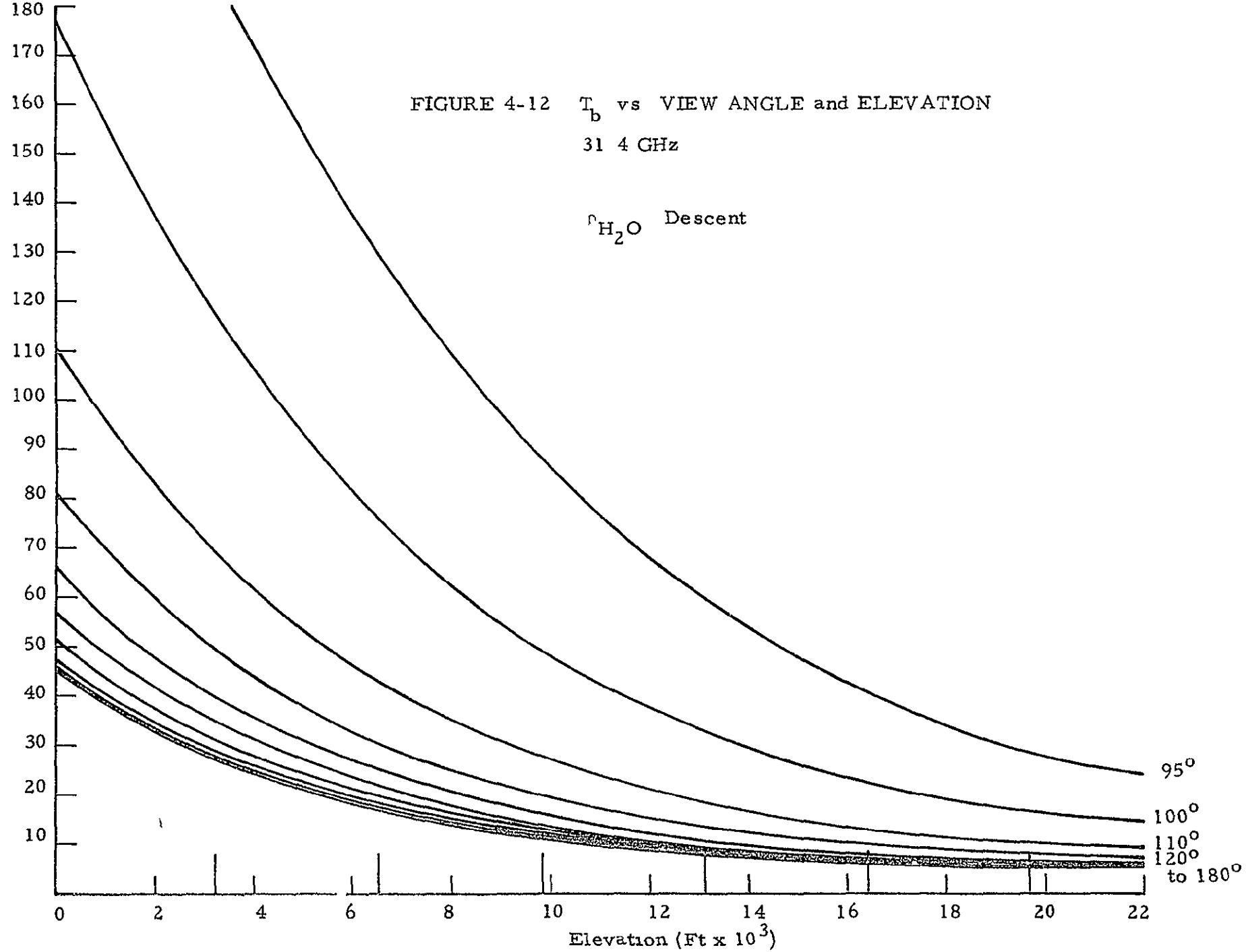

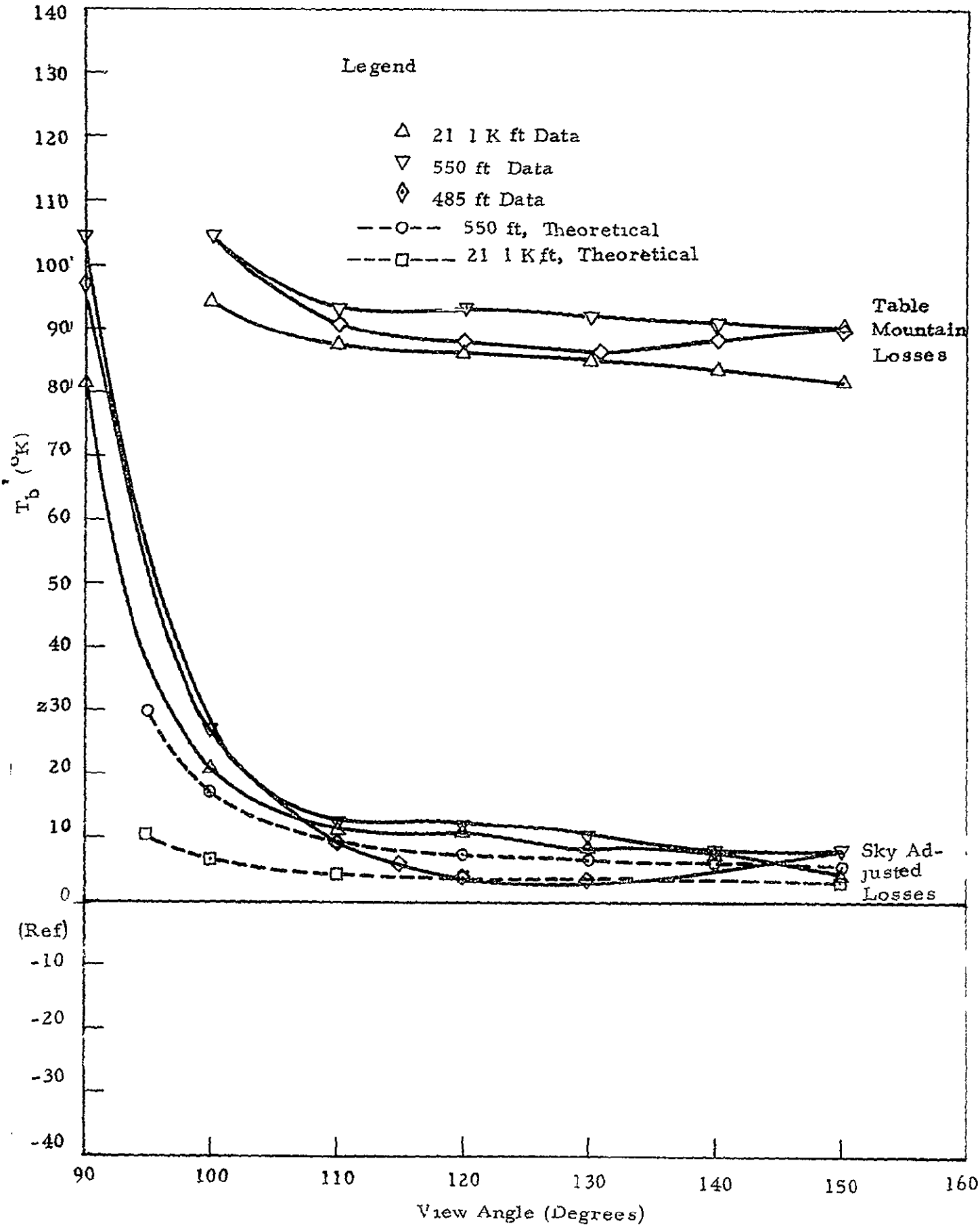

FIGURE 4-13. T_b VS VIEWING ANGLE, FIXED LOSS, 1 42 GHz

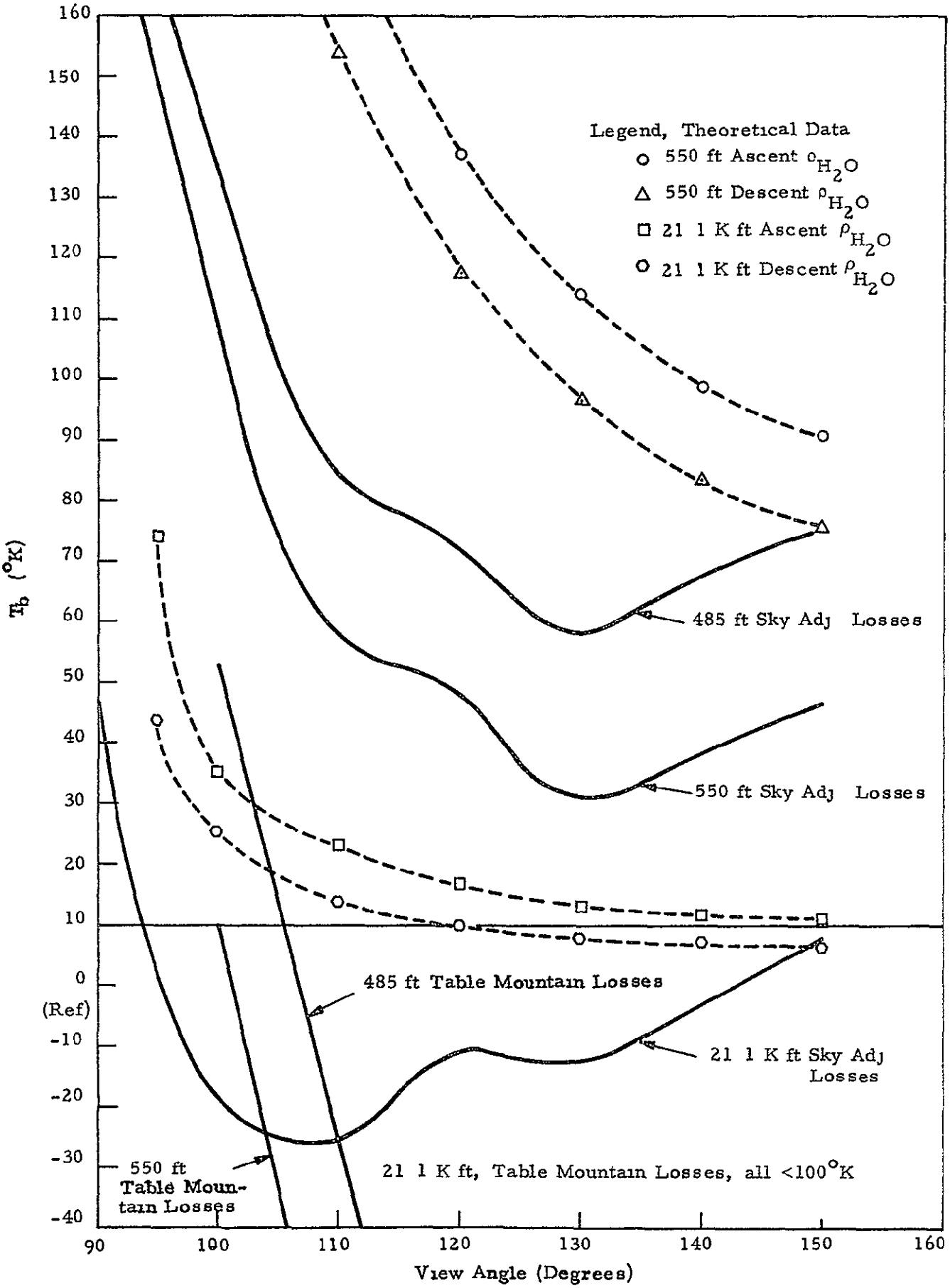

FIGURE 4-14 T_b vs Viewing Angle, Fixed Losses 22 235 GHz

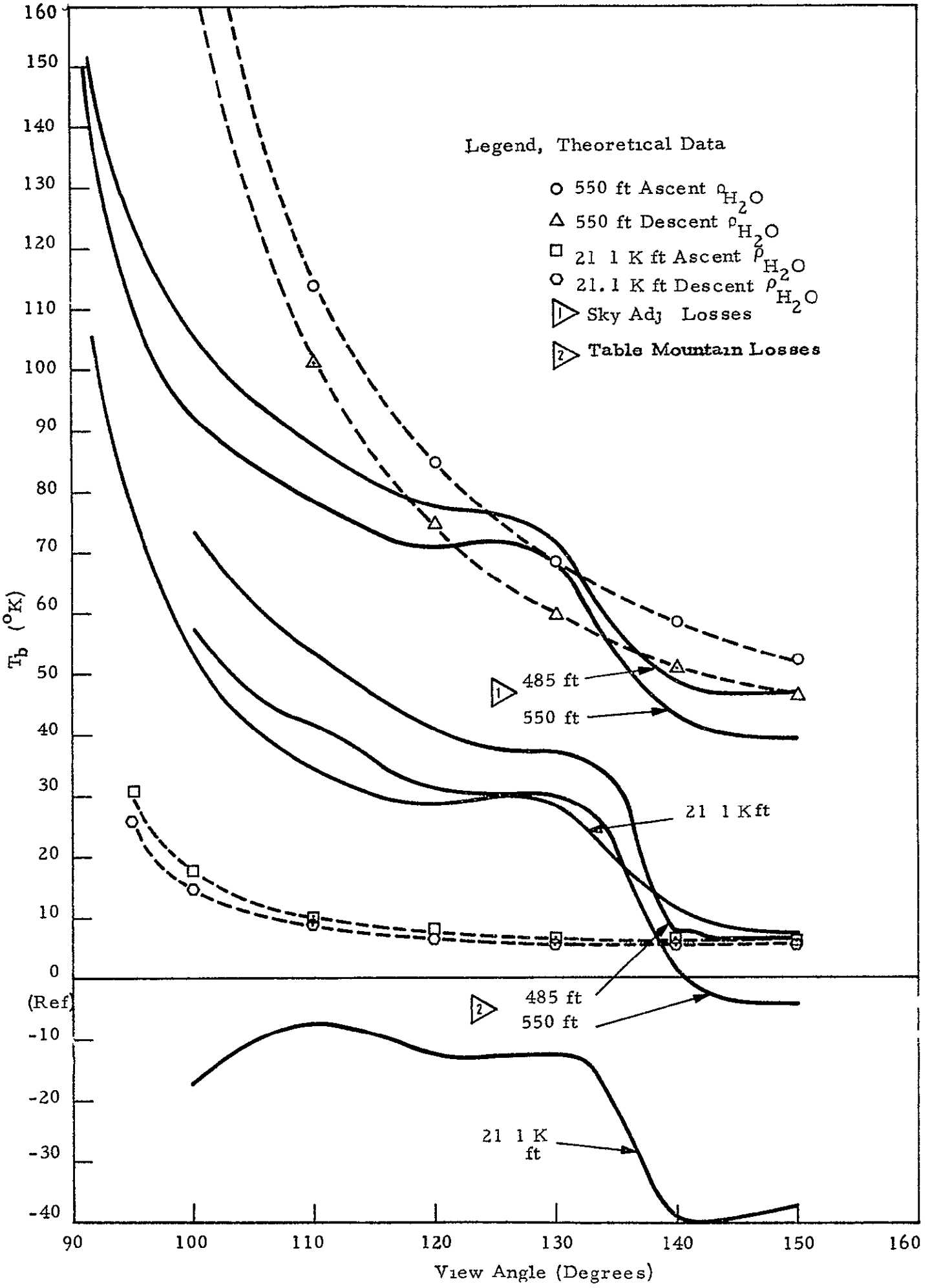

FIGURE 4-15 T_b vs VIEWING ANGLE, FIXED LOSSES, 31 4 GHz

In all of the discussion which follows we make the assumption that no significant error exists in the measured radiometer data. The validity of this assumption can only be determined after extensive measurements have determined the errors in each parameter used to obtain brightness temperature.

The first method of deriving results from the raw data consisted of applying the calibration data for the radome and antenna which were obtained at Table Mountain[1]. See Section 4.2.3. At all frequencies, totally unrealistic results were obtained. The most obvious errors are the large negative temperatures at 22.235, 22 355 and 31.4 GHz. Negative temperatures are physically meaningless.

Another difficulty that occurs with the Table Mountain calibration data is the oscillation in the sky temperature with angle (recall that we have assumed the measured data to be correct). In the absence of a region of strong absorption at a particular angle, the sky temperature should be a monotonically increasing function of angle in scanning from zenith to grazing (i e , from 180° to 90°). This behavior was not obtained in the measurements and cannot be ascribed to a possible local atmospheric anomaly because the aircraft was heading in different directions at different times, thus allowing the radiometers to observe several different portions of the atmosphere. Finally, the use of the Table Mountain calibration leads to an unexplainably high brightness temperature (above 70°K) at 1.42 GHz.

In view of the failure to obtain meaningful results with the prescribed calibration data, a second, approximate method was tried in order to test the sky temperature model. This consisted of empirically determining an overall loss factor (see Section 4.2.3) at each frequency and at an angle of 150° by forcing the sky brightness temperatures at 21,000 feet to agree with the theoretical results. This loss factor was then used to reduce the data at other angles at 21,000 feet as well as at 550 feet (for the ascent) and 485 feet (for the descent).

---

(1) "Table Mountain Calibration on P3A Multifrequency Microwave Radiometers and Radomes," Jet Propulsion Laboratory, Nov. 25, 1969.

With the second method of calibration, there is a distinct improvement in agreement with theory at all frequencies. The measurements near sea level are of the correct order of magnitude. Quantitative agreement, of course, cannot be expected because of the sensitivity of the results to the empirically determined loss factor. This factor could not be fixed precisely. The principal qualitative failure of the second calibration method is the peculiar oscillation in the brightness temperature which was previously noted in the use of the first calibration method. It must be concluded that allowance must be made for a loss factor which varies with angle.

Thus, a third approach was tried. This consisted of determining a loss factor as in the second method with the exception that a separate loss factor was assigned to each angle With this method, all of the data at 21,000 feet were used to establish the calibration so that the only check with theory is the data at lower altitudes (i.e., the 550 foot ascent data and the 485 foot descent data). The results are shown in Figures 4-16 to 4-18. A substantial improvement is made over the second method in that the magnitude of the undesirable oscillations is greatly decreased. Again, because of the sensitivity to the loss factor and approximations which were necessary, a precise quantitative check cannot be expected.

4.2.3 DATA REDUCTION PROCEDURES

In the computation of brightness temperatures from data recorded by the data acquisition system used in the flight test measurements, a number of operations take place. This section is concerned with presenting, in some detail, the operations which are needed to arrive at radiometer temperatures after the measured data has been supplied to Aerojet-General by the Computation and Analysis Division of the Manned Spacecraft Center in Houston, Texas.

The data acquisition system used in the aircraft samples and records each parameter of interest approximately 60 times per second. The values of each parameter can then be averaged using a computer program available at the Spacecraft Center with the time of measurement serving as

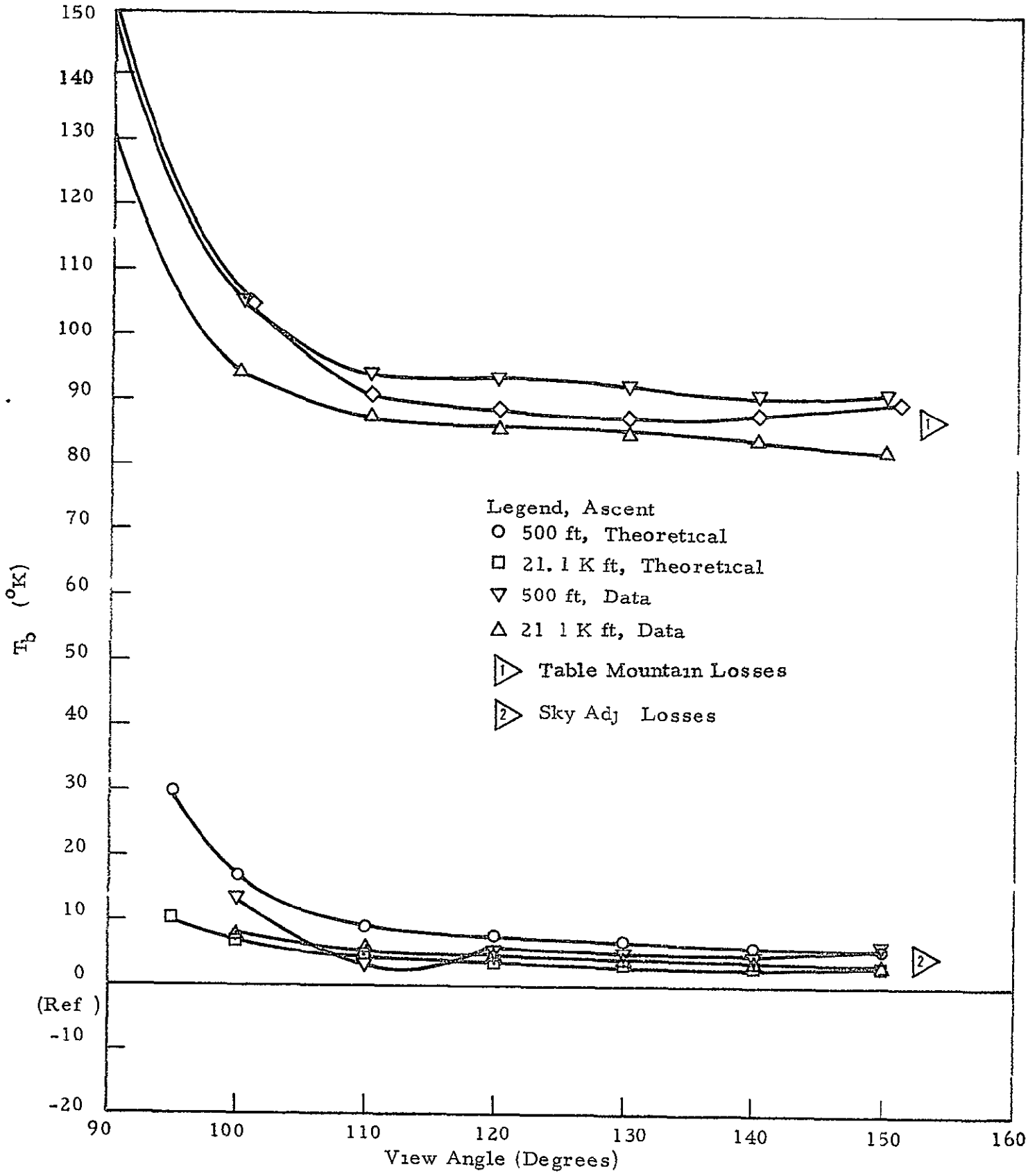

FIGURE 4-16 T_b VS VIEWING ANGLE, VARIABLE LOSSES
1 42 GHz

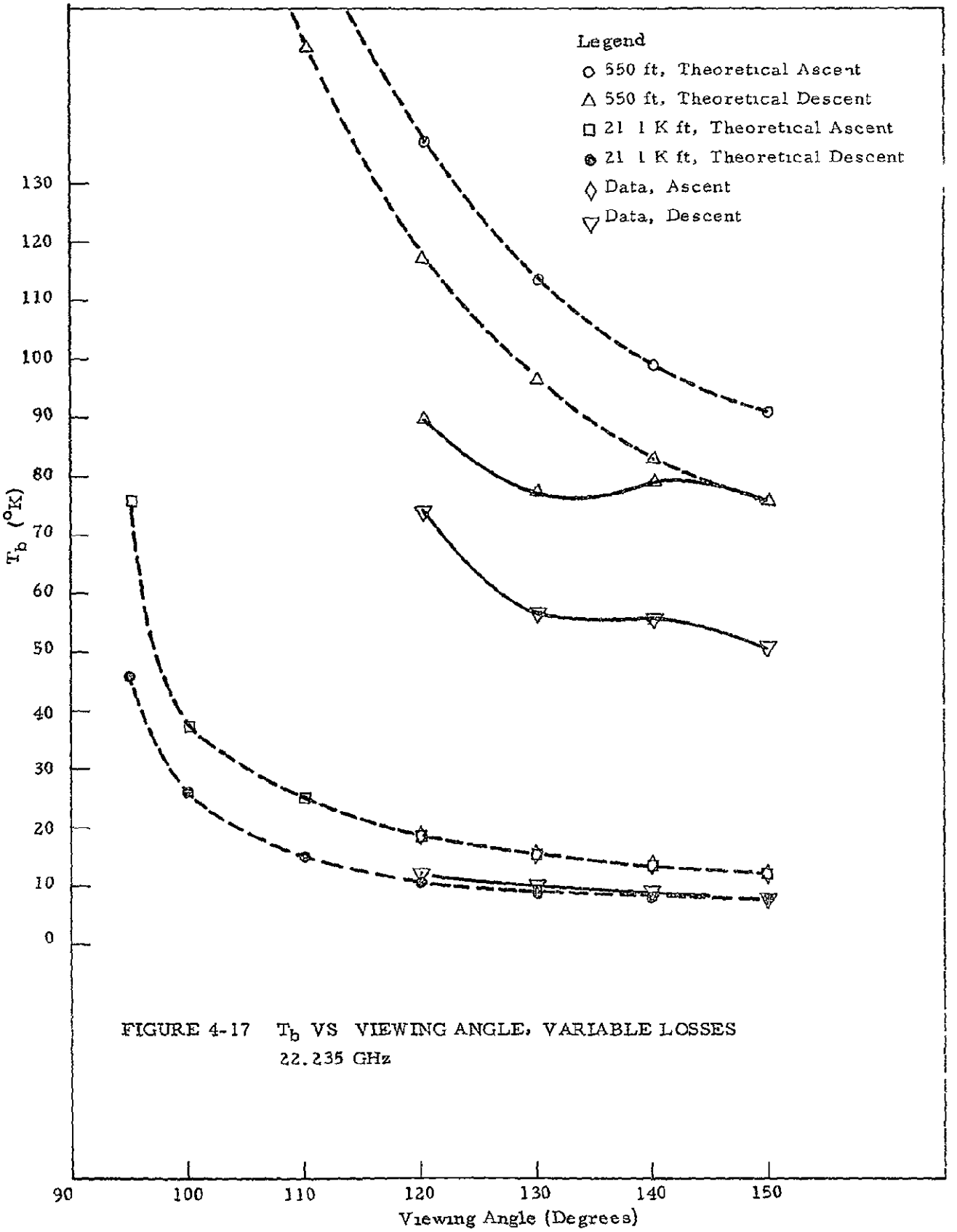

FIGURE 4-17 T_b VS VIEWING ANGLE, VARIABLE LOSSES
22.235 GHz

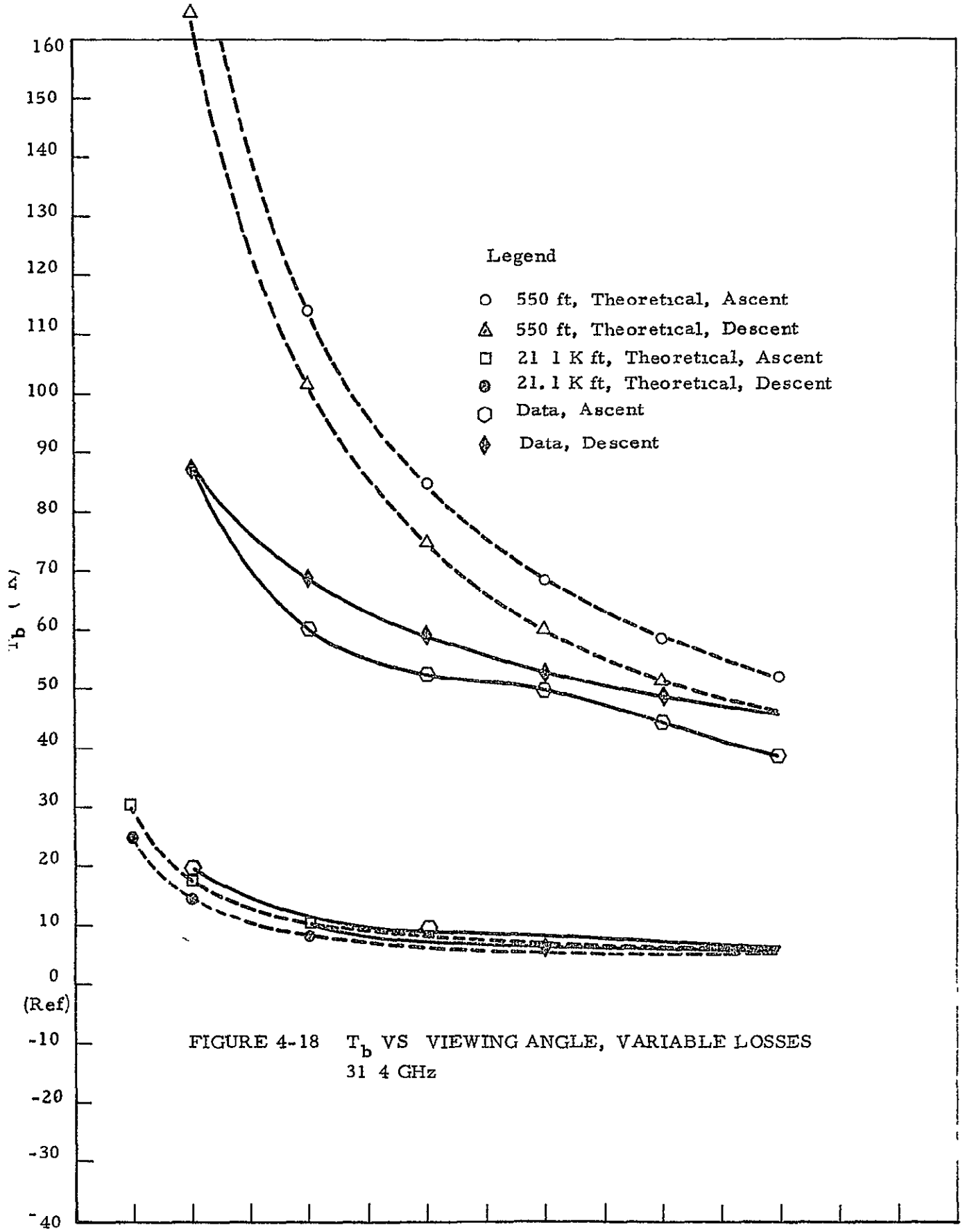

FIGURE 4-18 T_b VS VIEWING ANGLE, VARIABLE LOSSES
31 4 GHz

a means of identifying the data. Before the computer program can perform an average, however, two quantities must be supplied a time interval which specifies the number of values to be averaged and the time rate of printing the averaged values. The average value is printed out in the mid-point of the time interval. For example, when a five-second time interval and one-second time rate of printing is employed, 300 successive values of a parameter are used in the average with the average value printed out every second at the time corresponding to the mid-point of the five-second interval. For the data used in this report, a five-second time interval and a five-second time rate of printing was employed.

To readily determine the location in time of possible large noise fluctuations in the recorded data, an analog output on chart paper of the recorded data was examined. Locations which indicated large noise fluctuations were subsequently not considered as representing meaningful data.

Using averaged values of measured parameters supplied by the Manned Spacecraft Center, uncorrected brightness temperature T_b can be calculated as a function of time t

$$T_b(t) = \frac{T_{nt}\left(V_R(t) - V_{BL}(t)\right)}{V_c(t) - V_{BL}(t)} + T_{ref}(t)$$

where corrections for antenna and radome losses occur later

In the above equation

T_{nt} is the temperature of the noise tube,

T_{ref} is the reference tempeiature of the baseline (^{o}K),

V_c is the calibrate voltage,

V_{BL} is the baseline voltage,

and V_R is the radiometer voltage.

Measurements of the temperature of the noise tube were made before and after the flight test measurements by O'Hare* for all frequencies with the exception of pre-flight measurements at 22.235 and 22.355 GHz. Table 4-2 gives the values in ^{o}K As can be seen from the table, a relatively large uncertainty in T_{nt} exists for 1.420 and 10.625 GHz.

Table 4-2

Frequency (GHz)	Pre-Flight Measurements	Post-Flight Measurements	Average
1.420	123.1	119.4	121.2
10.625	94.4	89.6	92.0
22.235		107.3	107.3
22.355		124.2	124.2
31.400	85.8	85.5	85.6

The reference temperatures of the baseline during the flight measurements are shown in Figures 4-19 through 4-22 for each frequency. The error in the temperatures is usually less than $0.2^{o}C$ for the thermistors employed (YSI precision thermistors were used). Variations greater than $0.1^{o}C$ of the reference temperature during the flight measurements were included in the calculations of T_b .

The baseline and calibrate voltages were monitored before and after each radiometric measurement The maximum and minimum values at a fixed point in time of the five-second averaged data was observed to be approximately 30 millivolts for the 1.420 GHz radiometer. Variations of the same order of magnitude also exist at the other frequencies.

---

* Interdepartmental communication from W. M. O'Hare to N. M. Hatcher concerning MFMR calibration data on 3/30/70 at Manned Spacecraft Center, Houston, Texas.

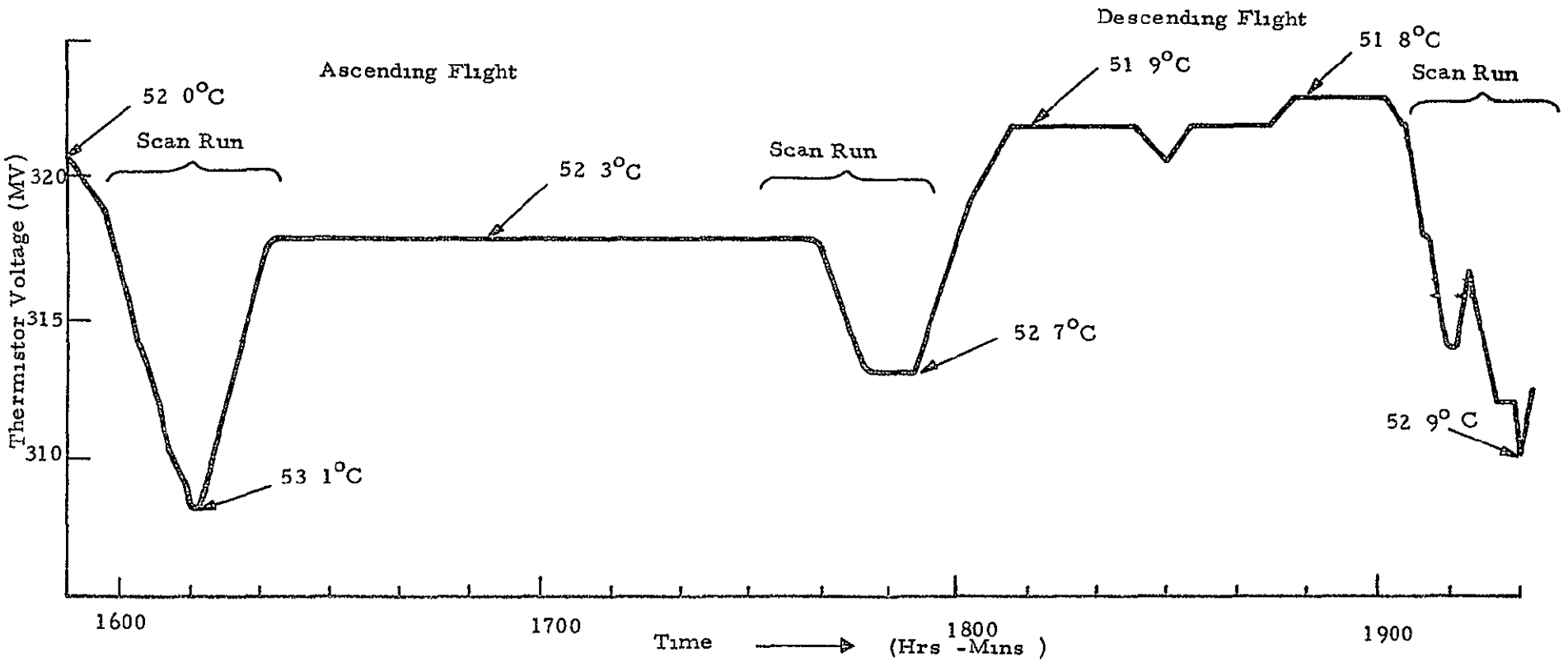

FIGURE 4-19. REFERENCE THERMISTOR (T_1)
VOLTAGE VS TIME - 1 420 GHz (L Band)
2/13/70

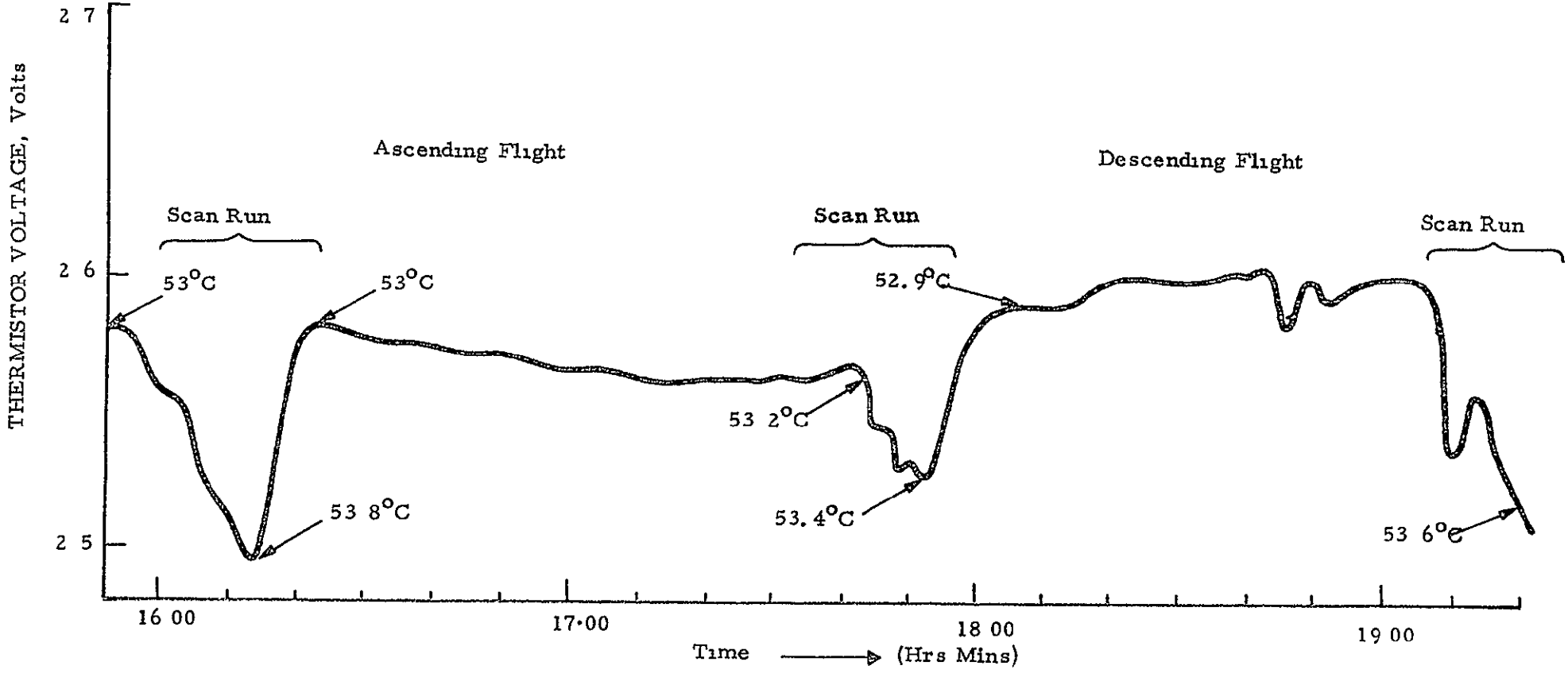

FIGURE 4-20 REFERENCE THERMISTOR (T_1) VOLTAGE VS TIME
10 625 GHz (X-Band), 2/13/70

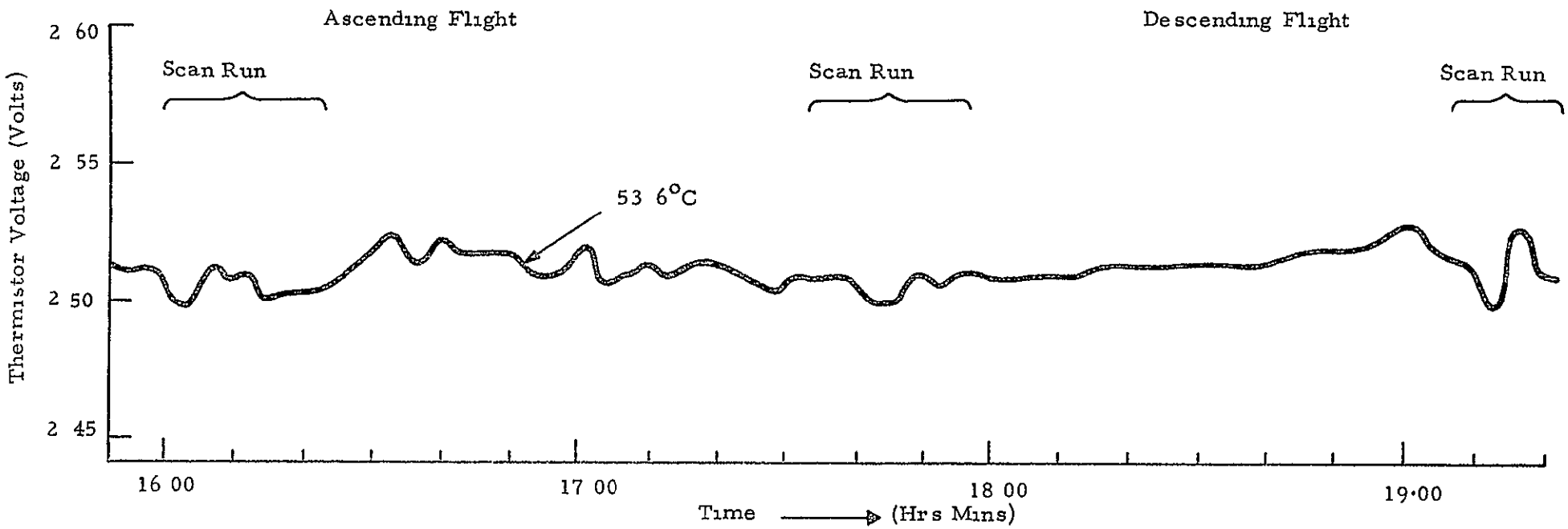

FIGURE 4-21 REFERENCE THERMISTOR (T_1) VOLTAGE VS TIME
22 235 and 22 355 GHz (K_1, K_2 Band), 2/13/70

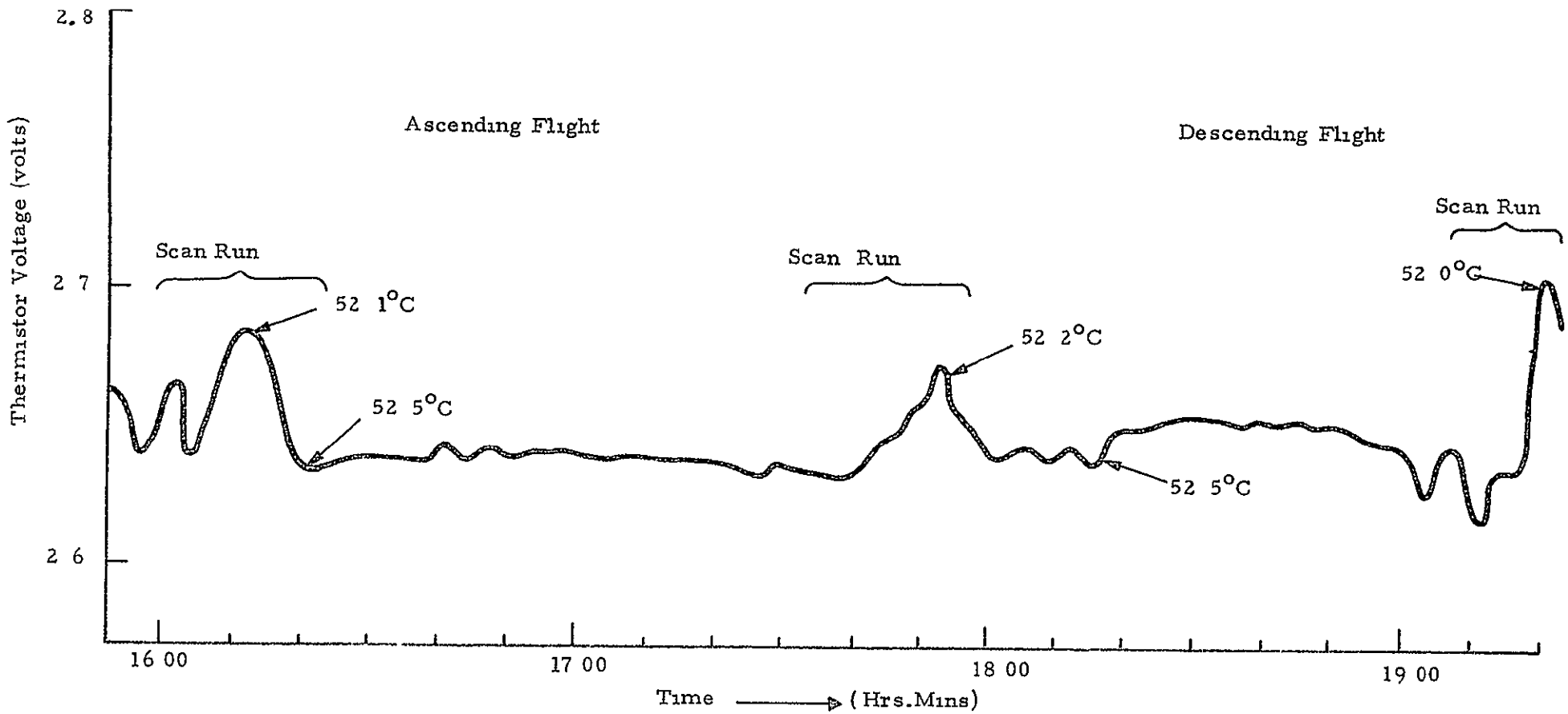

FIGURE 4-22 REFERENCE THERMISTOR (T_1) VOLTAGE VS TIME
31.4 GHz (K_a Band), 2/13/70

Since the variation of the average value of V_{BL} and V_c during the flight were roughly the same as the variations occurring at a fixed point in time, the variations of the average during the flight were considered to be due noise fluctuations rather than as real fluctuations of V_{BL} and V_c. Straight lines were constructed to pass through the average values and used in the calculation of T_b. See Figures 4-23 through 4-27. Each point in the figures is the average of more than 900 sampled values. It should be noted that, at times, values of calibrated voltages were not recorded by the PCM data system in the flights. In these cases linear extrapolations were used to approximate the calibrate voltages.

From an observation of the variations of V_c and V_{BL} in the figures it is apparent that detailed long-term measurements of these quantities would certainly be informative. The measurements would determine what portions of long-term variation of measured values of V_c and V_{BL} are due to real variations of V_c and V_{BL}.

Table 4-3 gives values of $T_b(t)$ corresponding to average values of $V_R(t)$ together with an rms error due to fluctuations in V_R. The number of points used in determining the average and rms is also given. As seen, the rms error is relatively large for the 22 235 and 22.355 GHz radiometers. Note also that two inexplicable large rms values occur at 31.4 GHz. As observed in the table, the rms error at 10.625 GHz is often 0.0. A preliminary observation indicates the possibility that voltages less than zero out of the radiometer are somehow recorded as zero volts. This possibility should be investigated.

Corrections of brightness temperatures for effects of losses of radome and antenna are usually made using the equation

$$T_{correct}(t) = \left(\frac{1}{1 - L_R}\right)\left(\frac{1}{1 - L_A}\right)\left[T_b(t) - L_A T_A(t) - L_R(1 - L_A)\, T_R(t)\right]$$

where L_R and L_A are the power loss fractions of the radome and antenna respectively and T_R and T_A are the thermal temperatures of the radome

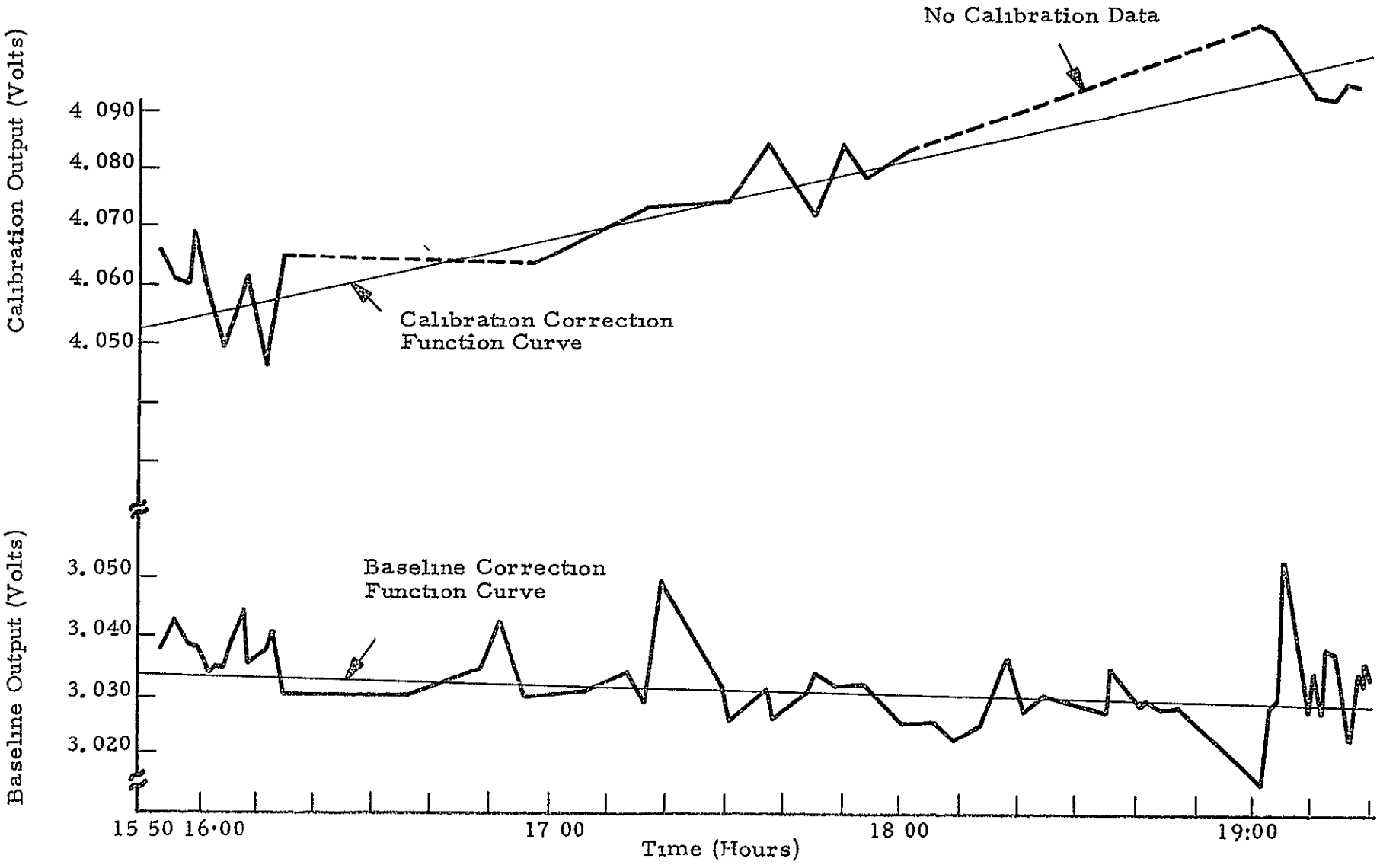

FIGURE 4-23 1 420 GHz (L-Band) BASELINE AND CALIBRATION VOLTAGE, 2/13/70

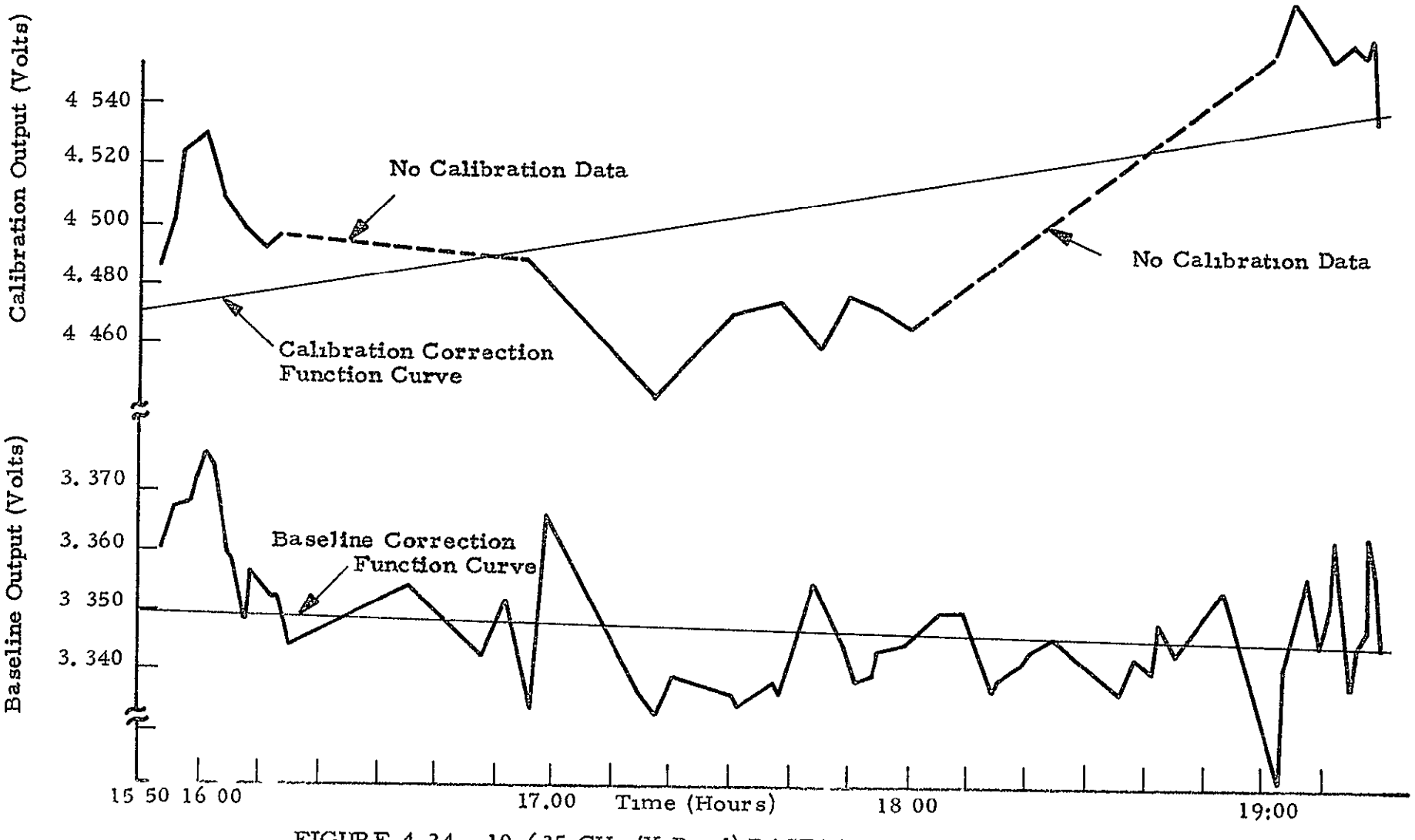

FIGURE 4-24 10 625 GHz (X Band) BASELINE AND CALIBRATION VOLTAGE, 2/13/70

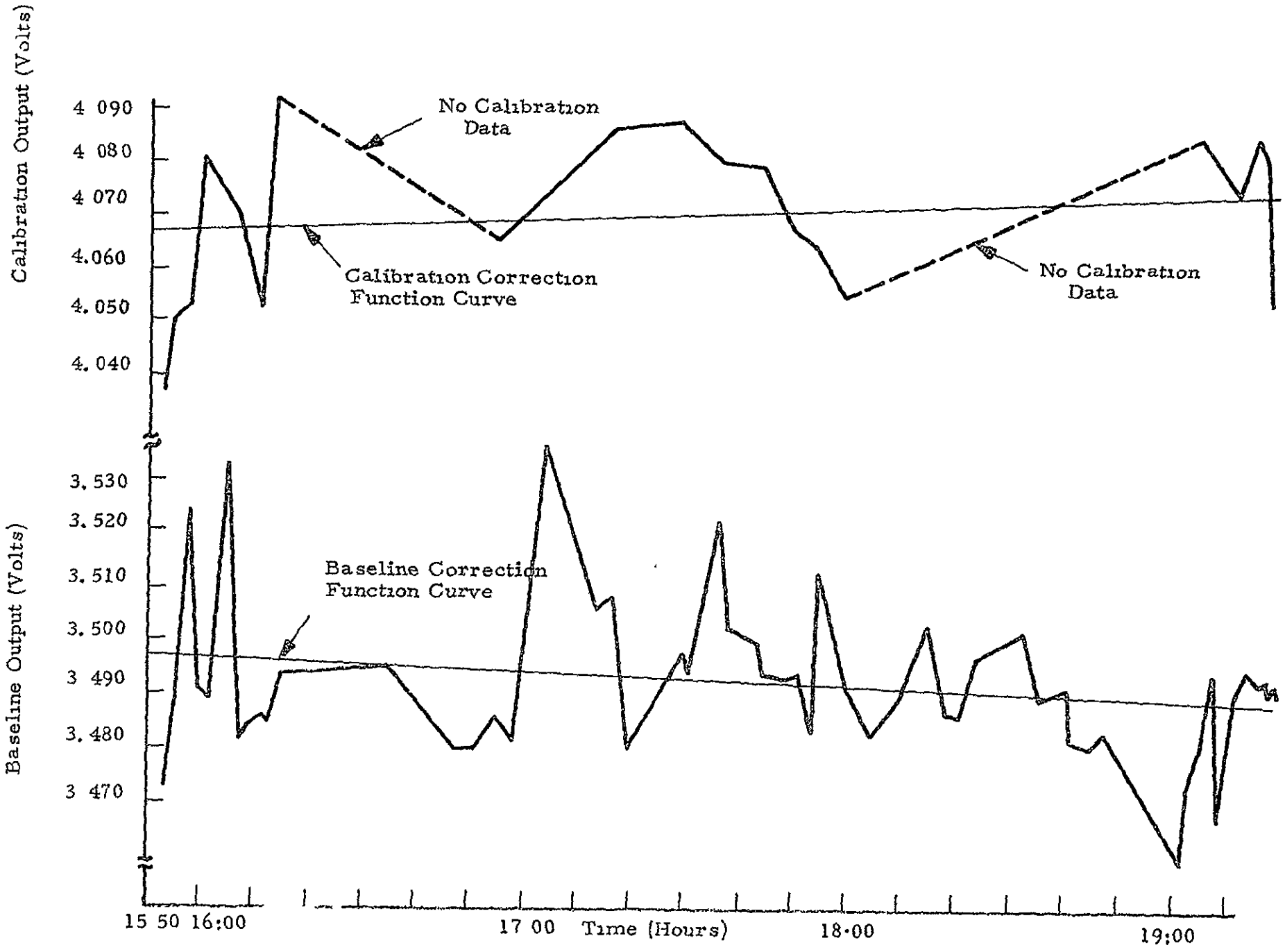

FIGURE 4-25 22 235 GHz (K_1 Band) BASELINE AND CALIBRATION VOLTAGE - 2/13/70

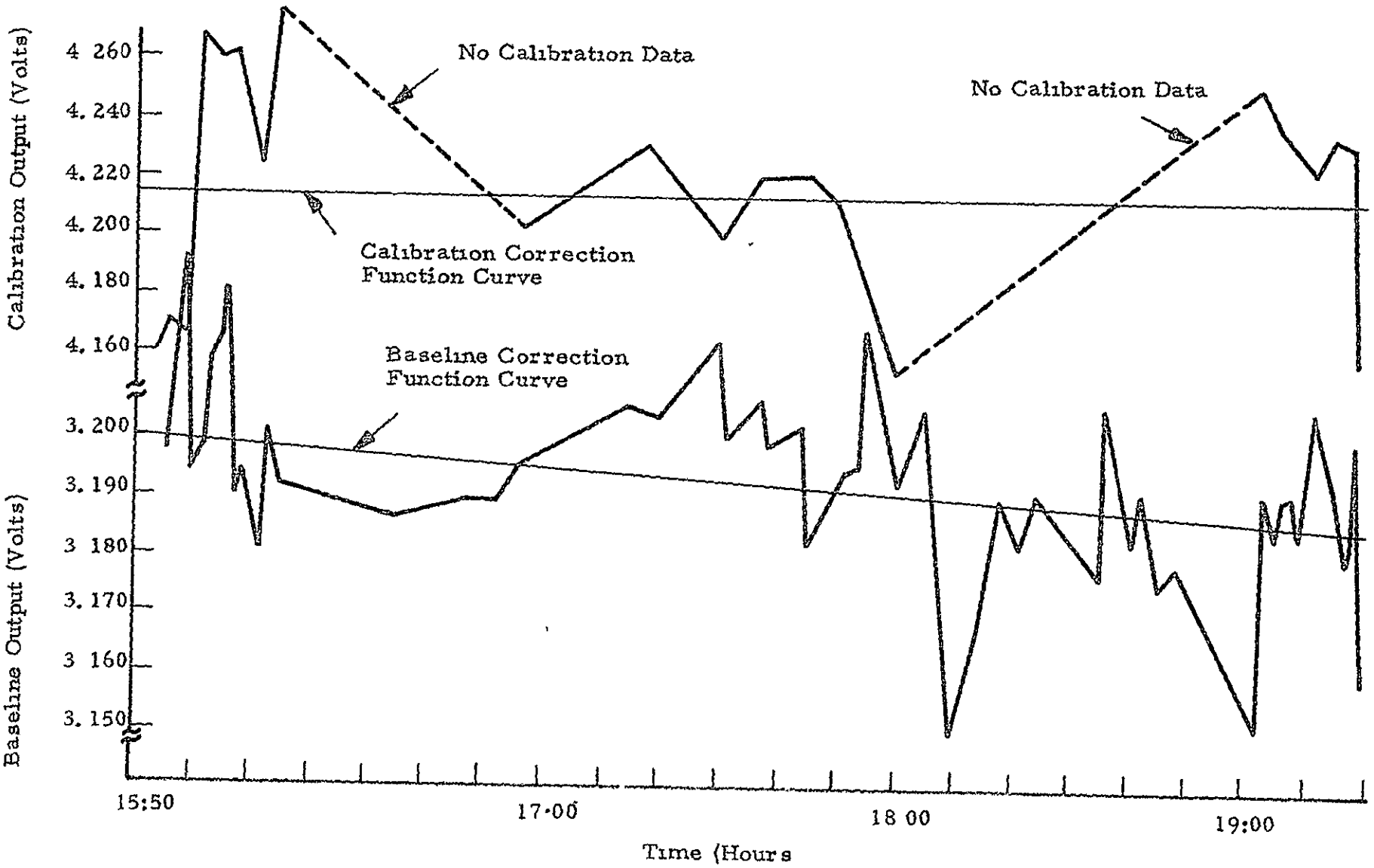

FIGURE 4-26. 22. 355 GHz (K_2 Band) BASELINE AND CALIBRATION VOLTAGE - 2/13/70

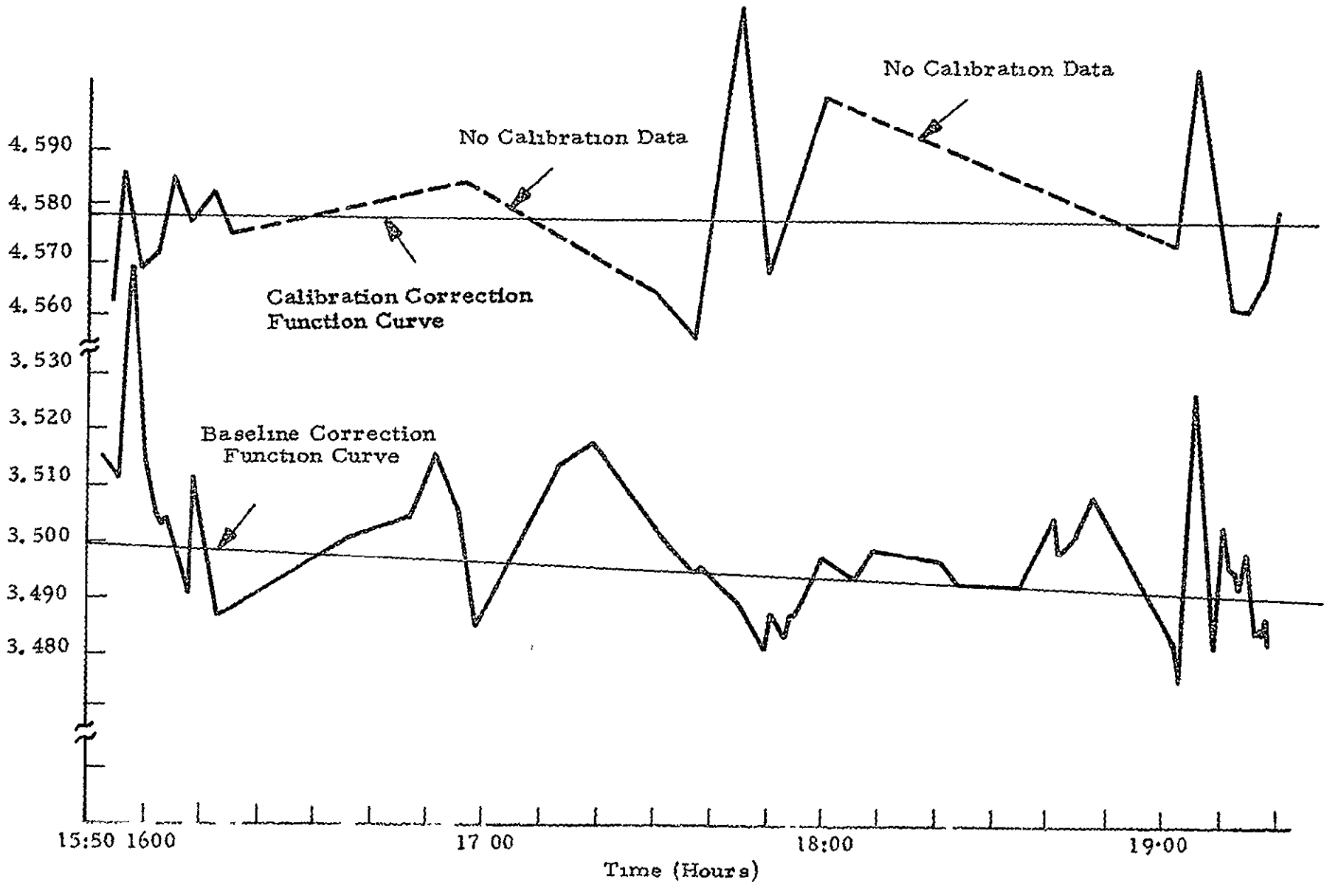

FIGURE 4-27. 31.40 GHz (K_a Band) BASELINE AND CALIBRATION VOLTAGE, 2/13/70

Table 4-3

UNCORRECTED BRIGHTNESS TEMPERATURES
AT THREE ALTITUDES*

Elevation & Angle	1.4200 GHz	10.625 GHz	22 235 GHz	22.355 GHz	31.400 GHz	No. of Points
Ascent						
550' & 100°	172.3 ±0.9	59.9 ±0.4	130.2 ±1.7	153.2 ±1.0	151.3 ±0.4	8
550' & 110°	164.7 ±0.9	53.3 ±0.1	84.6 ±1.6	110.5 ±1.7	141.7 ±0.2	7
550' &120°	165.2 ±0.5	53 7 ±0.1	77.8 ±1.4	104 8 ±1.4	122.8 ±30.5	7
550' & 130°	164.1 ±0.5	53.8 ±0.1	61.8 ±1.6	91.5 ±1.5	134.8 ±0.7	5
550' & 140°	163.1 ±0.9	54.1 ±0.1	68.8 ±1 7	96.4 ±1.3	116.0 ±0.7	6
550' & 150°	163.0 ±0.5	54.6 ±0.3	76.2 ±1.9	101.7 ±1.0	113.5 ±0.4	5
, 100' & 100°	157.5 ±1.1	65.5 ±0.4	15.6 ±1.6	51.5 ±0.7	96.8 ±0.4	9
, 100' & 110°	153.0 ±0 4	61.6 ±0.0	8.9 ±1.1	47.3 ±1.0	103.2 ±0.3	4
, 100' & 120°	152.6 ±0.8	61.8 ±0 0	22.7 ±1.4	57.9 ±2.1	99.5 ±1.0	4
, 100' & 130°	151.4 ±0.6	61.9 ±0 0	20.6 ±1.8	53.7 ±1.0	99.8 ±0.4	4
, 100' & 140°	151.2 ±0.5	62.0 ±0.0	28.1 ±1.2	62.4 ±0.8	71.9 ±16.0	3
, 100' & 150°	149.7 ±1.0	62.0 ±0.0	39.5 ±1.0	71.6 ±1 1	84.8 ±0.5	3
Descent						
485' & 100°	171.1 ±0.3	69.6 ±2.5	154.4 ±7.7	177.5 ±1.1	159.5 ±0.5	6
485' & 110°	162.6 ±0.7	69.0 ±1.1	108.6 ±1.5	133.2 ±1.2	147.2 ±0.5	5
485' & 120°	160.6 ±0.4	68.8 ±0.0	98.2 ±1 0	123.3 ±0.7	139.7 ±1.1	5
485' & 130°	159.9 ±0.5	68 8 ±0.0	85.9 ±1.8	110.5 ±1.2	137.1 ±0.3	4
485' & 140°	161.2 ±0 6	69.2 ±0.0	94 7 ±1 4	118.3 ±1.9	119.1 ±0.2	4
485' & 150°	162.5 ±0.7	69.3 ±0.0	101.5 ±1.3	124.6 ±1.2	118.6 ±0.7	5

* The rms error is calculated from fluctuations in V_R . The number of sample values used in arriving at an average V_R is 300 times the number of points given in the table.

and antenna respectively. A number of assumptions are made in using this relation

a. Reflections from radome or antenna are negligible.

b. Thermal gradients in the radome and antenna are negligible.

c. Variations of losses in the radome and along the antenna are negligible.

An investigation of the validity of these assumptions would allow an estimate of the error introduced into brightness temperatures using the above equation.

The values of L_R and L_A were taken from the Table Mountain calibration and are listed below*.

Table 4-4

LOSSES OF RADOME AND ANTENNAS

Frequency	L_R (Radome)	L_A (Antenna)
1.420	0.077	0.299
10.625	0.107	0.160
22.235	0.286	0.190
22.355	0.268	0.272
31.400	0.269	0.168

The thermal temperature of the radome was monitored by six thermistors located on top outside, left outside, left middle, left inside, bottom outside and bottom inside of the radome. Table 4-5 gives the average values measured at two elevations. An average of the readings at the corresponding altitude was used in the correction of measured brightness temperature.

* Table Mountain Calibration on P3A Multifrequency Microwave Radiometers and Radomes, Nov. 25, 1969, JPL.

Table 4-5

THERMAL TEMPERATURES AT DIFFERENT LOCATIONS AROUND THE RADOME IN °C

Elevation	Top Outside	Left Outside	Left Middle	Left Inside	Bottom Outside	Bottom Inside
Sea Level	23.4	24.4	23.7	23.1	21.0	21.4
21, 100 feet	-0.8	-5.0	-2.8	-2.4	-5.8	-4.0

The thermal temperature of the antennas and waveguides were monitored with two thermistors. Although RF loss occurs in the waveguide and coaxial leads, most of the loss occurs in the antennas. It is for this reason that the thermal temperature of the antenna is used with L_A. The thermal temperature of the waveguide is usually only a few degrees warmer than the antenna so that negligible error is introduced in using the thermal temperature of the antenna

Table 4-6 below gives the corrected brightness temperature corresponding to the uncorrected values in Table 4-3. As mentioned in the discussion of results, gross discrepancies occur between the theoretically predicted values and those in Table 4-6.

If one assumes that the measured data has no significant error, then one can calculate an equivalent loss of the entire radome-radiometer system. That is, if the quantity L_{eff} is selected from

$$L_{eff} = \frac{T_b - T_s}{T' - T_s}$$

where T_b is the measured brightness temperature of the sky, T_s is the theoretically predicted value and T' is some average thermal temperature of the radome and antenna, then all other measured data can be corrected for losses using

Table 4-6

CORRECTED BRIGHTNESS TEMPERATURE
USING THE LOSS VALUES DETERMINED ON TABLE MOUNTAIN
(See Table 4-4 for values of L_A and L_R)

Elevation & Angle	1 4200 GHz	10.625 GHz	22 235 GHz	22.355 GHz	31 400 GHz
Ascent					
550' & 100°	104.5	-17.9	10.2	21.8	57.8
550' & 110°	92.8	-26.7	-64.6	-36.6	42.1
550' & 120°	93.6	-26 2	-76.0	-44.3	31.7
550' & 130°	92.0	-26.0	-102.0	-62.6	30.9
550' & 140°	90.4	-25 6	-90.6	-55.8	0.0
550' & 150°	90.2	-25.0	-78.6	-48.6	-3.9
21, 100' & 100°	94.5	16.8	-173.0	-104.6	-17.4
21, 100' & 110°	87.6	17 0	-185.0	-110.5	-6.9
21, 100' & 120°	86.7	17 2	-161.0	-96.0	-13.0
21, 100' & 130°	85.0	17.4	-164.4	-101.8	-12.5
21, 100' & 140°	84.7	17.5	-151.5	-90.0	-40.1
Descent					
485' & 100°	104.0	-4.4	52.7	55.0	73.4
485' & 110°	91.0	-5.2	-26.4	-5.3	54.1
485' & 120°	88.0	-5.5	-44.5	-18.8	41.8
485' & 130°	86.7	-5.5	-65.5	-36.3	37.6
485' & 140°	88.8	-4 9	-50.5	-25.6	8.2
485' & 150°	90.8	-4.8	-38.8	-17.1	7.2

$$T_{correct} = \frac{1}{1 - L_{eff}} \left(T_b - L_{eff} T' \right)$$

The theoretically predicted sky temperature is computed from measurements of water vapor content, water droplet content, relative humidity, pressure and thermometric temperature profiles of the atmosphere. See Section 4.2.2.

In the figures comparing measured to corrected brightness temperatures with theoretically calculated temperature, the notation "sky adjust losses" refers to temperatures calculated using L_{eff}.

Values of L_{eff} calculated from sky measurements taken at 21, 100 feet are given in Table 4-7 where T' was determined using an average of the radome and antenna temperatures. The values were determined using the sky measurement at 150° from nadir.

Table 4-7

VALUES OF L_{eff} DETERMINED AT TWO ELEVATIONS*

Frequency, GHz	L_{eff}	
	550 Feet Elev	485 Feet Elev
1.420	0.542	0.542
10.625	0.215	0 216
22.235	0.104	0.118
22.355	0.226	0.238
31.400	0.292	0.295

* The 550 foot measurements corresponds to ascent data while the 485 foot to the descent data. Also, note that L_{eff} could be determined at each angle of observation. This was done and the results are discussed in Section 4.2.2.

4.3 EXPERIMENTAL VERIFICATION OF ANTENNA PATTERN EFFECTS CORRECTIONS

An antenna pattern effects experiment was designed to provide information suitable for verifying the techniques of the antenna pattern correction routine outlined in Section 3 and for demonstrating the magnitude of such corrections on brightness temperature data. The test design is described in Section 4.3.1 and flight testing was conducted on 16 February 1970. The antenna pattern flight test data were not analyzed because of the sizable uncertainties in MFMR data discussed in the preceding section These uncertainties preclude a meaningful analysis of the flight test data.

4.3.1 MISSION PLAN

An experimental mission was configured to test the validity of atmospheric correction routines developed in Section 3. The mission plan was approved by cognizant NASA/MSC personnel and is outlined below.

ANTENNA PATTERN MISSION PLAN

A. Flight Conditions

1) Flight should be over areas having sharp demarcation of media. Viz. water/land, land/concrete. Pairs of passes (using horizontal and vertical polarization) should be made over same flight line at six different altitudes. These flights should be accomplished using an antenna viewing angle of 0°, 30° and 150°, as indicated in Table 4-8.

2) Flight should be on a clear day. Time of day is unimportant.

3) Flights should be level and repeated passes made over the same flight line, in the same direction.

4) Flight passes should be perpendicular to boundaries. Record approxomately 30 seconds before and after each boundary interface.

5) Synchronize boresight camera imagery with each data run.

6) Specific flight lines will be in Houston area (within radius of 250 miles) and will be precisely defined prior to 12/31/69.

Table 4-8

ANTENNA PATTERN MISSION PLAN

(Flight Lines 2 and 3)

Run No.	Flight Line Pass	Absolute Flight Altitude	Record Time	Sensors 1	Laser Profilometer	Meteorological Data	Polarization	Antenna View Angle
1	2- 1	250	60 secs	Yes	Yes	Yes	Hor.	0°
2	2- 2	250	↑	↑	↑	↑	Vert.	0°
3	2- 3	250					Hor.	30°
4	2- 4	250					Vert.	30°
5	2- 5	250					Hor.	150°
6	2- 6	250					Vert.	150°
7	2- 7	500					Vert.	150°
8	2- 8	500					Hor.	150°
9	2- 9	500					Vert.	30°
10	2-10	500					Hor.	30°
11	2-11	500					Vert.	0°
12	2-12	500					Hor.	0°
13	2-13	1000					Hor.	0°
14	2-14	1000					Vert.	0°
15	2-15	1000					Hor.	30°
16	2-16	1000					Vert.	30°
17	2-17	1000					Hor.	150°
18	2-18	1000					Vert.	150°
19	2-19	2000					Vert.	150°
20	2-20	2000					Hor.	150°
21	2-21	2000					Vert.	30°
22	2-22	2000					Hor.	30°
23	2-23	2000					Vert.	0°
24	2-24	2000					Hor.	0°
25	2-25	4000					Hor.	0°
26	2-26	4000					Vert.	0°
27	2-27	4000					Hor.	30°
28	2-28	4000			↓		Vert.	30°
29	2-29	4000			Yes		Hor.	150°
30	2-30	4000					Vert.	150°
31	2-31	8000					Vert.	150°
32	2-32	8000					Hor.	150°
33	2-33	8000					Vert.	30°
34	2-34	8000					Hor.	30°
35	2-35	8000					Vert.	0°
36	2-36	8000	60 secs	Yes		Yes	Hor.	0°

Note 1. Sensors include multifrequency radiometers, boresight camera, analog recorder.

2. Altitudes should be flown exactly as listed ±30 ft, all passes level

B. Recorded Flight Data

1) Radiometer outputs and radiometer calibration data on PCM system and 4-pen analog recorder (use one sec integrators) (Record 4 frequencies plus time.) Be sure that in-flight calibrations are PCM recorded.

2) Radiometer Frequencies

L-Band	1.42 GHz
X-Band	10.625 GHz
K-Band	22.2 GHz
K_A-Band	31.4 GHz

3) Complete ADAS

4) Boresight camera and RC8 imagery during all recording periods. (Must be time or frame correlated with radiometer data.)

5) Air temperature at each elevation.

6) Air pressure at each elevation.

7) Humidity at each elevation.

8) Occurrence of water droplets (if any) at each elevation. Quantitative cloud cover - note height of cloud base and cloud tops in flight line (if any).

9) Record laser altimeter data at applicable lower elevations.

C. Ground Truth Data

1) Nominal wind speed (steady or gusting).

2) Nominal wind direction.

3) Nominal wave height.

4) Nominal water temperature.

5) Description of weather in general area. (Meteorological maps.) Presence of fronts, cloud cover descriptions, ceiling (if any).

6) Cold load and hot load calibrations should be run within a day or two "before" and "after" the flight.

7) Types of materials traversed during passes (e.g., sand, grassland, trees, crops, etc.).

The major difficulty in accomplishing the antenna pattern mission is in locating suitable targets. Ideally, a site should be selected where there are a small number of well-defined terrain types. Within each type there must be negligible variation of the microwave properties of the surface, but from type to type there must be considerable variation Also, all but one of the terrain types must occur in patches whose sizes appear to be many tens of beamwidths wide at the lowest altitude at which the aircraft will fly, and from one to a few beamwidths wide at the highest altitude. The remaining terrain type would be the "background" within which the patches of the other terrain types lie. (It would probably be acceptable if there were no single background, as long as all of the patches met the size requirements stated above.)

The aircraft would then be flown over the site at high and low altitudes. The sidelobe correction procedure would be applied to the high altitude data, where sidelobe effects would be expected to introduce significant errors. The corrected results should then be the brightness temperatures of each of the terrain patches. To confirm this, the low altitude data would be used, because, in the low altitude case, both the main lobe and the sidelobes would generally be seeing the same patch of terrain. Thus, except for "glitches" when crossing a boundary, there would be no significant sidelobe errors.

It would, of course, be necessary to assure that there were no effects due solely to the different path lengths at the two altitudes (or, that such effects were adequately compensated for). This could be done by finding large terrain patches at the same site or at a nearby site. These patches would have to be many tens of beamwidths wide even at the high altitude. Flights over such patches would then produce data where errors due to sidelobes would be negligible from both high and low altitudes. Thus, any effects due to altitude itself would be isolated.

Antenna pattern flight test data were collected over various dikes in Galveston Bay, over a pond located in farmland area, and over the end of a cement runway. These data are less than ideal but can be used as a check on the validity of the antenna pattern correction scheme.

Section 5

CONCLUSIONS

Equations, flow diagrams and data reduction routines have been developed to correct MFMR data for atmospheric contributions and antenna pattern effects. The equations and techniques for performing these corrections are discussed in this report. Computer programs are being developed by Manned Spacecraft Center to apply these corrections to MFMR data. Equations and technical details for programming and debugging of the MFMR data correction routines were provided as part of the data study.

MFMR missions are flown for a variety of purposes and requirements for atmospheric and antenna pattern corrections vary from mission to mission. Flexible data correction techniques have been developed to accommodate the range of experimental conditions The effectiveness of these correction techniques depends on proper mission planning and experimental procedures. MFMR mission planning must include consideration of data requirements and mission constraints for performing adequate corrections.

Atmospheric contributions to MFMR measurements can be determined by (1) computation of atmospheric attenuation and emission using suitable mathematical expressions and known or estimated meteorological conditions, and (2) direct MFMR measurements of atmospheric radiation at selected heights above the terrain. Each approach possesses advantages and limitations. Both are useful for MFMR data analysis. The first method consists of assuming that atmospheric conditions are sufficiently well known (e.g , from data supplied by a nearby Weather Bureau station or by direct meteorological measurements from the aircraft) that an a priori calculation of the atmospheric effects can be made. The second approach assumes that the necessary parameters for an a priori calculation are not known (or known only partially) and thus requires that some measurements be performed before atmospheric corrections can be made. The latter approach

is more general, but has the concomitant disadvantage of requiring some flight time to be set aside specifically for atmospheric measurements. In addition, the calibration of the radiometers must be accurate for the second method to succeed. Both approaches are utilized in the microwave radiometer data study The reported equations and methods are sufficiently broad in scope for use with other microwave radiometers such as a C-Band system which is being considered for use in the Earth Resources Aircraft Program

The effect of antenna patterns on MFMR measurements can be estimated from a knowledge of the antenna gain functions and the corresponding brightness temperature of each solid angle element where the antenna gain is significant The available patterns appear to be adequate for determining the total power in the sidelobes. Determination of the brightness temperatures for each significant solid angle element is made difficult by the ground scan which is along a single line. For most types of terrain, information will be needed on the terrain on all sides of the main lobe. It is expected that temperature values accurate enough for this purpose can be estimated using the optical photography obtained at the same time as the microwave data. The antenna pattern correction can be time consuming and use of this correction is impractical for complex terrain data where a large catalog of brightness temperature signatures is required

Flight experiments and test procedures were developed and implemented to substantiate the equations and data reduction procedures for correcting MFMR data Experimental data taken to substantiate the atmospheric correction routine were inconsistent Unrealistic brightness temperatures were obtained using antenna and radome loss values furnished for use in this study. Significant improvement was achieved by using an empirically determined loss factor. However, quantitative results could not be obtained due to the sensitivity of measurement data to the empirically determined loss factor. After an adequate calibration of the MFMR is achieved, verification tests of the atmospheric and antenna pattern routines can be completed The microwave radiometer data processing routines developed under Phase II of the data study will, for the first time, enable routine application of atmospheric and antenna pattern corrections. These refinements will facilitate use of MFMR data by the scientific community